

THE THERMAL AND FLUID SCIENCES CENTER

SMU

RESEARCH REPORT NUMBER 67-1

SYMMETRICAL AND UNSYMMETRICAL FLOW
SEPARATION IN SUPERSONIC NOZZLES

by

Roy A. Lawrence

Sponsored by
National Aeronautics and Space Administration
Multi-Disciplinary Research Grant NGR 44-007-006
Principal Investigator: Dr. Edmund E. Weynand

GPO PRICE \$
CFSTI PRICE(S) \$
Hard copy (HC) 3.80
Microfiche (MF) 1.65

653 July 65

N68-15974

(ACCESSION NUMBER)

(THRU)

April 6, 1967

(PAGES)

(CODE)

(NASA CR OR TMX OR AD NUMBER)

(CATEGORY)

FACILITY FORM 502

SOUTHERN METHODIST UNIVERSITY
INSTITUTE OF TECHNOLOGY
DALLAS, TEXAS, 75222

Research Report Number 1

on

SYMMETRICAL AND UNSYMMETRICAL FLOW SEPARATION
IN SUPERSONIC NOZZLES

by

ROY ALBERT LAWRENCE

(B.S. University of Oklahoma, 1951)
(M.S. Southern Methodist University, 1961)
(Ph.D. Southern Methodist University, 1967)

Sponsored by
National Aeronautics and Space Administration
Multi-Disciplinary Research Grant NGR 44-007-006

Principal Investigator
Dr. Edmund E. Weynand
Professor of Mechanical Engineering
and Thermal and Fluid Sciences
Southern Methodist University
Institute of Technology
Dallas, Texas

April 6, 1967

ABSTRACT

Flow separation in supersonic nozzles was investigated to determine the characteristics and cause of unstable and unsymmetrical flow behavior which occurs at low chamber pressures, and to resolve the reasons for the difference between separation correlations for contoured nozzles as opposed to those for conical nozzles.

The flow structure in several contoured and straight-walled, two-dimensional nozzles was examined by means of schlieren photography with single-frame and high-speed motion picture cameras, and with short-exposure shadowgraphs. Symmetrical, unsymmetrical and unstable separation in contoured and conical axi-symmetric nozzles was investigated by making transient and time-average measurements of static pressures along several sides of the nozzle walls simultaneously.

These studies indicate that separation in nozzles is a two-part problem; of which one part is a jet-entrainment problem to determine the local back pressure in the immediate vicinity of separation, and the other part is the conventional boundary-layer separation problem for supersonic flow. Evidence is presented to show that this approach to the problem resolves apparent differences in separation behavior resulting from the effects of noz-

zle geometry, and that the approach is also valid for wall-attached flows in two-dimensional nozzles.

Unstable and unsymmetrical separation in axisymmetric nozzles is shown to be a consequence of the combined effects of entrainment, and of the shock and flow-turning angles associated with separation. The effects of boundary-layer transition are also considered. The results of experiments to produce and control the deflection of two-dimensional and axisymmetric jets by means of forced separation are presented.

ACKNOWLEDGEMENTS

Several individuals have been of great assistance to the author during the course of this investigation and throughout the doctoral program with which this study is associated. Much is owed to Dr. C.W. Tittle for inviting the author to participate in the program, and for his assistance during the earlier stages of the work.

The author is particularly indebted to his advisor, Dr. E.E. Weynand, for originating the research project and acquiring the financial support necessary for its execution, for the devotion of much of his time and effort to the project, and for taking on numerous other burdens associated with the advisory capacity.

Thanks are due to Dr. H.A. Blum for lending the multi-channel oscillograph to the project and to Mr. T. S. Ashley for his cooperation in the use of this instrument, to Mr. L. Carruth for the use of his personal photographic equipment on numerous occasions, to Mr. J.A. Anderson for machining the two-dimensional nozzle fixture, and to Mr. B. Clark for contributing his personal time to various machining operations in support of the project.

Part of the studies on forced separation were a

cooperative effort with Mr. Larry Chasteen. Mr. Chasteen has since extended these studies.

Mr. R.L. Woods performed much of the programming of the data-reduction and plot routines, and provided general assistance on the project. His generous devotion of time and effort extended far beyond the normal requirements of the assignment and materially contributed to the success of the project.

Appreciation for typing this dissertation is extended to Mrs. Jacquelyn Newbury and to Mrs. Eva Helms, who also suffered through the confusing hieroglyphics of the rough draft and review copies and devoted their personal time so that deadlines could be met. The author also appreciates the assistance of various members of the Thermal and Fluid Sciences Center and Mechanical Engineering Department in expediting the review and publication of this document.

This research was conducted under the auspices of Research Grant NGR 44-007-006 administered by the National Aeronautics and Space Administration. Financial support during the graduate program was provided the author by a National Defense Education Act fellowship. The author is most grateful to the American Taxpayer for providing these funds -- and eagerly anticipates the moment when he makes the transition from the receiving end to the giving end.

Thanks, Dee.

TABLE OF CONTENTS

	Page
ABSTRACT	
ACKNOWLEDGEMENTS	
LIST OF TABLES	
LIST OF ILLUSTRATIONS	
I. INTRODUCTION	1
II. HISTORICAL BACKGROUND	6
Nozzle Separation in General	6
Investigation of Contoured Nozzles	17
III. EXPERIMENTAL SET UP	20
Basic Considerations	20
General Arrangement	20
Air Dryer.	23
Two-Dimensional Nozzles	25
Axi-Symmetric Nozzles	36
Pressure Instrumentation	43
Optical Instrumentation	47
Data Processing	52
IV. EXPERIMENTAL RESULTS; TWO-DIMENSIONAL NOZZLES	54
10-Degree Nozzle (D-2)	54
30-Degree Nozzle (D-3a)	67
30-Degree Nozzle with Extension (D-3b)	73

	Page
30-Degree Nozzle with Curved Throat Exit (D-3c)	76
Contoured Nozzle with Large Initial Divergence Angle (D-4)	78
Contoured Nozzle with Small Initial Divergence Angle (D-5)	82
V. EXPERIMENTAL RESULTS; AXI-SYMMETRIC NOZZLES	86
9-Degree Conical Nozzle (A-1)	86
15-Degree Conical Nozzle (A-2)	97
30-Degree Conical Nozzle; 0.190-inch Throat Diameter (A-3)	103
30-Degree Conical Nozzle; .390-inch Throat Diameter (A-4a)	105
30-Degree Conical Nozzle with Extensions (A-4b,c)	105
Mach-4, Contoured Nozzle (A-5a,b,c)	108
Mach-5, Contoured Nozzle (A-6a,b,c,d)	110
VI. ANALYSIS	113
Separation Pressure Ratios	113
Two-Dimensional Flow Structure.	128
Unstable and Unsymmetrical Behavior	131
VII. CONTROLLED DEFLECTION STUDIES	158
VIII. SUMMARY OF RESULTS AND CONCLUSIONS	167
IX. RECOMMENDATIONS FOR FUTURE WORK	172
APPENDICES	
A. LIST OF SYMBOLS	174
B. TWO-DIMENSIONAL CONTOURED NOZZLES	177
BIBLIOGRAPHY	193

LIST OF TABLES

Table	Page
1. Two-dimensional nozzle parameters	31
2. Axi-symmetric nozzle parameters	40
3. Results of transient pressure measurements; Nozzle D-2	64
4. Data for two-dimensional, sharp-cornered, nozzles	180

LIST OF ILLUSTRATIONS

Figure	Page
1. Types of flow adjustments in overexpanded supersonic nozzles	2
2. Correlations of separation pressures in 15-degree conical nozzles [after Green (7)] . . .	9
3. Separation of two-dimensional flow by abrupt step	10
4. Separation correlation based on Mach number [after Arens and Spiegler (17)]	14
5. Separation data for contoured nozzles [after Ahlberg, Hamilton and Migdal (26)]	18
6. Schematic of experimental arrangement	21
7. Photographs of experimental arrangement	22
8. Two-dimensional nozzle assembly	27
9. Two-dimensional nozzle contours	30
10. Axi-symmetric nozzle assembly	37
11. Axi-symmetric nozzle contours	39
12. D.C. Amplifier	46
13. Flow visualization arrangements	48
14. Flow patterns; 10-degree, two-dimensional nozzle	55
15. Typical wall static-pressure for 10-degree, two-dimensional nozzle	56
16. Pressure fluctuations in 10-degree, two-dimensional nozzle	62

Figure	Page
17. Oscillating-flow configuration	66
18. Flow patterns; 30-degree, two-dimensional nozzle	68
19. Wall static pressures; 30-degree, two- dimensional nozzle	71
20. Flow patterns; 30-degree nozzle with straight extension	75
21. Flow patterns; 30-degree nozzle with curved throat exit	77
22. Flow patterns; contoured nozzle with large throat exit angle (D-4)	79
23. Wall static pressures; contoured nozzle, D-4	83
24. Flow patterns; contoured nozzle with small throat exit angle (D-5)	84
25. Wall static pressures; 9-degree, conical nozzle (A-1)	87
26. Flow symmetry for 9-degree, conical noz- zle - lower pressures	89
27. Flow symmetry for 9-degree, conical noz- zle - higher pressures	90
28. Exhaust appearance for symmetrical and un- symmetrical flow in conical nozzle	92
29. Oscillograph record of flow switching	94
30. Fluctuating pressure distributions in 9-degree, conical nozzle	96
31. Pressure distributions for deflected jet in ventilated, 9-degree conical nozzle	98
32. Wall static pressures; 15-degree conical nozzle (A-2)	100
33. Exhaust patterns for 15-degree, conical nozzle (A-2)	102

Figure	Page
34. Unsymmetrical pressure distributions; 30-degree, conical nozzle with .190-inch throat diameter (A-3)104
35. Wall static pressures; 30-degree, conical nozzle with .390-inch throat diameter (A-4 _a)106
36. Wall static pressures; 30-degree, conical nozzle with straight extension (A-4 _b)107
37. Wall static pressures; Mach-4, contoured nozzle (A-5)109
38. Wall static pressures; Mach 5, contoured nozzle111
39. Separation correlation based on pressure ratio114
40. Separation correlation based on Mach number124
41. Separation correlations for 10-degree, two-dimensional nozzle127
42. Separation-shock angles129
43. Flow structure in axi-symmetric nozzles133
44. Illustration of the possibility of a double solution to the nozzle-flow and separation equations136
45. Separation correlation based on Reynolds number [after Shapiro (44)]138
46. Shadowgraphs of flow in 10-degree, two-dimensional nozzle142
47. Flow turning angle at separation145
48. Deflections due to differential pressure151
49. Control volume for determination of nozzle forces153
50. Forced separation in 9-degree conical nozzle160

Figure	Page
51. Pressure profiles for forced separation . . .	161
52. Forced flow deflection in two-dimensional nozzle at high chamber pressure	164
53. Illustration of data for contoured nozzles .	179

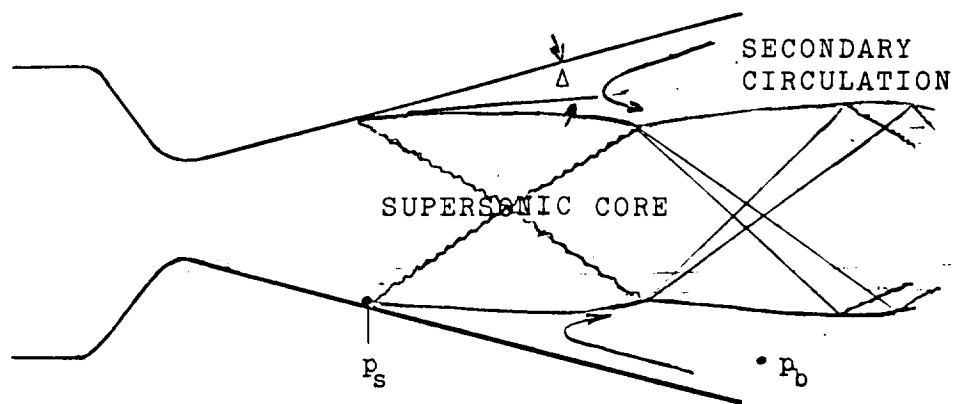
INTRODUCTION

The objective of the research which is reported in this document is to provide additional information and greater understanding regarding supersonic flow separation in nozzles.

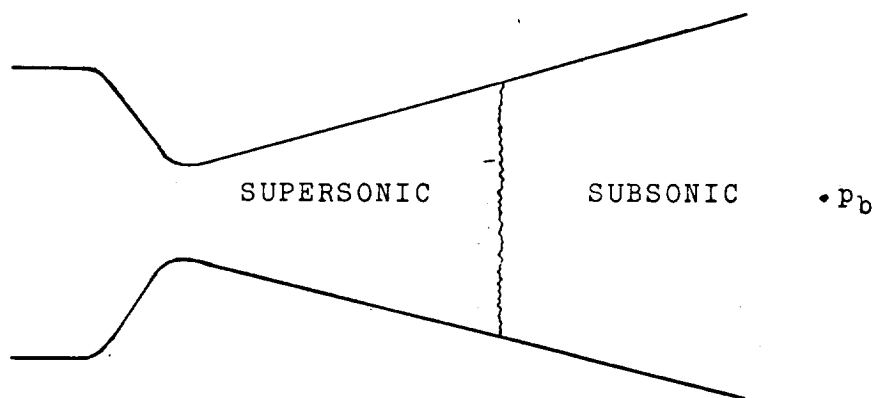
Numerous investigations have revealed that when supersonic nozzles operate in an environmental pressure which is greater than that for which the nozzle is designed, that is, when the nozzle is overexpanded; usually oblique shock waves will occur and the flow will separate from the walls and exit as a supersonic jet which fills only a portion of the cross-sectional area for expansion.

This behavior is in contrast with the "classical" model of flow in overexpanded supersonic nozzles which provides for flow adjustments exterior to the nozzle accompanied by oblique shocks, but requires that adjustments occurring inside of the nozzle be through a normal, or series of normal shocks, positioned so that beyond the shock(s), subsonic flow will completely fill the nozzle and diffuse to match the environmental pressure at the exit.

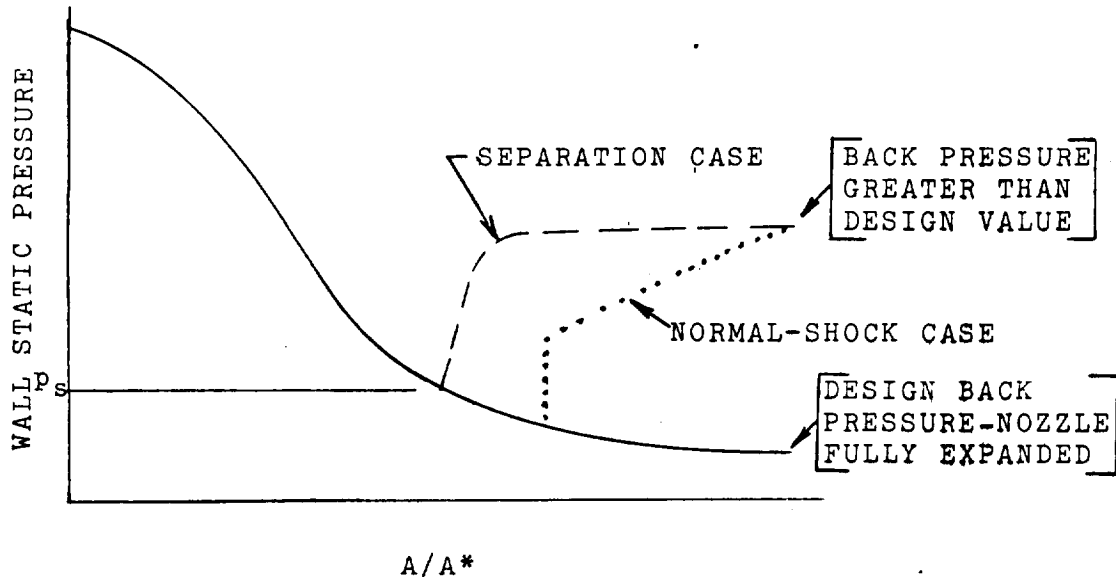
Figure 1 illustrates the difference between the two cases. Because the flow does not fill the nozzle, separation - when it occurs - always takes place upstream of the



a. separation case



b. normal-shock case



c. wall static pressure distributions

Fig. 1.--Types of flow adjustments in overexpanded supersonic nozzles.

position where a normal shock would theoretically occur. With separation, flow expands from a supply total pressure, p_0^\dagger , to a minimum wall static pressure, which is designated (somewhat inaccurately) as the separation pressure, p_s . The wall pressure then abruptly rises to the approximate value of the back pressure, p_b (which is usually the local atmospheric pressure, p_a). Internal wall pressures less than the pressure of the environment produce a loss of thrust. Because separation occurs upstream of where a normal shock would occur, and because the pressure rise is more abrupt than that associated with subsonic diffusion, separation results in higher internal pressures in the expansion region and therefore, appreciably improved performance over that associated with the case of the normal shock. Obviously, knowledge of the point of separation and of the pressure profile which follows is essential if one is to be able to predict performance.

Nozzles which are designed for optimum performance at high altitudes will be overexpanded at lower altitudes and therefore, susceptible to separation. Since this situation is a matter of practical concern in many rocket applications, separation has been the subject of numerous investigations. The major results of these investigations are as

[†]Appendix A lists the symbols used in this document unless otherwise defined at the location in the text where the symbol is used.

follows[†]:

1. Some evidence has been accumulated to the effect that separation in nozzles is a boundary layer phenomenon with characteristics similar to the shock-boundary layer interactions which occur when turbulent supersonic flow over a flat plate encounters an obstruction. However, other evidence is offered which tends to contradict this hypothesis.
2. Empirical correlations have been made which permit one to predict the position of separation in conical nozzles.
3. Flow instabilities and unsymmetrical flow patterns have been observed at low upstream stagnation pressures. However, this behavior has received only cursory investigation.
4. Only a few data have been published regarding flow separation in contoured nozzles. These data are inconsistent, but they indicate that the location of separation cannot be reliably predicted by the correlations mentioned in item 2, above. Consequently, there is an uncertainty regarding the nature of separation in contoured nozzles.

[†]Information summarized here will be discussed in greater detail and referenced in the following chapter.

Despite the apparent success in correlating separation in conical nozzles, several uncertainties still remain which are worthy of investigation. Knowledge of the separation shock geometry and the behavior of the core of supersonic flow immediately beyond the separation point could provide information regarding the validity of the separation models which have been proposed. Also, such knowledge would contribute to a better understanding of the principles governing the behavior of fluid amplifiers and switches utilizing supersonic flow.

Also, the discrepancy between the separation correlations for conical and contoured nozzles indicates that understanding of the phenomenon is not complete. In particular, the effects of differences in pressure gradients, internal flow structure, and wall contour are not known.

Finally, the unsymmetrical and unstable flow behavior pose fundamental questions regarding the stability of supersonic flows in confined regions. This subject is of importance in the development of fluidic devices as well as to the behavior of thrust-producing nozzles.

These topics are the focal points of the study reported herein.

II. HISTORICAL BACKGROUND

Nozzle Separation in General

The phenomenon of separation was noticed during the course of early investigations of flow in converging-diverging nozzles conducted by Buchner (1904), Prandtl (1907), Meyer (1908), Flügel (1917), Stanton (1926) and Stodola (1927). These findings are discussed by Stodola in his book on steam and gas turbines (1).[†]

With the advent of rocket propulsion following World War II, flow separation became a matter of practical importance, and interest in the subject grew. A series of experiments conducted at the Jet Propulsion Laboratory (JPL) of the California Institute of Technology by Foster and Cowles (2), (3); McKenney, (4); and Summerfield and Swan (5) provided some of the first quantitative correlations relating the location of separation in conical and two-dimensional nozzles as a function of chamber pressure.

These investigators ascertained that the location of separation could be predicted reasonably well by assuming that the flow is turned through a wedge angle, Δ , in the

[†]Numbers in parentheses refer to corresponding references listed in the bibliography.

region of separation (as indicated in Figure 1) and then applying two-dimensional-shock theory to determine the pressure rise across the shock. In this approach, the pressure downstream of the shock is taken to be the back pressure, p_b . The interesting, and potentially significant, discovery was made that the experimental data were best fitted if the wedge angle was assumed to have a constant value which was almost independent of the divergence angle of the nozzle, nozzle length, pressure ratio, and gas temperature. This result was quite surprising because one would expect the flow to be turned approximately parallel to the axis of the nozzle. Thus, one could guess that the turning angle would be nearly that of the divergence angle of the nozzle. As a consequence of these investigations, Summerfield observed that separation occurred at a value of $p_s/p_b \approx 0.4$. For several years, this value served as a guide for locating the point of separation. However, considerable evidence which indicates that this ratio is not a constant has since been accumulated, as will be made apparent in the following discussion. The series of experiments at JPL also revealed the occurrence of unsymmetrical and unstable flow behavior in two-dimensional and conical nozzles when operated at low chamber pressures.

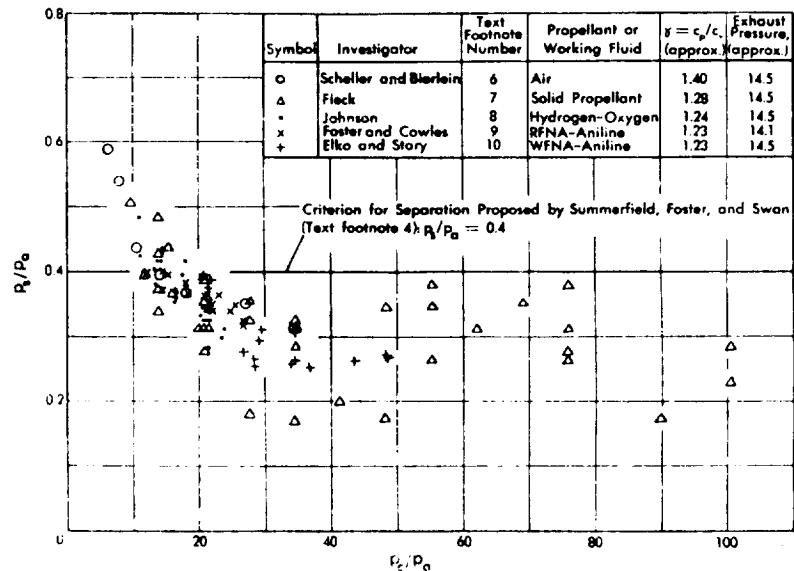
Scheller and Bierlein (6) obtained separation data for dry air flowing through conical nozzles having divergence angles of 5, 15 and 33 degrees. Their results disagreed with the foregoing data of Summerfield, et al, in that the

separation pressure was found to be strongly dependent on the divergence angle of the nozzle. These results also indicated that the assumption of two-dimensional shock relations with a constant wedge angle would not provide a generally satisfactory model for determining separation pressures.

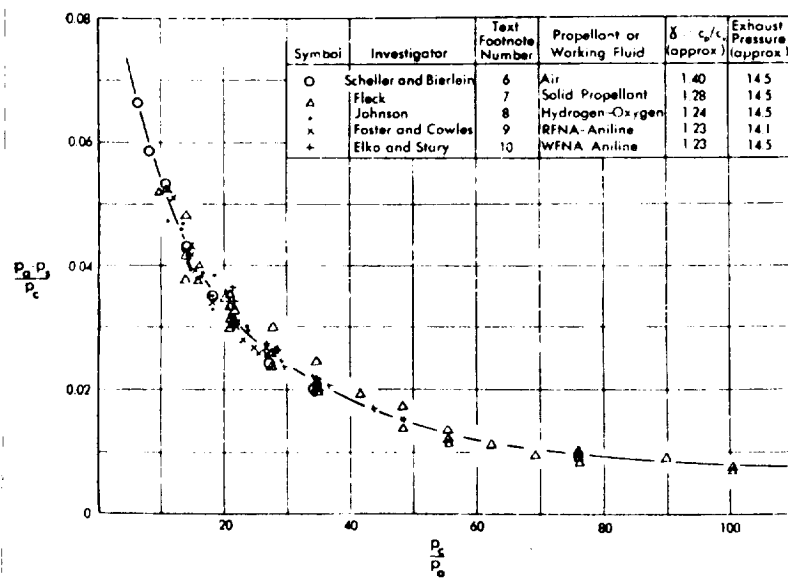
Green (7) attempted to correlate data regarding the separation pressure ratios for 15-degree conical nozzles which had been reported by a number of investigators prior to 1952. Figure 2a shows the relationship of separation pressure ratio to chamber pressure ratio as compiled by Green. Green replotted these data in terms of the variable, $(p_a - p_s) / p_c$. This correlation is indicated in Figure 2b. Although this latter correlation inherently tends to suppress the scatter of the data, it does permit a general curve fit which is esthetically more appealing than that of Figure 2a.

Mager (8) contributed significantly to the understanding of flow separation in nozzles by making the association that separation in nozzles is basically the same phenomenon as the separation produced by the shock-boundary layer interaction which occurs when a supersonic stream flowing over a flat plate encounters an obstruction - such as an abrupt step.

Figure 3 indicates this type of flow situation as determined from investigations such as those by Gadd (9), Lange (10), and Bogdanoff and Kepler (11). Mager observed



a. usual representation



b. Green's correlation

Fig. 2.--Correlations of separation pressures in 15-degree conical nozzles [after Green(7)]

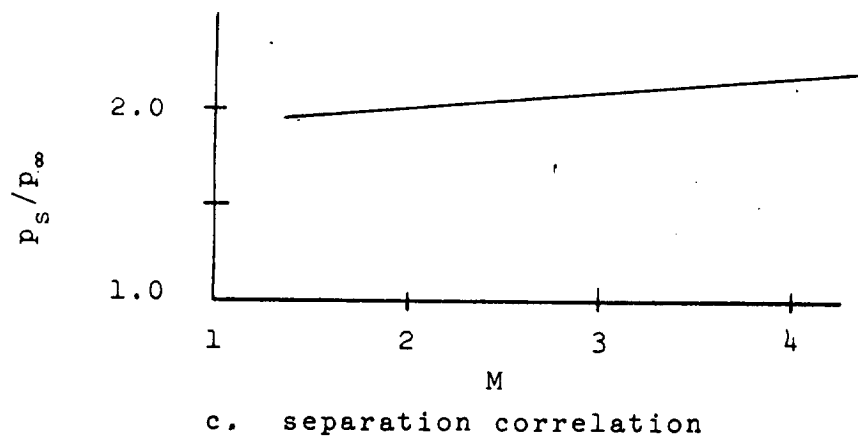
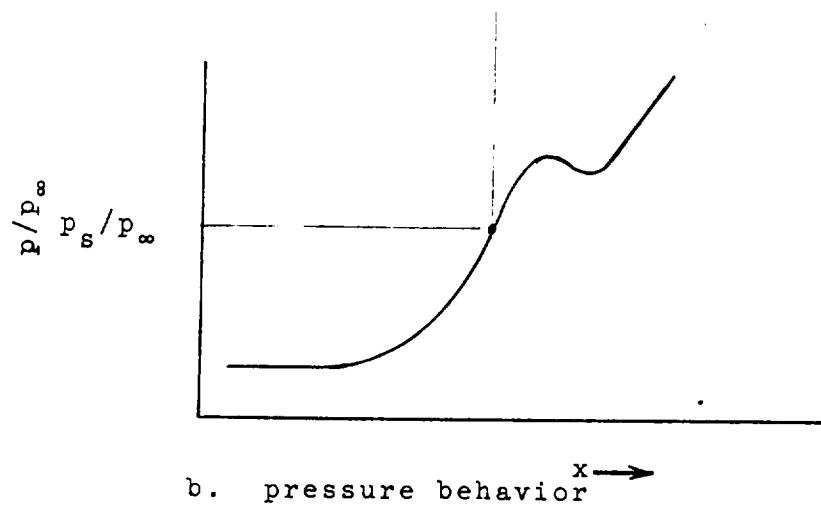
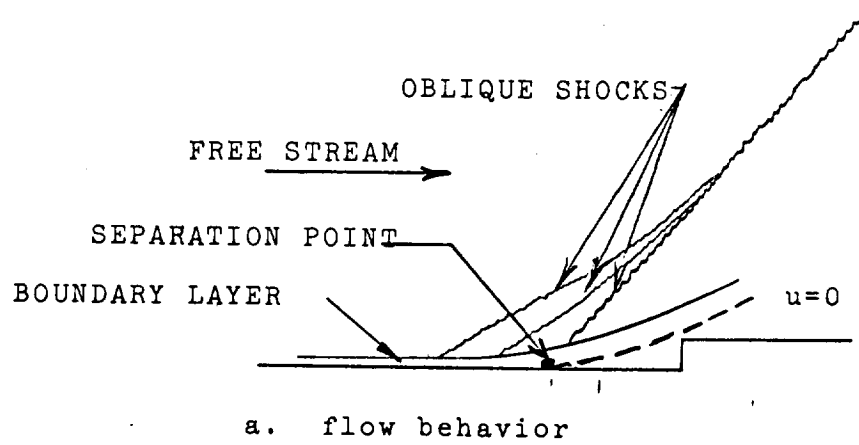


Fig. 3. --Separation of two-dimensional flow by abrupt step

that while the pressure behind the point of separation (taken to be the point of zero velocity gradient in the boundary layer) depended on the nature of the obstacle, the static pressure ratio p_s/p_∞ was a reasonably well known function of Mach number such as indicated in Figure 3c. He then formulated a model to relate the pressure ratio across the separation shock, p_b/p_∞ to the separation pressure ratio, p_s/p_∞ . By this means he was able to provide a reasonably good fit to McKenney's experimental data for separation pressure ratios in a two-dimensional nozzle.

Frazer, Eisenklam, and Wilkie (12) investigated separation in a variety of nozzles which were equipped with extensions of different geometries to alter the back pressure. This study led these investigators to conclude that for a given general type of nozzle geometry, there is only one separation pressure for each back pressure. Furthermore, the ratio of separation pressure to back pressure was believed to be a function of nozzle geometry only and independent of separation Mach number, reservoir pressure, throat area, etc. For conical nozzles, the ratio of separation pressure to back pressure was found to be 0.36. These results appear to be at odds with the model proposed by Mager, and with the observation of Summerfield, regarding turning of the flow through a constant wedge angle. Unsymmetrical and unstable flow tendencies at low reservoir pressures were also observed.

Campbell and Farley (13) made a very practical

contribution to the state of the art by developing empirically-based correlations for determining wall static-pressure distributions over the entire length of conical nozzles in which separation occurs. By means of this correlation, they were able to predict thrust ratios to within about one per cent for conical nozzles having expansion half angles ranging from 15 to 30 degrees. They also found that the ratio of static pressure to total pressure at separation, p_s/p_o , could be predicted quite well from two-dimensional, oblique-shock theory if one assumed a Mach-number ratio across the shock of approximately 0.76; a value which is in good accord with experimental data for the shock-induced separation of turbulent boundary layers over flat plates (14).

Farley and Campbell employed air, but other experiments conducted by the National Aeronautics and Space Administration (NASA) (15) indicated that the separation pressures in conical nozzles employing JP-4 and oxygen could also be predicted by utilizing a suitable Mach-number ratio across an oblique shock.

Page (16) proposed a theory to predict the pressure rise associated with separation of two-dimensional turbulent boundary layers. The theoretical results were in reasonably good accord with some of the experimental data for 15-degree nozzles, and with the empirical curve of Figure 2b.

Arens and Spiegler (17) conducted experiments and compiled data of other investigators to demonstrate that

separation pressure ratios, p_s/p_b , in conical and two-dimensional nozzles consistently decreased with increasing Mach number in a manner very similar to that observed for forward facing steps, compression surfaces, etc. These authors utilized the assumption, first suggested by Gadd (18), that the pressure rise associated with separation must be sufficient to stagnate a characteristic velocity in the boundary layer, u_s^* . They found that the theory could predict the experimentally-determined dependence of separation pressure ratio on Mach number if a value for $u_s^*/u_s = 0.6$ was assumed; where u_s is the free stream velocity at separation. Figure 4 shows the analytical and experimental Mach number dependence.

During the course of their investigations, Arens and Spiegler conducted tests at low chamber pressures where they noted unsymmetrical and unstable flow behavior. They also pointed out that if the separation model was correct, the pressure ratio required to separate the boundary layer at a Mach number of 1.13 is 1.7, a value which is greater than the pressure ratio across a normal shock at this Mach number. They therefore concluded that oblique shock separation was unlikely for nozzle pressure ratios, (p_o/p_b) less than approximately 1.7.

This analysis and associated experimental observations led the authors to classify flow in overexpanded conical nozzles into five distinct regimes, which are in order

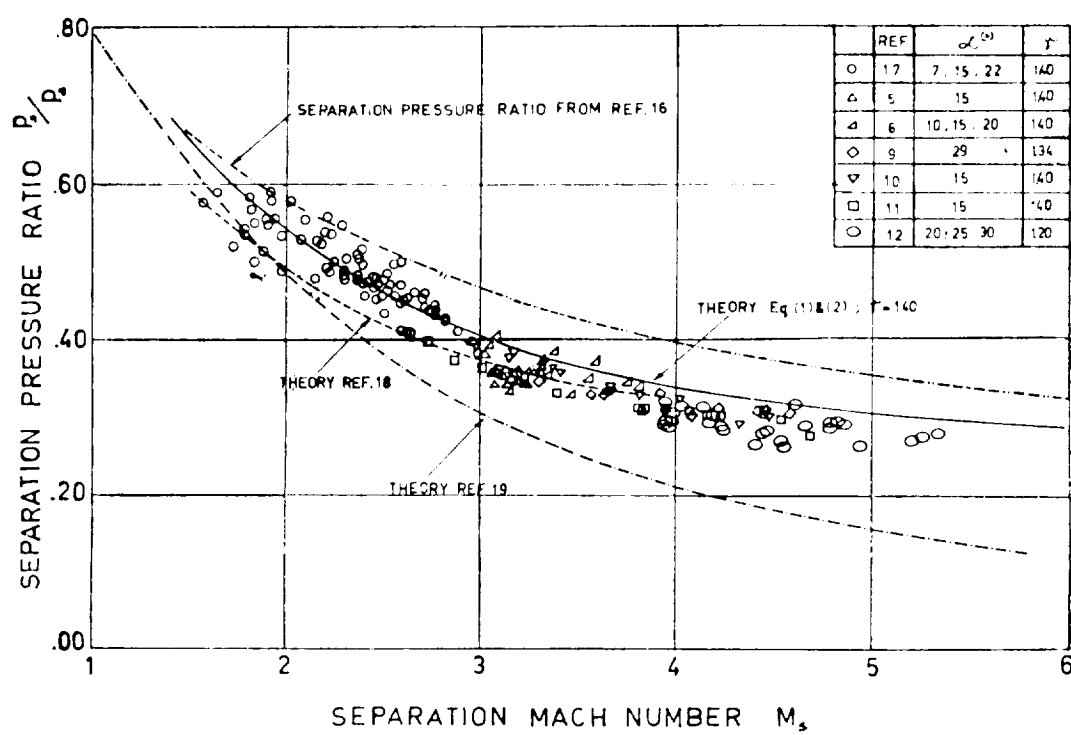


Fig. 4 --Separation correlation based on Mach number
[after Arens and Spiegler(17)]

of increasing pressure ratio:

1. Essentially one-dimensional flow with a normal shock just downstream of the throat.
2. Unstable and asymmetric flow with oblique-shock boundary layer separation.
3. Stable flow with oblique-shock boundary layer separation.
4. Same as 3 but with shocks occurring in the immediate vicinity of the nozzle exit, but within the nozzle.
5. Undisturbed flow in nozzle but with oblique shocks initiating in the nozzle exit plane.

Moore (19) and Simon (20) attempted to categorize nozzle pressure ratios associated with the first three of the above regimes. Moore investigated flow in a small conical nozzle of 15-degree divergence angle. Simon utilized a 10-degree nozzle which was cut off at successively shorter lengths to determine the effects of varying the area ratio. Their results are tabulated below:

<u>p_o/p_a</u>	<u>Type Flow</u>
1.7 - 2.1	stable, unsymmetrical
2.1 - 3.7	unstable, unsymmetrical
3.6 - 11	stable, unsymmetrical
> 11	stable, symmetrical

Simon found that changing the area ratio had no effect on the pressure limits of the various regimes, but that the smaller nozzle divergence angle appeared to slightly

increase the upper limit of pressure ratio for the stable, unsymmetric regime.

Sunley and Ferriman (21) compared the edge positions of soot bands produced by combustion products expanding on a conical nozzle with the positions of minimum wall static pressure and concluded that the point of separation, as evidenced by the termination of soot, occurred at an area ratio which was 10 to 20 per cent higher than that for minimum pressure; a conclusion which is consistent with the data for separation caused by steps as shown in Figure 3. These investigators also concluded that separation occurring at area ratios greater than approximately 80 per cent of the exit area ratio was characterized by higher separation pressure ratios than for separation occurring further upstream in the nozzle. They attributed this effect to reduced entrainment of external air, but did not investigate the matter in detail.

Kalt and Badal (22) established an empirical basis for determining rocket thrust under separated flow conditions. In the course of their work, they were able to fit experimental data for separation pressure ratios such as those represented in Figure 4 by the relationship:

$$\frac{p_s}{p_a} = \frac{2}{3} \left[\frac{p_c}{p_a} \right]^{-0.2}$$

They also ascertained that the region of rapid pressure rise immediately beyond the point of incipient separation

in nozzles agreed reasonably well with other observations related to flat plates (11,23,24) that the length of interaction of the turbulent boundary layer is approximately 10δ , where δ is the boundary layer thickness at the point of separation. Thus, for a conical nozzle of fixed expansion angle, the authors could relate the initial and final area ratios associated with the abrupt pressure rise. By these means they were able to determine pressures along the entire length of the nozzle and thereby determine the performance penalty associated with operation in the overexpanded regime.

Investigations of Contoured Nozzles

Very little information has been published regarding flow separation in contoured nozzles, despite the popularity of such nozzles for rocket applications. The data that are available indicate that the usual correlations which are successful for conical nozzles, such as the one in Figure 2, are not applicable. Farley and Campbell (25) investigated separation in three contoured nozzles and observed that flow overexpanded to a greater extent before separation occurred than in conical nozzles. Figure 5, which was compiled by Ahlberg, Hamilton, Migdal, and Wilson (26) provides a general indication of the differences. The foregoing authors also conducted tests with a cylindrical shroud around a nozzle to inject air for the purpose of determining the effect of external flow. They observed that the separation correlation was identical to the values shown in Figure 5 if the actual

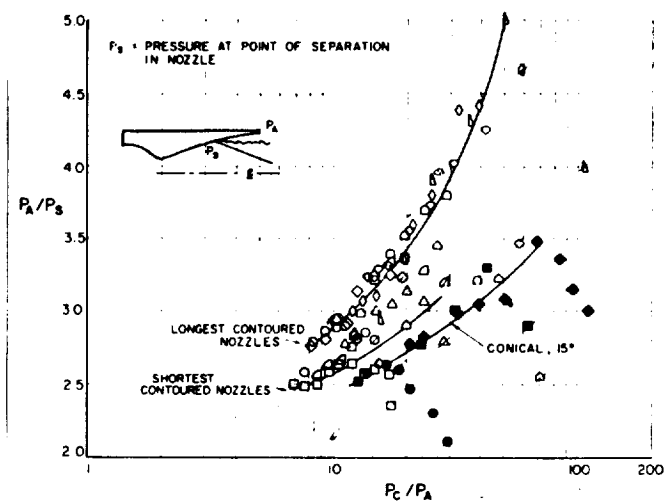




Fig. 5.--Separation data for contoured nozzles.
[after Ahlberg, Hamilton and Migdal(26)]

base pressure instead of the ambient pressure was used in determining chamber-pressure ratios. Another interesting aspect of their investigation was the observation that cooling of the nozzle walls retarded separation.

Roschke and Massier (27) found that separation pressure ratios were larger, and the separation area ratios smaller in a contoured nozzle than in a conical nozzle, and that the discrepancy between the two nozzle types increased with increasing chamber pressure. These results are just the opposite of those of Farley and Campbell.

Ionov (28) used schlieren photography to examine the flow patterns in two plane-contoured nozzles designed for exit Mach numbers of 1.55 and 2.0. By varying the back pressure on the nozzle, he was able to vary the air mass flow rate while maintaining a fixed pressure ratio across the nozzle. He noted that, for a fixed pressure ratio, the shock pattern changed from "bridge-like  " to "oblique  " as the back pressure was reduced. Presumably, the first of these patterns is associated with separation of a turbulent boundary layer and the second with a laminar boundary layer, since the length Reynolds number would be higher with the higher back pressure.

In view of the conflicting reports, one concludes that a universally acceptable model for separation in nozzles has not been advanced - or if it has, it has not been generally recognized.

III. EXPERIMENTAL SET UP

Basic Considerations

The experimental program was oriented to achieve several objectives. One of these was to gain a better understanding of unstable flow behavior. To accomplish this objective, the approach was; (1) to attempt to gain insight regarding the controlling phenomena by visual indications of the flow behavior in two-dimensional nozzles with transparent walls and, (2) to acquire knowledge of the flow dynamics by suitable pressure measurements in both two-dimensional and axi-symmetric nozzles. For the visual studies, high-speed, motion-picture photography was used in conjunction with the schlieren and shadowgraph visualization techniques. Electrical pressure transducers were utilized to determine the characteristics of the pressure fluctuations.

Other objectives of investigating flow structure, unsymmetrical flow behavior, and separation in contoured nozzles were approached in a similar manner; except that still photography and steady-state pressure measurements were employed.

General Arrangement

Figures 6 and 7 show the experimental arrangement. Air, employed as the working fluid, was supplied from a

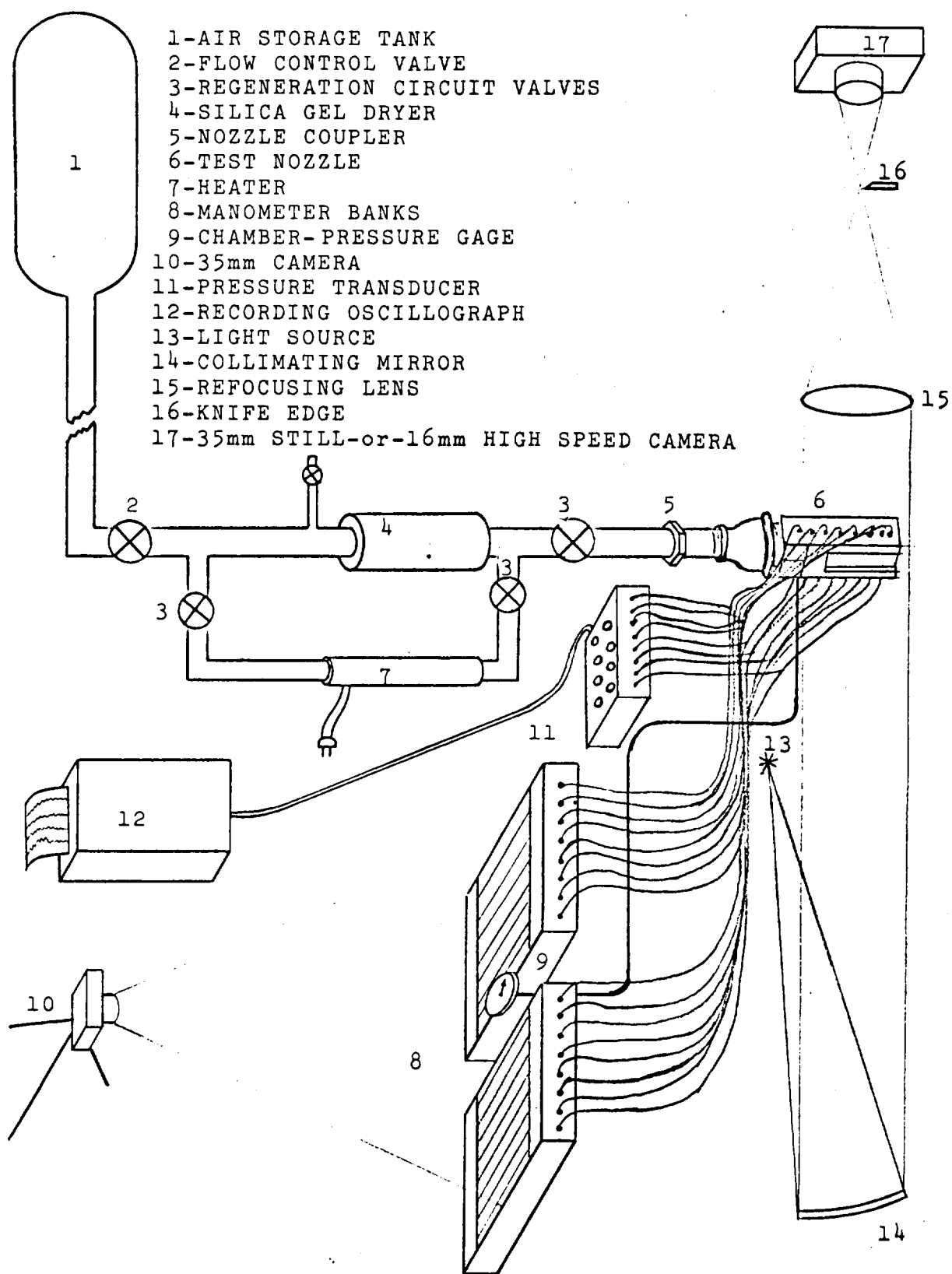
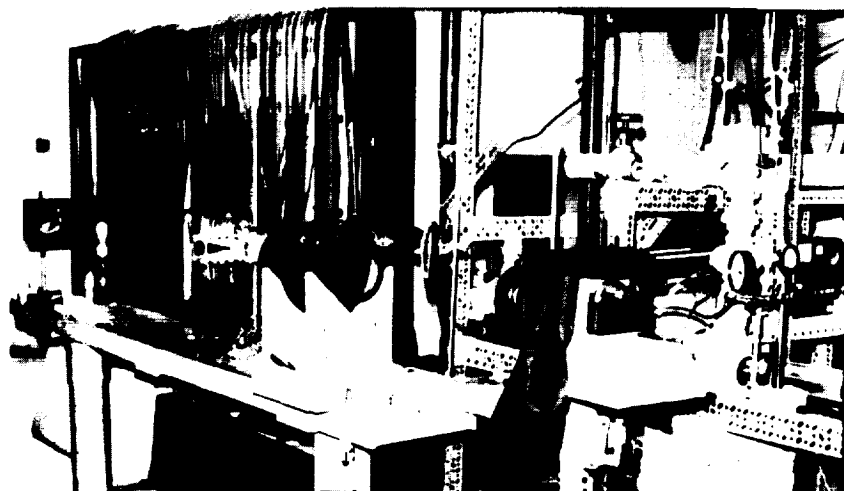
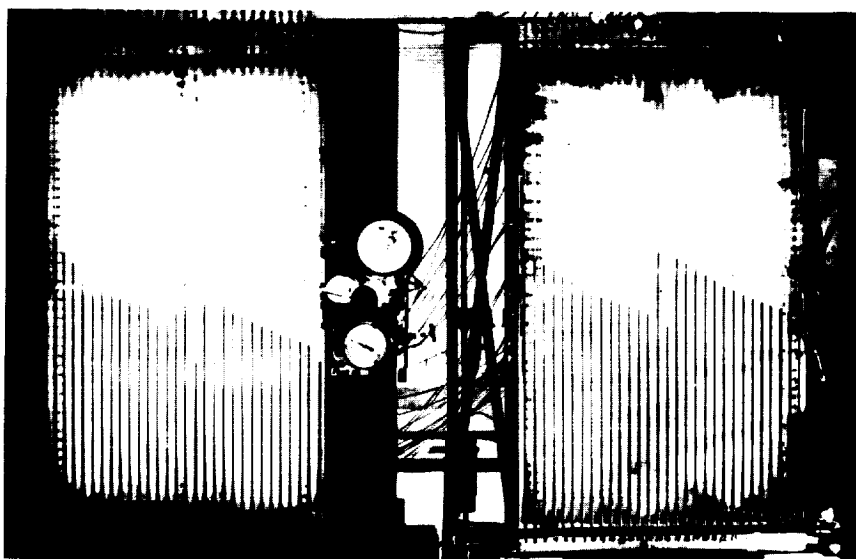


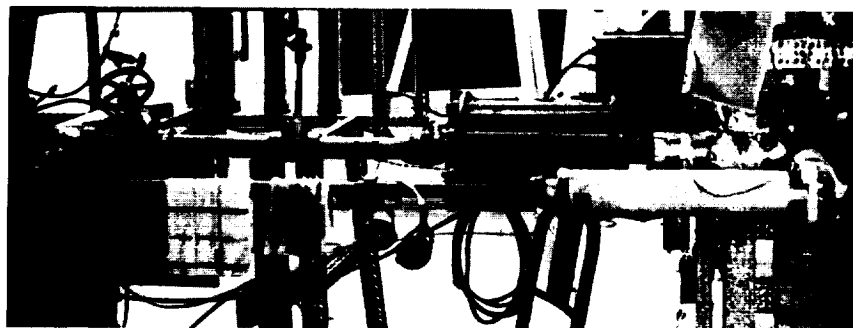
Fig.6.--Schematic of experimental arrangement.



a. schlieren set-up



b. manometer boards



c. air-dryer and regenerator

Fig. 7.--Photographs of experimental arrangement

storage tank having a capacity of 2400 cubic feet at a maximum pressure of 500 psi. The supply line from the tank to the test location consisted of approximately 100 ft. of 2-inch diameter pipe.

In the immediate vicinity of the nozzle, the air flowed through a hand-operated globe valve which was used for flow control; a thin polyurethane particle filter, a silica gel bed for on-stream moisture removal; an open globe valve; a short section of 2-inch diameter pipe equipped with a thermometer well; a pipe fitting to accommodate the particular nozzle being investigated; flow straighteners, and then to the nozzle.

Various optical arrangements suitable to schlieren and shadow photography were utilized. The nozzles were equipped with numerous wall pressure taps which were connected to two banks of manometers and a bank of electrical pressure transducers by means of plastic tubing. The output of the pressure transducers was recorded on a 20-channel oscillograph.

Air Dryer

To eliminate the effect of condensation on flow behavior and flow visualization, efforts were extended to reduce the moisture content of the air. The first step in this direction was to maintain high pressures in the supply tank. A nominal value was 400 psig. At this pressure, the moisture fraction was approximately 0.0011 or less,

depending on the storage temperature.

To reduce the moisture content further, a silica gel dryer was fabricated and incorporated in the supply line leading from the tank to the nozzle. The dryer consisted of a 15-inch section of 8-inch diameter high-pressure steel pipe clamped between two 1/2-inch thick steel plates by means of eight 3/4-inch threaded steel rods. The silica gel was supported internally by stainless steel screens positioned to provide a 1-inch plenum at each end of the dryer.

The dryer was loaded with 20 lbs of 6-16 mesh silica gel. Mass transfer computations indicated that this loading would reduce the moisture concentration in the air to the equilibrium concentration in the silica gel. In practice it is found that the frost point for such conditions will be approximately -60°F . The corresponding Mach number for the nominal conditions of the tests is approximately 1.2.

The rate of moisture accumulation by the silica gel was sufficiently rapid that frequent regeneration was necessary. Accordingly, a drying loop was incorporated in the set-up. Between experimental runs, air from the supply tank was passed first through a heater where its temperature was raised to approximately 330°F and then through the silica gel bed in a direction opposite that of the flow during a test. The heater consisted of a 20 x 1 x 1/2 inch resistance-heating element imbedded in aluminum chips and contained within a section of 2-inch-diameter pipe. The heater operated on

220 volts and dissipated 2 kilowatts. A thermocouple placed at the inlet of the silica gel bed was used to monitor the air temperature. Temperature control was accomplished merely by adjusting the rate of air flow through the heater by means of a hand-operated valve.

A second thermocouple placed at the outlet of the silica-gel bed indicated the exit air temperature and thus, provided an indication of the status of the regeneration. In practice, the outlet temperature climbed to a value of approximately 150°F in a period of 50 minutes, remained at this level for another 50 minutes, then climbed again to a value of 240°F over another 50-minute period, and then remained at 240°F indefinitely. The latter phase served as an indication that regeneration was complete.

Two-Dimensional Nozzles

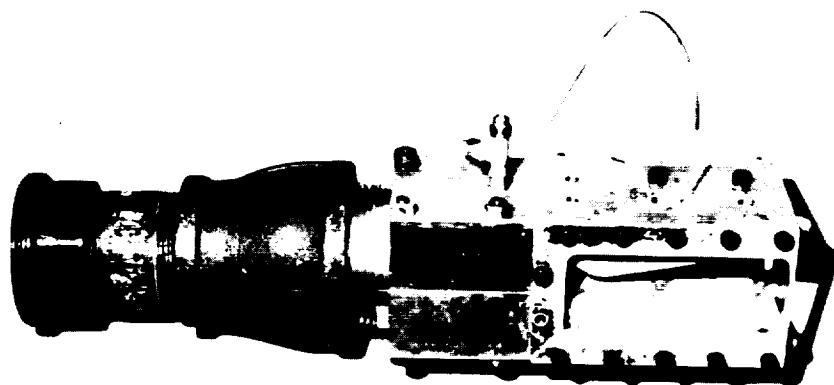
Nozzle fixture.— At the outset of the project the decision was made that an investigation of the flow characteristics in several different two-dimensional nozzles would be desirable. Accordingly, a fixture was designed which would mate with the air supply piping, and which would also accomodate a variety of nozzle blocks of different wall contours in such a manner as to minimize the fabrication expense and the assembly problems associated with a number of different configurations.

The size of the fixture was influenced by the maximum

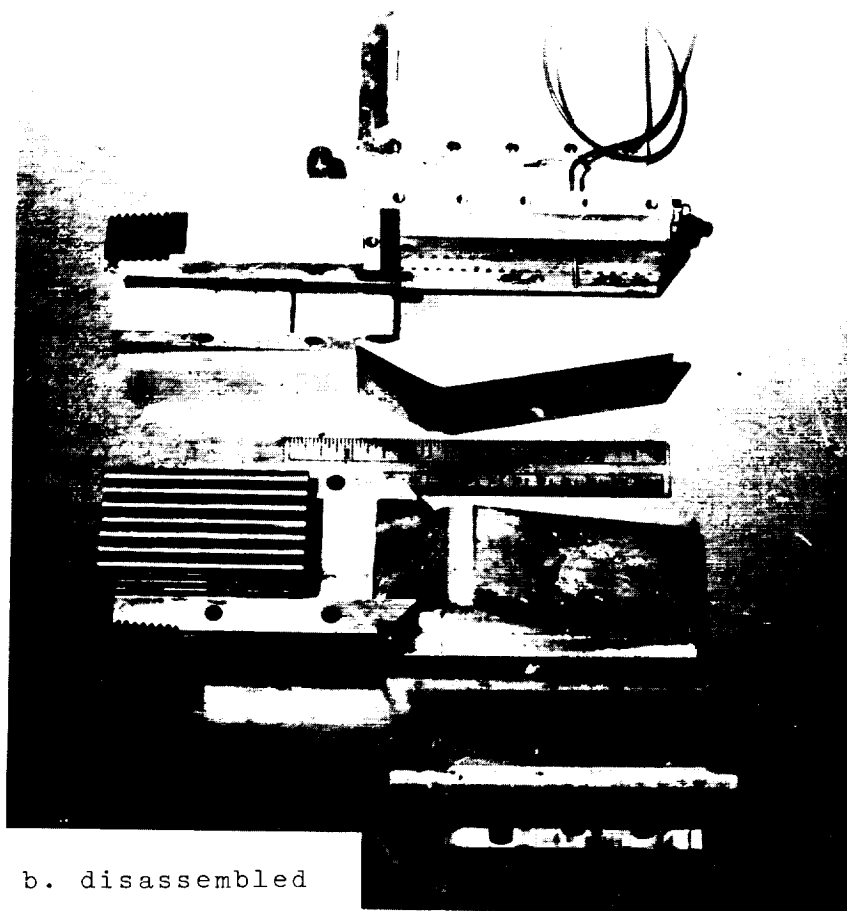
dimensions of the schlieren optics, by the capacity of the air supply, and by the maximum flow which could be accommodated without excessively large pressure drops in the supply line and air dryer - a factor which dictated a nozzle throat area less than approximately 1 square-inch. Another consideration was the desire to make the dimension of the nozzle parallel to the optical axis as large as possible so as to minimize the relative importance of boundary layer effects on the glass walls, provide a closer approach to two dimensionality, and enhance the amount of light refraction by density variations in the test zone.

Figure 8 shows the nozzle fixture which resulted from these considerations. Both the width of the flow region and the maximum expansion width are 1.75 inches. The viewing area is 1.75 x 4.0 inches. Recessed regions 0.375 in. deep were milled around the viewing area on both sides of the fixture to provide seats for transparent windows. The windows were made from "Parallel-o-Plate" glass having a nominal thickness of 3/8 inch. The windows were held in place by two flat cover clamps which were secured to the body by numerous socket-head machine screws. Each side of the fixture contained 40 holes of 1/16 inch diameter. These holes accommodated steel tubes for transmission of wall static pressures. The holes were positioned on 0.2-inch centers in two rows spread 0.2 inch on either side of the mid-plane of the nozzle.

Nozzle blocks were attached to the fixture by means



a. assembled



b. disassembled

Fig. 8. --Two-dimensional nozzle assembly.

of machine screws after first being aligned. After attaching the blocks to the fixture in proper alignment, the 1/16 inch diameter holes in the fixture were extended through the back of the nozzle blocks to within 0.050 inch of the nozzle surface. The blocks were then removed from the fixture and 0.025-inch diameter holes were drilled in the face of the blocks to meet the larger holes.

Wall static pressures were transmitted through 1/16-inch diameter stainless steel tubes inserted through the fixture into the nozzle blocks. The tubes were sealed to the external surface of the fixture with household cement. Leakage between the outside of the tubes and the walls of the holes in the nozzle blocks was eliminated by achieving a tight fit between the tubes and the walls of the holes, and by the use of a grease or plastic sealant between the nozzle blocks and the fixture. A pressure tap for measurement of chamber pressure was incorporated in a straight section of the fixture upstream of the nozzle blocks. This tap consisted of a 0.060-inch-diameter hole connected to a larger hole which was drilled and tapped to accommodate a 1/8-inch pipe fitting.

Immediately upstream of the chamber-pressure fitting, the internal walls of the fixture were milled out slightly to hold a flow straightener. The flow straightener consisted of a cluster of straight aluminum tubes, 3 inches long and 0.25 inches in diameter bundled into a rectangular configuration. The cluster was held together by a thin coating of epoxy

glue between the tubes.

The upper end of the nozzle fixture was threaded to mate with a conventional 2-1/2 to 2 inch pipe reducer which, in turn, was connected to a pipe coupling through a short length of a 2 inch diameter pipe. The fixture, reducer, and half of the coupling comprised a convenient assembly which could be quickly connected to and disconnected from the air supply system.

Two, 2-inch diameter, 30-mesh, stainless-steel screens were installed in the coupling-end of the fixture assembly to serve as a back-up filter to those installed in the ends of the silica gel bed. These screens were supported by a 1/4-inch thick steel disc perforated with small holes.

Nozzle contours.—Figure 9 shows the two-dimensional nozzle contours employed in this study. Table I lists the appropriate dimensions of each of the nozzles. The selection of these shapes was based on the following considerations:

Nozzle D-1 has a contour nearly identical to that of another nozzle with opaque sides which had previously been observed to undergo violent oscillations. Thus, it was expected that Nozzle D-1 would exhibit the same oscillatory behavior. Nozzle D-2 is the same nozzle as D-1 except for the smoothing of the throat contour to eliminate supersonic flow zones which were observed in the throat of D-1. It was also intended that Nozzle D-2 would exhibit the flow characteristics

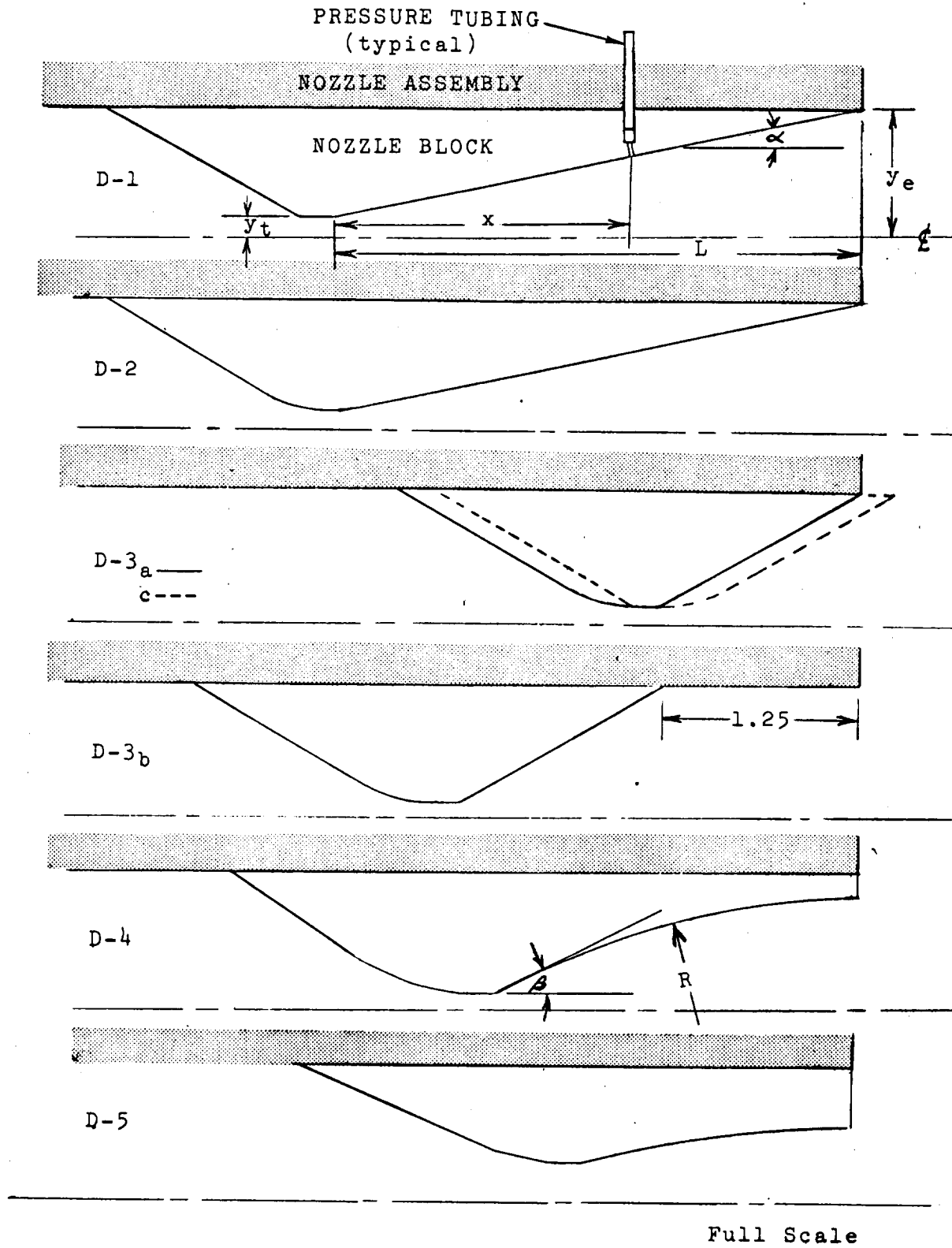


Fig.9. --Two-dimensional nozzle contours

TABLE 1.-- Two-dimensional nozzle parameters;
straight-walled nozzles

	D-2	D-3
α	$\frac{10^\circ}{10^\circ}$	$\frac{30^\circ}{30^\circ}$
L(in)	3.45	1.32
R(in)	-	-
y_e (in)	.795	.870
y_t (in)	.131	.120
A^* (ft ²)	.00322	.00291

Pressure Tap Data

A/A*

D-2		D-3	
top	bottom	top	bottom
1.84 [†]	1.67 [†]	1.21	1.34
1.16 [†]	1.05 [†]	1.43	1.69
1.01	1.23	2.12	2.65
1.12	1.50	2.40	3.23
1.30	1.55	3.15	3.62
1.42	1.89	3.40	4.16
1.58	2.09	4.10	4.58
1.70	-	4.39	5.10
1.85	2.38	5.08	5.55
1.99	2.46	5.35	6.02
2.16	2.65	6.05	6.54
2.27	2.76	6.34	
2.45	2.95		
2.57	3.04		
2.72	3.25		
2.86	3.33		
3.00	3.52		
3.14	3.62		
3.30	3.81		
3.43	3.91		
3.58	4.10		
3.72	4.14		
3.88	4.39		
4.01	4.51		
4.18	4.67		
4.29	4.80		
4.47	4.96		
4.59	5.10		

[†]upstream of throat

TABLE 1. (continued) -- Two-dimensional nozzle
parameters; contoured nozzles

	D-4 28°	D-5 15°
β		
L(in)	2.40	1.81
R(in)	5.0	7.0
y_e (in)	.715	.495
y_t (in)	.102	.250
A^* (ft ²)	.00246	.00625

Pressure Tap Data

A/A*

D-4				D-5			
top		bottom		top		bottom	
x	A/A*	x	A/A*	x	A/A*	x	A/A*
.02	1.12	.10	1.51	.004	1.004	.096	1.096
.09	1.47	.20	1.99	.20	1.20	.17	1.16
.17	1.86	.28	2.39	.30	1.28	.29	1.27
.28	2.39	.40	2.89	.41	1.36	.37	1.34
.38	2.81	.48	3.22	.51	1.44	.50	1.44
.47	3.20	.58	3.60	.60	1.51	.57	1.50
.59	3.65	.69	4.00	.71	1.58	.70	1.57
.66	3.92	.77	4.30	.81	1.64	.77	1.61
.76	4.26	.89	4.66	.90	1.69	.91	1.69
.85	4.55	.99	4.96	1.00	1.74	.97	1.72
.95	4.85	1.08	5.20	1.10	1.77	1.12	1.78
1.06	5.17	1.17	5.43	1.20	1.81	1.17	1.80
1.15	5.41	1.30	5.47	1.29	1.84	1.32	1.84
1.25	5.63	1.38	5.91	1.42	1.87	1.47	1.88
1.34	5.82	1.47	6.08	1.49	1.88	1.52	1.88
1.49	6.10	1.58	6.25	1.59	1.89	1.67	1.90
1.54	6.19	1.67	6.40	1.71	1.90	1.67	1.90
1.69	6.42	1.77	6.52				
1.78	6.48	1.86	6.62				
1.89	6.64	1.95	6.70				
1.94	6.69	2.05	6.77				
2.07	6.78	2.16	6.83				
2.12	6.81	2.56	6.86				

associated with nozzles of relatively small divergence angles. Nozzle D-3 served to exhibit the flow characteristics associated with nozzles of relatively large divergence angles. For Nozzle D-3a the exit edges of the nozzle blocks were aligned flush with the edge of the fixture in the conventional manner. Nozzle D-3b is the same as D-3a except that the blocks were moved forward in the fixture to determine the effects of downstream flow straightening on the separation behavior. Nozzle D-3c was the same as D-3a except that the blocks were reversed to provide a rounded throat exit. Nozzle D-4 was a contoured nozzle with a relatively large initial divergence angle. For reasons which will be discussed more thoroughly later, investigations of the flow in contoured nozzles having a relatively small initial angle in the second instance, were desirable. To eliminate many of the arbitrary variables which would be associated with contoured nozzles, the decision was made to use nozzles having sharp-cornered throats with the straightening contour extending from the throat to the exit. For this type of nozzle, the exit Mach number and area ratio is uniquely determined by the initial divergence angle. Thus, the height of the nozzle throat is governed basically

by the initial divergence angle and by the practical necessity for maintaining nozzle dimensions which will fit within the nozzle fixture and which are satisfactory for optical studies. The initial divergence angle of Nozzle D-4 was 28 degrees. This value corresponds to a theoretical exit area ratio of 5.89 and exit Mach number of 3.35. Nozzle D-5 was the small initial-divergence-angle counterpart of D-4. The initial divergence angle in this instance was 15 degrees and the theoretical exit area ratio and Mach number were 1.89 and 2.13 respectively.

The theoretical profiles for both of the contoured nozzles were computed by the method of characteristics for a sharp-cornered nozzle with the aid of a digital computer. The computations were based on the field method (29). The computer was programmed to determine wall contours, the coordinates of the inter sections of the characteristics and the properties of the flow in each of the fields enclosed by the characteristics. The program and nozzle parameters for nozzles of initial divergence angles ranging from 0 to 30 degrees is presented in Appendix B.

Because of fabrication limitations it was necessary

to approximate the theoretical nozzle profile with the arc of a circle. In the case of Nozzle D-5 the contour was obtained by utilizing a radial saw having a blade of 14 in. diameter. The contour for Nozzle D-4 was obtained by first making a series of cuts on a horizontal milling machine equipped with a 5-inch diameter cutter, and then grinding and lapping the resulting surfaces on a tool of the proper radius (5 inches) which had been machined with a lathe. Although, the resulting contours departed somewhat from the theoretical profiles, the effects of the departure were of little importance to the separation phenomena.

The blocks were made from aluminum and clear acrylic plastic. In each instance with the exceptions of Nozzles D-3b and D-3c the exit edges of the nozzle blocks were positioned so that they were flush with the exit face of the nozzle fixture. Thus, the hole positions in the backs of the various blocks corresponded to that of the fixture as measured from the downstream edge. When short nozzle blocks were employed such as D-3, the holes in the fixture upstream of the blocks were plugged.

In order to minimize the error in pressure measurement, the pressure tap-holes were of small diameter (0.025 in.) and the holes were drilled normal to the nozzle wall. Although accomplishment of the latter sometimes proved to

be a stimulating experience in machine shop practice, hindsight indicates that the refinement probably was not necessary.

The holes were positioned to within 0.003 in. of the desired location by utilizing a milling machine with precise traverse indicators to drill the holes.

Assembly considerations.-Satisfactory alignment and installation of the nozzle blocks and glass windows proved to be rather difficult. The major problems involved the lateral alignment of the nozzle blocks, sealing of the edges of the nozzle blocks against the surfaces of the windows, and breakage of the windows due to clamping stresses. All of these problems resulted from slight variations in dimensional tolerances in the nozzle fixture and the glass blocks.

In this regard, it is probably worthwhile to note that the use of transparent acrylic plastic was tried for the windows after repeated breakage of glass windows in the early stages of the project. The plastic could easily be machined to give a very good fit with the nozzle fixture. However, the plastic proved undesirable because density variations in the plastic (which were probably aggravated by clamping stresses) produced schlieren effects of sufficient magnitude to mask some of the flow phenomena being studied.

Axi-Symmetric Nozzles

General features.-Figure 10 shows the axi-symmetric nozzle arrangement. The complete assembly was comprised of

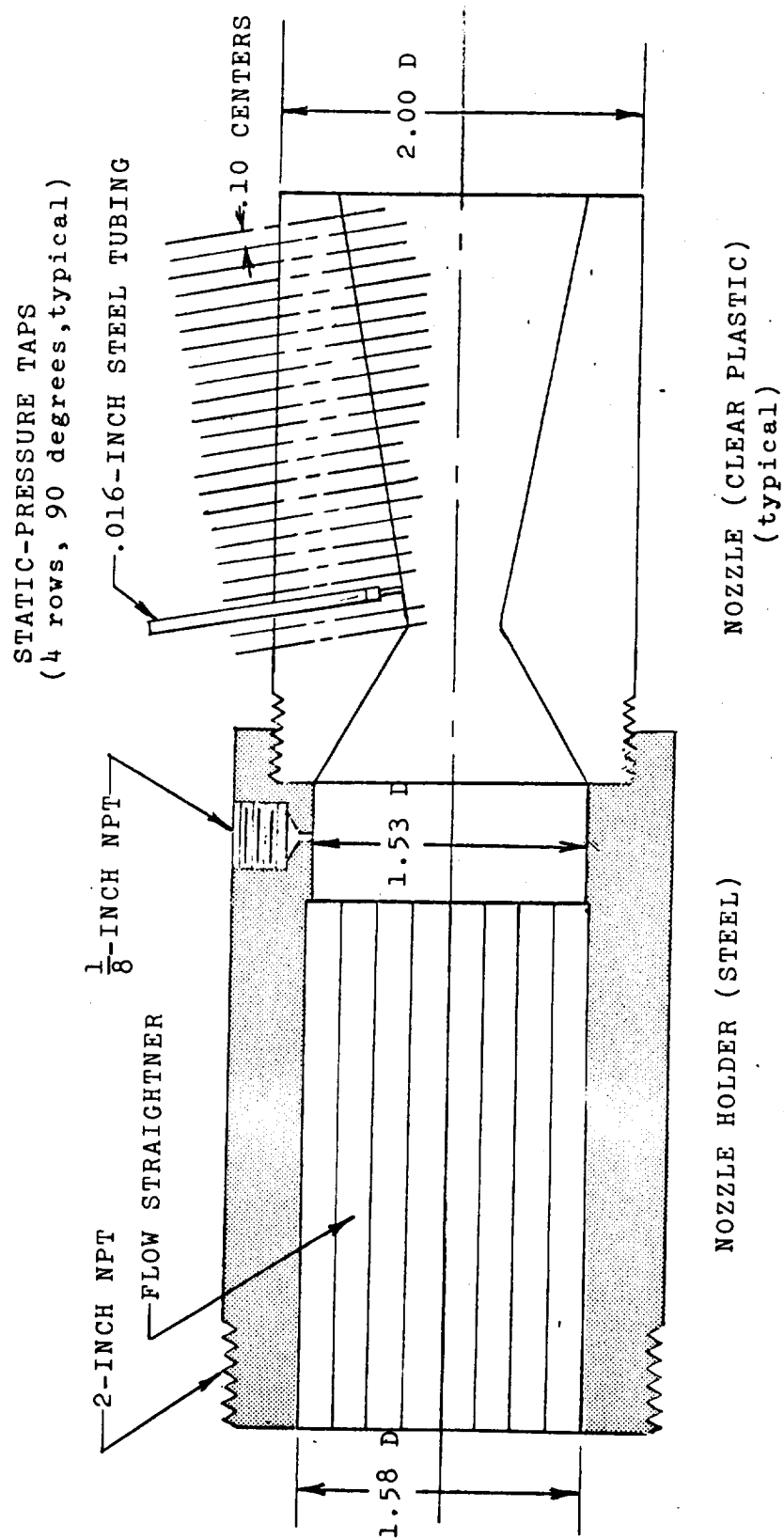


Fig. 10. --Axi-symmetric nozzle assembly

two sections; an "adapter" and a "nozzle." The adapter served as a convenient device for mating with the supply piping, for holding flow straighteners, and for housing a chamber pressure tap.

The nozzles were made from rods of clear acrylic plastic having an external diameter of 2 inches. The nozzles were mated to the adapter by means of a straight, threaded section. Pipe sealing compound was used on the threads to prevent air leakage.

Wall pressure taps were spaced on 0.1 inch centers in one or more rows for each of the nozzles employed. The pressure taps consisted of a relatively long hole of 1/16 inch diameter, which served to hold a short length of 1/16 inch diameter steel tubing which, in turn, provided a means for connecting plastic tubing leading to the pressure instrumentation. The hole penetrating the nozzle wall was .025 inches in diameter. For the nozzles with straight walls, the pressure taps were normal to the flow surface. However, for the contoured nozzles, the taps were normal to the cylindrical surface forming the exterior wall of the nozzle.

Axi-symmetric-nozzle contours.-Figure 11 shows the axi-symmetric-nozzle contours which were used and Table 2 lists the nozzle parameters.

Nozzle A-2 was the one used by Moore in his study (19). This nozzle was built in one piece and was made of aluminum, but the internal arrangement was the same as that

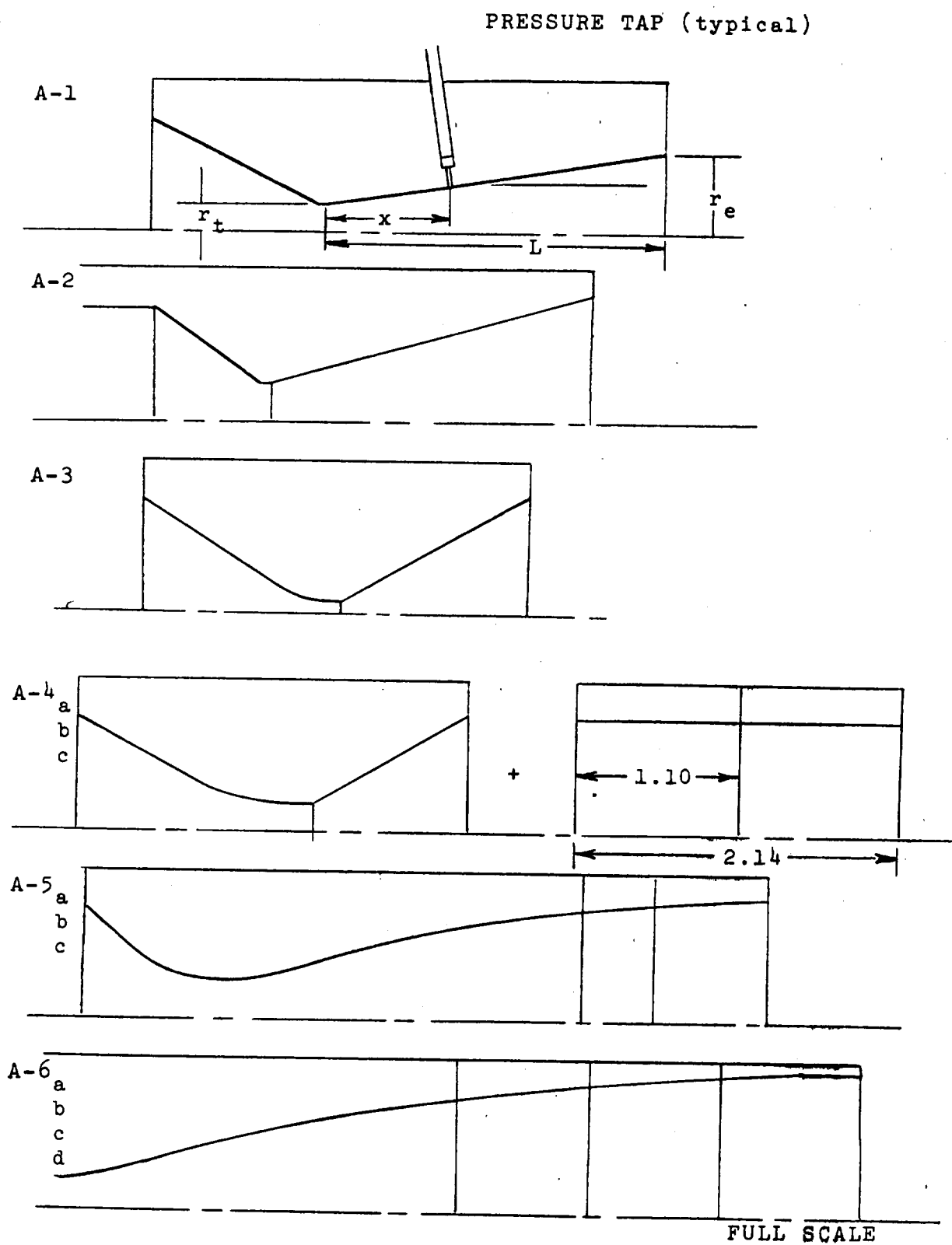


Fig.11. -- Axi-symmetric nozzle contours

TABLE 2. -- Axi-symmetric nozzle parameters

	A-1	A-2	A-3	A-4	A-5	A-6
L(in)	2.22	1.64	1.22	1.04	several	see below
r _e (in)	.548	.678	.800	.800	several	see below
r _t (in)	.204	.251	.094	.195	.261	.200
A* (ft ²)	.0009	.00035	.0002	.0008	.0015	.00088

Pressure Tap Data							
A-1	A-2	A-3	A-4	A-5		A-6	
<u>A/A*</u>	<u>A/A*</u>	<u>A/A*</u>	<u>A/A*</u>	<u>x</u>	<u>A/A*</u>	<u>x</u>	<u>A/A*</u>
1.03	1.24	1.25	1.10	.15	1.04	.2	1.10
1.30	1.74	2.70	1.69	.25	1.10	.3	1.22
1.48	2.32	4.71	2.42	.35	1.20	.4	1.43
1.66	3.00	7.27	3.27	.45	1.35	.5	1.73
1.88	3.75	10.39	4.25	.55	1.53	.6	2.10
2.08	4.59	14.07	5.36	.65	1.78	.7	2.60
2.30	5.33	18.30	6.60	.75	2.10	.8	3.10
2.54	6.54	23.08	7.96	.85	2.42	.9	3.65
2.78	7.00	28.42	9.50	.95	2.75	1.0	4.25
3.04		34.32	11.08	1.05	3.10	1.1	4.82
3.33	x4	40.97	12.83	1.15	3.42	1.2	5.45
3.59		47.77		1.25	3.80	1.3	6.10
3.88		55.34	x4	1.35	4.10	1.4	6.70
4.19				1.45	4.49	1.5	7.36
4.50		x4		1.55	4.80	1.6	7.98
4.83				1.65	5.15	1.7	8.61
5.17				1.75	5.49	1.8	9.22
5.51				1.85	5.80	1.9	9.88
5.87				1.95	6.10	2.0	10.48
6.25				2.15	6.70	2.1	11.10
				2.32	7.30	2.2	11.74
x4*				2.55	7.85	2.3	12.31
				2.65	8.10	2.4	12.84
				2.85	8.55	2.6	13.27
				3.05	8.95	2.8	15.08
*number of rows of pressure taps				3.25	9.32	3.0	16.09
				3.45	9.60	3.4	17.82
				3.65	9.90	3.8	19.56
--nozzle cut-off locations						4.2	20.74
					x2	5.3	23.10

x1

illustrated in Figure 10.

As is indicated in Figure 11, Nozzle A-3 was equipped with extensions and the contoured nozzles were successively cut off from a "long" configuration to a relatively "short" geometry. This was done to investigate a hypothesis of the author that the major reason for the anomalous behavior of the contoured nozzles, such as that reported in Reference 26, was due to entrainment of air in the "dead air" space surrounding the jet; and that the characteristics of the entrainment were dependent on the length and contour of the nozzle.

Contoured nozzles.-As a basis for selecting shapes of the contoured nozzles, it was desired that the flow be turned to within a few degrees of axial in the "long" configuration and that the relationship between area ratio and length be such that separation could be made to occur over a significant range of distances downstream from the throat with the chamber pressures which were available. Local contour angles of at least 15 degrees in the initial expansion region were also desired. This latter requirement conflicted with the first two, so the resulting profiles represented somewhat of a compromise.

Non-dimensional profiles were taken from a report by Chow (30) and scaled to fit the existing needs. In the case of the Mach 4 nozzle, the radial dimensions were increased

by the amount: $\delta^* = 0.004 \frac{x}{r_t}$, where x is the distance downstream from the throat and r_t is the radius of the throat, to compensate for the boundary layer displacement thickness.

The contoured nozzles, besides being different because of the contour itself, were also different in the respect that the contour was continuous in the throat region, whereas the throats of the conical nozzles had sharp corners.

The conical nozzles were machined on a lathe in a straightforward manner. The contoured nozzles were fabricated as follows: A template of the wall contour was made from 1/8-inch-thick sheet of acrylic plastic. The contour was transferred to the plastic by installing the point of a scribe in the arbor of a vertical milling machine, attaching the plastic to the bed of the machine, and indexing the bed underneath the scribe to various positions of the theoretical contours. At each position, a small mark was made on the plastic by making contact with the scribe. A smooth curve was then drawn between the marks. The resulting contour was cut out and ground to shape by moving the plastic past a small rotary grinder by hand. The template contour which resulted was estimated to be within ± 0.010 inch of the desired value.

The template was properly aligned and fastened to the bed of a lathe and a dial indicator affixed to the tool rest. The nozzle contour was then obtained by moving the

tool with the longitudinal and cross-feeds of the lathe in such a manner as to maintain a constant reading on the dial indicator. Except for one rather drastic mistake, the template contour was easily followed to within ± 0.001 inch.

Pressure Instrumentation

Time-integrated-average pressure measurements.-

Measurements of the time-integrated-average static pressures along the nozzle walls were made with two multi-tube manometer boards. The manometer fluid was mercury. Each of the manometers had an active length of 50 inches. One board contained 30 manometers connected to a common reservoir. The other board consisted of two sections of 15 manometers, with each section connected to a common reservoir. One manometer in each section was referenced to atmospheric pressure. Thus, a total of 57 pressure readings could be obtained simultaneously.

The manometers were connected to the pressure taps in the nozzle wall by 8-foot lengths of flexible plastic tubing having a nominal inside diameter of 0.050 inch.

Nozzle chamber pressures were measured with two Bourdon pressure gages. One gage covered a range from 0 to 60 psig and the second gage covered the range of 0 to 500 psig. A hand valve placed in the line to the low pressure gage permitted isolation of this gage during high pressure runs.

Both gages were mounted on the manometer boards.

The method of recording pressure data was simply to photograph the manometers and the pressure gages with a 35mm camera. Each of the manometer boards was backed by a grid of horizontal lines spaced 0.2-inches apart which was back-lighted with fluorescent lamps. The pressure gages were illuminated from the front by a high-intensity lamp.

A film reader was utilized to determine the manometer and pressure gage readings. With this technique, the manometers could be read to within ± 0.05 inch, the low-pressure gage to within ± 0.2 psi, and the high-pressure gage to ± 1 psi. The errors caused by these and other uncertainties will be discussed later.

Transient-pressure measurements.—Pressure fluctuations were measured with a bank of 20 strain-gage pressure transducers. The outputs of these transducers were recorded by a 20-channel optical recording oscillograph. Each transducer was connected to its respective pressure tap in the nozzle wall by a length of 0.050-inch diameter plastic tubing which was usually shorter than 12 inches. These connections were made in parallel to the manometer connections.

The pressure transducers operated off of 6 volt d.c. and produced an output of approximately 2 millivolts per psi-differential. The transducers, associated resistors for matching the impedance of the transducers to the oscillograph galvanometers, and potentiometers for voltage balance were mounted in a metal box.

The natural frequency of the galvanometers was 40 Hz. The response to pressure oscillations at frequencies greater than this value dropped off rapidly. Therefore, to provide assurance that the transient measurements made with the oscillograph were valid, measurements were also occasionally made with a single transducer connected to an oscilloscope.

Figure 12 shows a schematic of the d.c. amplifier (31) which was assembled to boost the voltage signal from the transducer to a level sufficient to drive the oscilloscope. The amplifier had a voltage gain of 100 and a flat frequency response from d.c. to 1 MHz.

Accuracy of pressure data.—The pressure gages were calibrated with a dead-weight tester. The accuracies of these calibrations are estimated to be within ± 0.2 psi and ± 1 psi for the low and high-pressure gages, respectively. By determining the uncertainties from:

$$\Delta y = \left[\sum_i \left(\frac{\partial y}{\partial x_i} \right)^2 \Delta x_i^2 \right]^{\frac{1}{2}}$$

where:

Δy = uncertainty in dependent variable, y

Δx_i = uncertainties in independent variables, x_i ;

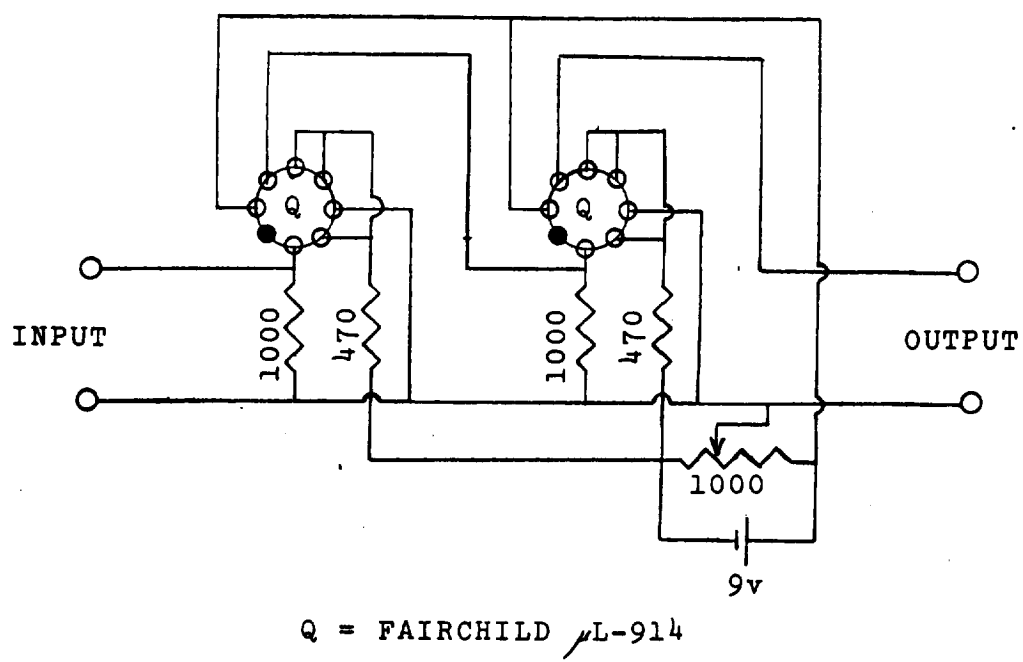


Fig.12. -- D.C. Amplifier

the following errors for the major variables of concern are determined:

$$p_s/p_a \approx 0.5\%$$

$$p_s/p_c \approx 1\% \text{ @ } p_c = 30 \text{ psia}$$

$$\approx 2\% \text{ @ } p_c = 75 \text{ psia}$$

The error in the variable, p_s/p_c , decreases as either of the two values for p_c given above is increased.

Optical Instrumentation

Figure 13 shows several variations of the schlieren and shadowgraph optical arrangements which were employed during the course of the study. Still photographs were taken with a 35mm Minolta SR-1, single-lens-reflex camera. Motion pictures at rates up to 6000 pictures per second (pps) were taken with a Red Lakes, Model K2001 16mm high-speed motion picture camera.

The light source for most of the photographic work was a No. 1141, 12-volt automobile light bulb which had a straight filament approximately 0.020-inch wide and 0.30 inches long. The bulb was connected to a d.c. power supply. The light intensity was regulated by means of a variac which controlled the input voltage to the power supply. The dimensions of the filament were such that the bulb could be used directly as a light source for schlieren work without the necessity of a condensing lens and aperture. The light output was sufficient that adequate exposure could be

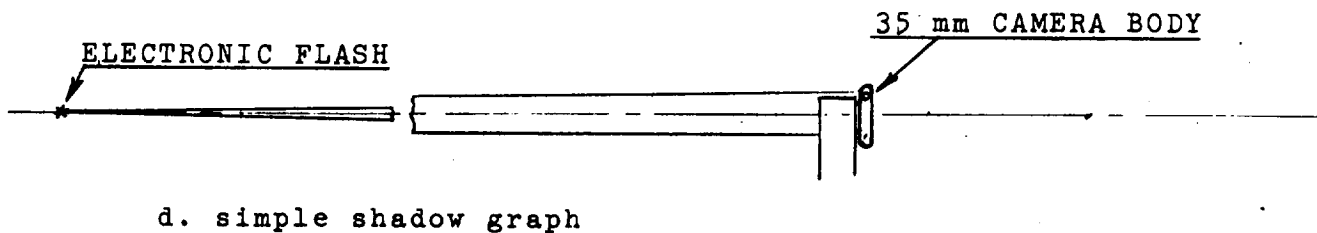
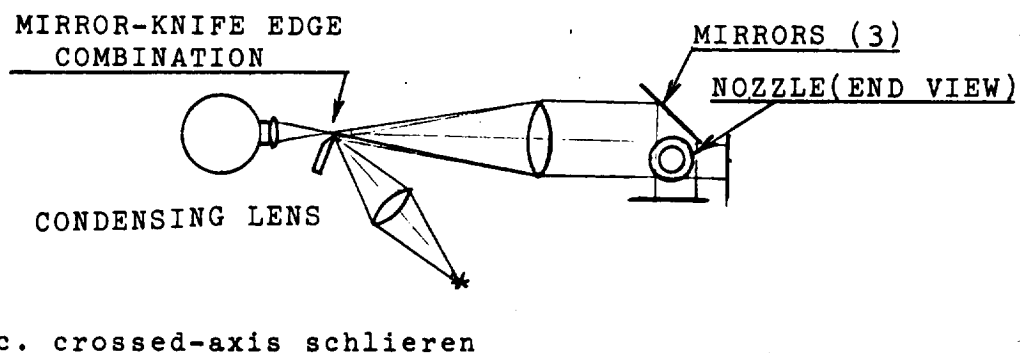
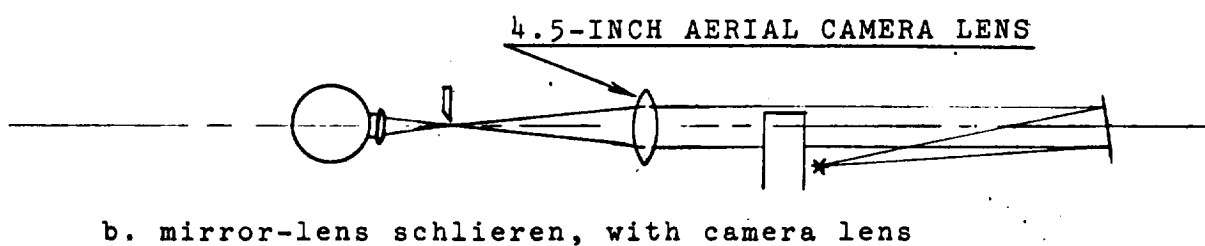
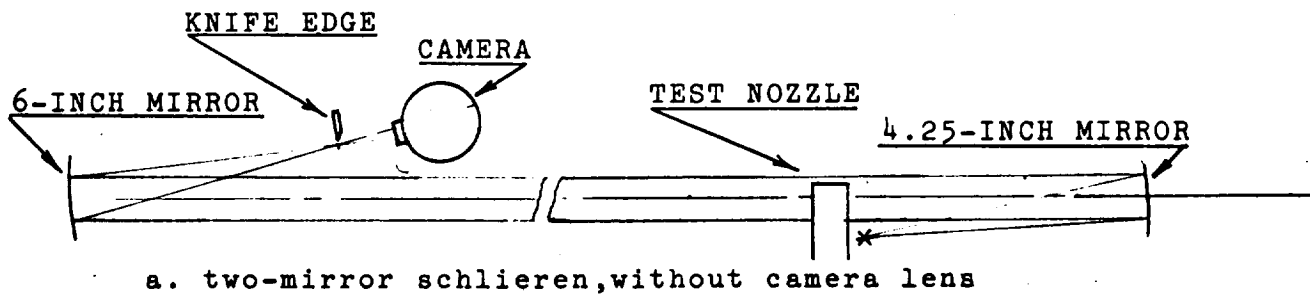


Fig.13. -- Flow visualization arrangements

obtained at picture-taking rates up to 6000 pps with the 16mm motion picture camera on Eastman Kodak Tri-X Reversal film (ASA 160); and at shutter speeds of 1/250 second with the 35mm camera on Eastman Kodak Panatomic-X film (ASA 32).

An alternating-current, mercury-vapor lamp was also used for some of the work. Filters were employed to obtain a light output which was, essentially, monochromatic. However, photographs made with this light source were not noticeably better than those obtained with the incandescent bulb. Also, objectional a.c. flicker was encountered in the motion pictures.

A few photographs were made with a simple shadow-graph arrangement as indicated in Figure 13d. For these photographs a Minneapolis Honeywell, Model 660 "Autostrobnar" electronic flash gun was used. This unit produced a light flash of approximately 20 micro-seconds duration. In order to approximate a point source, a mask with a 1/2-inch diameter aperture was placed over the face of the unit and the unit was positioned as far from the test section as possible, consistent with adequate exposure.

As indicated in Figure 13, several optical arrangements were used. Figure 13a shows the configuration employed during the early stages of the project. In this arrangement, two front-surface mirrors of 45-inch focal length were

used. Both of the mirrors were intended for use in small telescopes. The surface of the collimating mirror was spherical and the mirror had a diameter of 4.25 inches. The surface of the refocusing mirror was parabolic and the diameter was 6 inches.

The refocusing mirror also served to focus the image of the test section on the film. This arrangement, while being advantageous in that distortions due to intervening optics were eliminated, had the following disadvantages:

- 1) It was necessary to position the refocusing mirror and camera at a considerable distance from the test section in order to achieve the proper image size - this situation resulted in operational problems.
- 2) Scattered light could enter the camera - therefore, operation at night was required to avoid fogging of the film.
- 3) Positioning of the camera to obtain a sharp focus was very touchy, particularly with the movie camera.
- 4) Two different positions for the refocusing mirror were required to achieve the proper image size for both the 16mm and 35mm photographs. Thus, the system had to be frequently realigned.

Figure 13b shows the arrangement employed for most of the work. This system utilized an $f/8$, 36-inch focal length, aerial-camera lens for refocusing the light beam. With a lens used for this purpose instead of a mirror, it was possible to move the refocusing lens close to the test section and photograph the resulting virtual image with the camera lens placed immediately behind the knife edge. Such an arrangement was not practical when a mirror was used for refocusing because the optics would have had to be arranged so that the nozzle exhaust would have traversed the refocusing beam.

A satisfactory image size for the 35mm photographs was obtained by adapting a 7-inch focal length "Aero Ektar" lens to mate with the 35mm camera body. Similar results were obtained by adapting a lens of 2-inch focal length to fit the motion-picture camera. With the arrangement of Figure 13b, all of the disadvantages mentioned in the previous photograph were eliminated. However, the schlieren sensitivity was decreased slightly from that of Figure 13a.

One aspect of the study was to determine the deflection of exhaust streams resulting from unsymmetrical separation in axi-symmetric nozzles. The arrangement shown in Figure 13c was used for this purpose. An image of the filament of the 12-volt light bulb was focused first on the edge of a small steel mirror which was positioned so that the image was at the focal point of the 36-inch-focal-length

aerial camera lens. Mirrors, arranged as shown in Figure 13c, split the parallel light into two beams which crossed the axis of the nozzle at right angles to each other and which were then reflected back through the lens which refocused the two beams in the vicinity of the primary image of the filament on the small steel mirror. With the system properly aligned, the two refocused images could be brought into superposition just on the edge of the steel mirror, which then served as a single knife edge for the schlieren effect for both beams.

The system shown in Figure 13d was a simple shadow-graph arrangement. In this instance the body of the 35mm camera without the lens served as a film holder and was placed immediately behind the test section. The electronic flash unit mentioned previously was placed on the optical axis of the nozzle at a distance of approximately 40 ft.

Data Processing

A typical test comprised approximately 1000 data points. A computer program was written to process the resulting copious data. Manometer readings, in inches of mercury, and chamber-pressure readings, in psig, were key-punched directly as they were read from the film reader. The computer program corrected the manometer readings for parallax incurred at the camera position, converted the readings to psia, and for each pressure-tap position; computed the ratio of wall static pressure to chamber total

pressure (p/p_o), length and diameter Reynolds numbers, and momentum flux. Graphs of the ratio of wall static pressure to atmospheric pressure (p/p_a) as a function of area ratio (A/A^*) were also plotted automatically by a digital plotter.

IV. EXPERIMENTAL RESULTS: TWO-DIMENSIONAL NOZZLES

10-Degree Nozzle (D-2)

Flow patterns and pressure distributions: Figure 14 shows the various types of characteristic flow patterns observed in the 10-degree, two-dimensional nozzle. These flow patterns are believed to be representative of the general types of flow in nozzles with relatively narrow divergence angles.* Figure 15 shows wall static pressures for the nozzle. Five types of flow patterns can be identified:

- (1) Type 1. Flow at low chamber pressures char-
acterized by indistinct shock patterns: As a rule, this behavior (Figure 14a) occurred over a range of chamber pressures extending from a value of approximately 50-60 psia. Over this pressure range, the flow exhibited a roughness in tonal quality as if the sound were comprised of a mixture of frequencies of various amplitudes. Probing the flow with a total-pressure probe, threads and cotton tufts indicated that exhaust stream filled only about 75 per cent of

*In many of the photographs which follow, the pressure gage can be seen. The pressure readings are in psig, but the pressures quoted in the text are in psia.

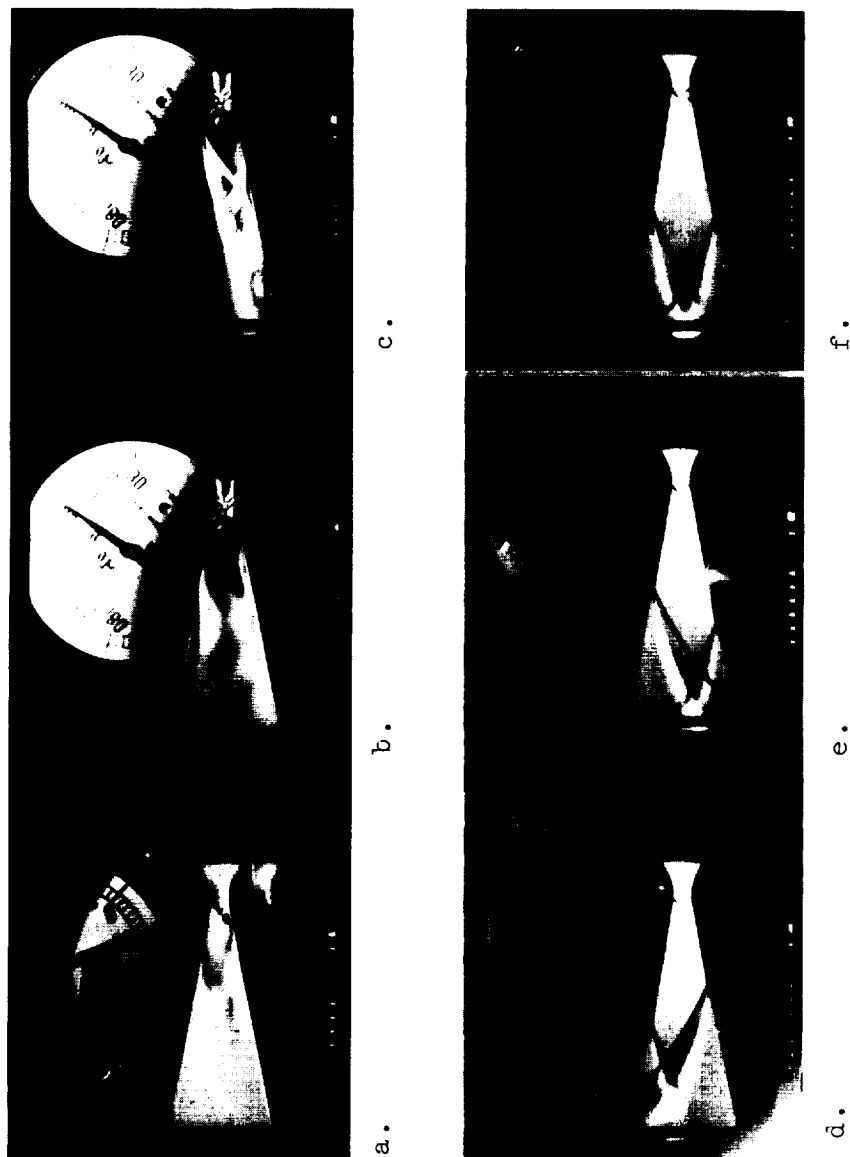


Fig. 14. --Flow patterns; 10-degree,
two-dimensional nozzle.

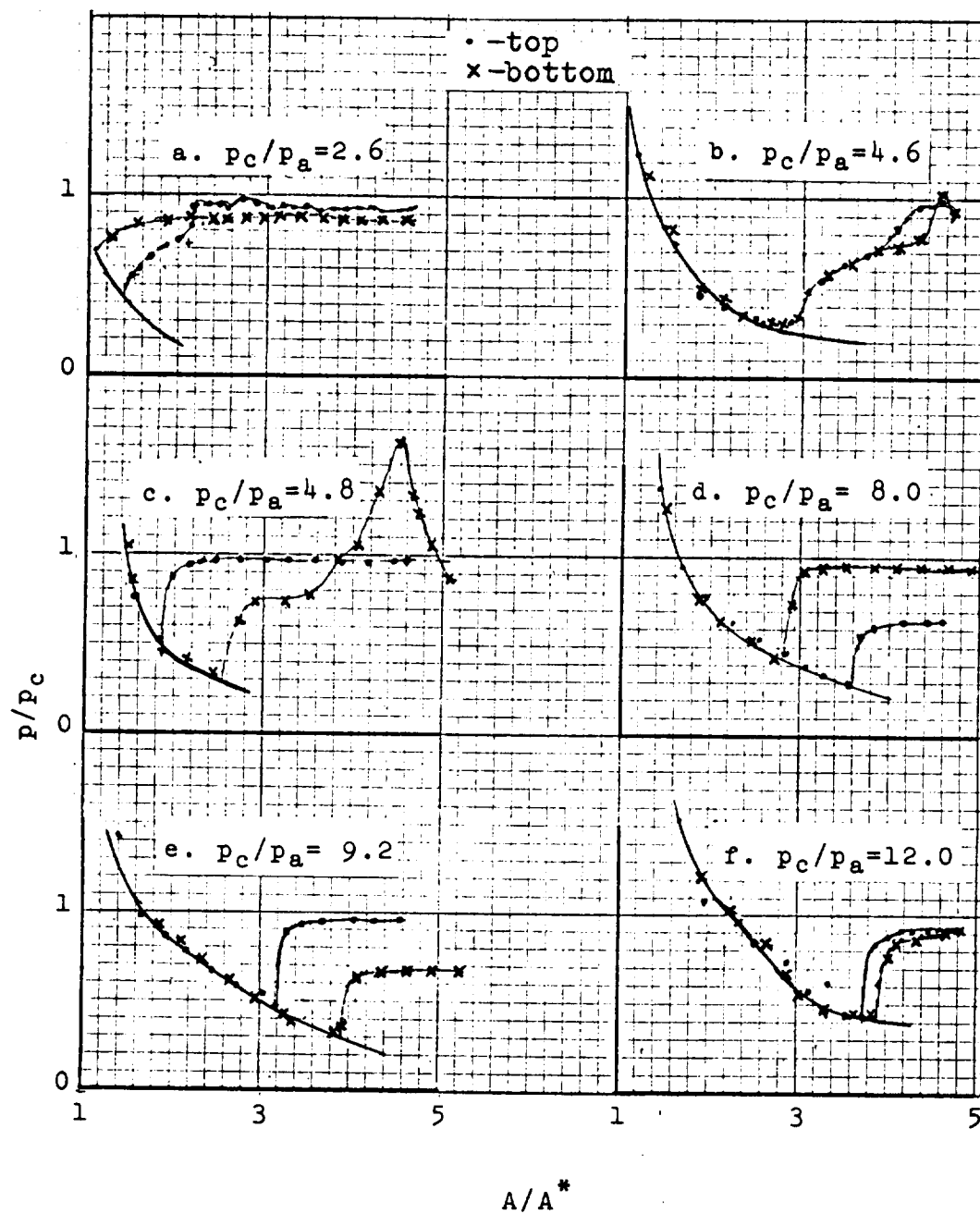


Fig. 15. --Typical wall static-pressures for 10-degree, two-dimensional nozzle.

the nozzle at the exit. A pronounced suction, or region of reverse flow, existed along one edge of the nozzle. As the chamber pressure was raised toward the upper limit of the range, the shock patterns became distinct in the manner indicated in Figure 14c. Figure 15a shows the static pressure distributions along the nozzle walls corresponding to this type of flow. The solid curve is the experimentally-determined full-flow pressure distribution for the nozzle.

- (2) Type 2. Flow at low chamber pressure characterized by symmetrical shock pattern: Figure 14b shows a second type of flow pattern which also occurred at low pressures. When this type of flow occurred, it would prevail until a chamber pressure of approximately 75 psia was reached, and then suddenly switch to the pattern of Figure 14c. For this type of flow, the exhaust invariably attached to one of the glass walls.

Figure 15b shows a pressure profile which is characteristic for this type of flow. The particular profile shown is for a chamber pressure just below the value at which the flow switched.

- (3) Type 3. Flow attached to one wall. When the chamber pressure reached the limiting value

for Type-2 flow, the flow became attached to one of the diverging walls of the nozzle and remained attached until a chamber pressure of 135 psia was reached. Figure 14c shows the flow pattern. Throughout this flow regime the shock pattern was quite distinct. If Type 1 flow prevailed over the low range of chamber pressures, the transition to Type 3 flow was gradual; the main differences between the two types of flow being the difference in clarity of the shock pattern and a rougher sound associated with Type-1 flow.

Figure 15c shows a characteristic pressure distribution associated with Type-3 flow. The particular distribution shown is for a chamber pressure just above the value necessary to switch from Type 1. A comparison of Figures 15b and 15c reveals that the point of initial separation moves upstream, and that the pressure rise downstream of separation is much more rapid, after the flow switches to attach to the wall. Indeed, the Type-2 pressure profile seems to indicate behavior rather like a normal shock. However, the point where the pressure starts to increase in Figure 15b is appreciably upstream of where a normal shock would theoretically occur. Also,

Figure 14b indicates that the separation shock is oblique, but becomes normal in the center of the stream. This point will be discussed in greater detail in Chapter VI. Also worthy of mention, is the fact that once the flow had switched from Type 2 to Type 3, the chamber pressure could be reduced and the flow behavior would become that of Type 1.

Type-3 flow is of special interest because the angle of the thrust vector is the maximum possible -- namely; the divergence angle of the nozzle. A significant parameter is the maximum value of the momentum flux which could be turned through this angle. This value was approximately 75 pounds-force; a value which was determined by computing the product $\dot{w}\bar{u}_\infty$, where \dot{w} , is the mass flow rate and \bar{u}_∞ , is the local jet velocity in the region where the flow is initially deflected.

- (4) Type 4. Flow deflected off axis but not attached: This type of flow occurred over the limited range of chamber pressures extending from approximately 135 to 155 psia for Nozzle D-2. The flow pattern is shown in Figure 14e and the pressure distribution in Figure 15e. An unusual characteristic of the flow which would

sometimes occur, was a switching of the jet from the "top" wall of the nozzle to the "bottom" wall at a chamber pressure of approximately 120 psia. At lower pressures, the jet would attach to either of the two diverging walls with about equal probability. But switching would occur only if the jet was first attached to a particular wall which happened to be the upper wall of the nozzle. Figures 14d and 14e show the flow pattern before and after switching and Figures 15d and 15e show the pressure profiles.

The switching appears to be associated with a low-pressure pocket in the recirculation region which is just downstream of the separation point, (Figure 14d). The flow switches when the downstream edge of this pocket just reaches the edge of the nozzle block to which it is adjacent.

In the case where the flow switched, it is believed that slight asymmetries in geometry existed which permitted the formation of a confined separation pocket adjacent to the opposite wall. When the chamber pressure was raised to such a value that the

confined pocket could no longer exist because of the presence of the exit edge of the nozzle, the downstream pressure on both sides of the jet tended to become equal and the jet straightened out.

- (5) Type 5. Symmetrical flow pattern: For chamber pressures greater than approximately 150 psia, the jet became symmetrical with respect to the axis of the nozzle. The flow pattern and pressure profiles are shown in Figures 14f and 15f respectively.

One of the characteristics of the flow in the 10-degree nozzles was that the flow could easily be switched from one wall to the other by introducing an obstruction either into or across the suction side of the exhaust. However, the flow was extremely resistant to attempts to change the behavior by placing an obstruction across the exhaust stream in such a manner as to back-load the system. This behavior, the switching behavior at high pressures, and other indications which will be made apparent later in this report, provide evidence that the pressure immediately downstream of the separation shock is very important to the behavior of separated flows.

Unsteady Flow Behavior: Figure 16 is a reproduction of several sections of an oscillograph record showing

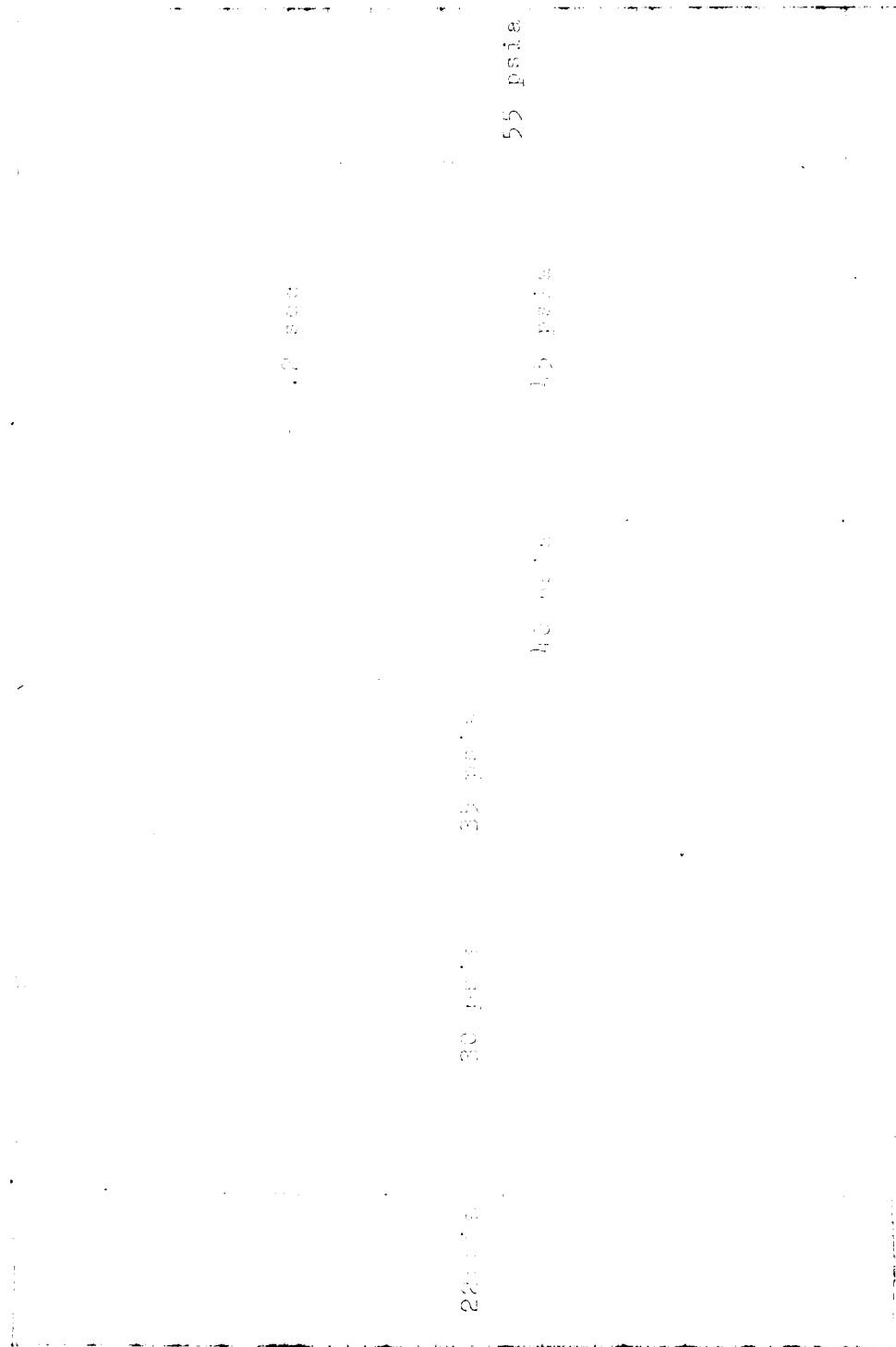


Fig.16. --Pressure fluctuations in 10-degree, two-dimensional nozzle

pressure fluctuations in the 10-degree, two-dimensional nozzle. The general alignment of the record is such that the top traces represent static pressures along one side, and the bottom traces represent pressures along the other side of the nozzle. The distances of the pressure taps from the nozzle throat represented by the traces increase from top to bottom within each of the two groups of traces. Most of the pressure taps were located downstream of the point of separation for chamber pressures less than 35 psia. At higher pressures, the positions of separation moved downstream of some of the pressure taps. The oscillograph records reveal that fluctuations no longer occur when the separation moves downstream of the pressure tap. Thus, the conclusion is reached that fluctuations in upstream pressure are not the cause of the flow disturbance. Table 3 provides a summary of information determined from the oscillograph record.

One notes that the general behavior agrees with that observed photographically in the respect that smooth flow occurs above 60 psia. The transient measurements for a chamber pressure of 30 psia reveal that the pressure fluctuations on opposite sides of the nozzle occur in opposite sense; thereby indicating that the flow was switching from one side of the nozzle to the other. The switching action occurred only over a very narrow range of

TABLE 3.-- Results of transient pressure
measurements; Nozzle D-2

p_c (psia)	General Behavior	Approximate Frequency of Disturbance (Sec ⁻¹)	Amplitude Disturbance (psia)
< 25	smooth	-	-
30	flow switch- ing from side to side	~ 30	0.8-1.0
35-40	very slight fluctuations	~ 40	0.2
40-45	modest fluctuations	~ 28-35	0.6-0.8
50	slight fluctuations	~ 28	0.4
> 60	smooth	-	-

chamber pressures. For example, at pressures of 25 and 35 psia - chamber pressures which bracketed the pressure at which switching occurred - the flow was relatively quiescent. It should be noted that switching was not observed for many of the tests. Fluctuations occurring at chamber pressures other than the switching pressure appear to be in phase, thereby indicating that the disturbance is symmetrical.

High-speed motion pictures of the flow with chamber pressures less than approximately 35 psia revealed that the positions of separation moved rapidly back and forth over a distance which was nominally about 0.1 inch, but frequently was as great as 0.2 inch. The movement of the oblique shock waves associated with separation was particularly apparent. These fluctuations occurred with a frequency of approximately 600 oscillations per second. The fluctuations appeared to be either the result of - or the cause of - severe disturbances in the main body of the jet. Figure 17 shows a sketch of the flow situation.

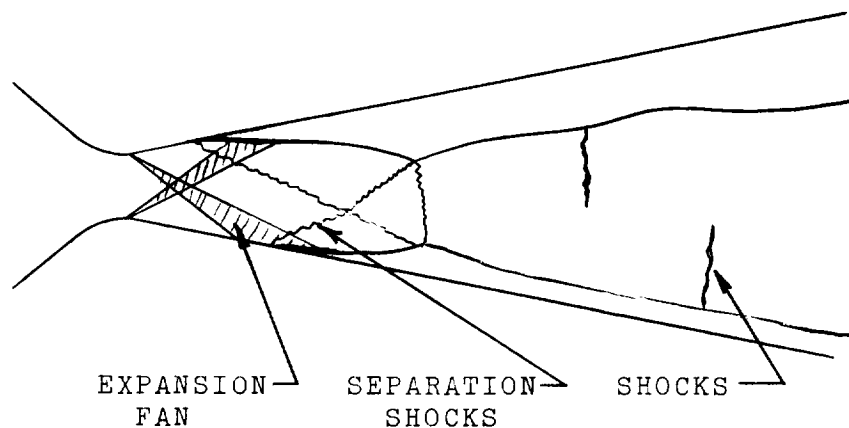


Fig. 17 --Oscillating-flow configuration

The jet is inclined toward one wall, but is not attached. Normal shocks are formed in the region where the oblique separation shocks intersect the opposite boundary of the supersonic stream. It is at this location that much of the flow disturbance seems to originate. The photographs show severe fluctuations in the strength and texture of the normal shocks, and these disturbances, in turn, appear to effect the entire flow structure downstream. At times, the edge of the downstream flow nearest the center of the nozzle appears to jump toward the opposite wall.

This action occurs with such speed that the motion is difficult to follow even with picture-taking rates of 6000 pps.

Instabilities of the type described above, occur when the point of separation lies inside the expansion fan originating at the corners of the throat. As the chamber pressure is raised, the point of separation emerges from the fan on one side of the nozzle. The magnitude of the disturbance then diminishes somewhat. A further increase in pressure causes the point of separation on the opposite side to emerge from the fan, and when this occurs, the flow becomes much more stable. This condition occurred at a chamber pressure of approximately 55 psia.

For pressures greater than 55 psia, the oblique shocks still fluctuated at the same frequency (~ 600 oscillations per second). However, the amplitudes of the fluctuations were smaller and there was no significant disturbance of the flow behavior.

30-Degree Nozzle (D-3a)

Flow patterns and pressure distributions: Figure 18 shows typical flow patterns in the 30° -two dimensional nozzle. The dial in the upper right of each photograph indicates the chamber-pressure in psig. These photographs are believed to be indicative of the types of flow structure occurring in nozzles of relatively wide

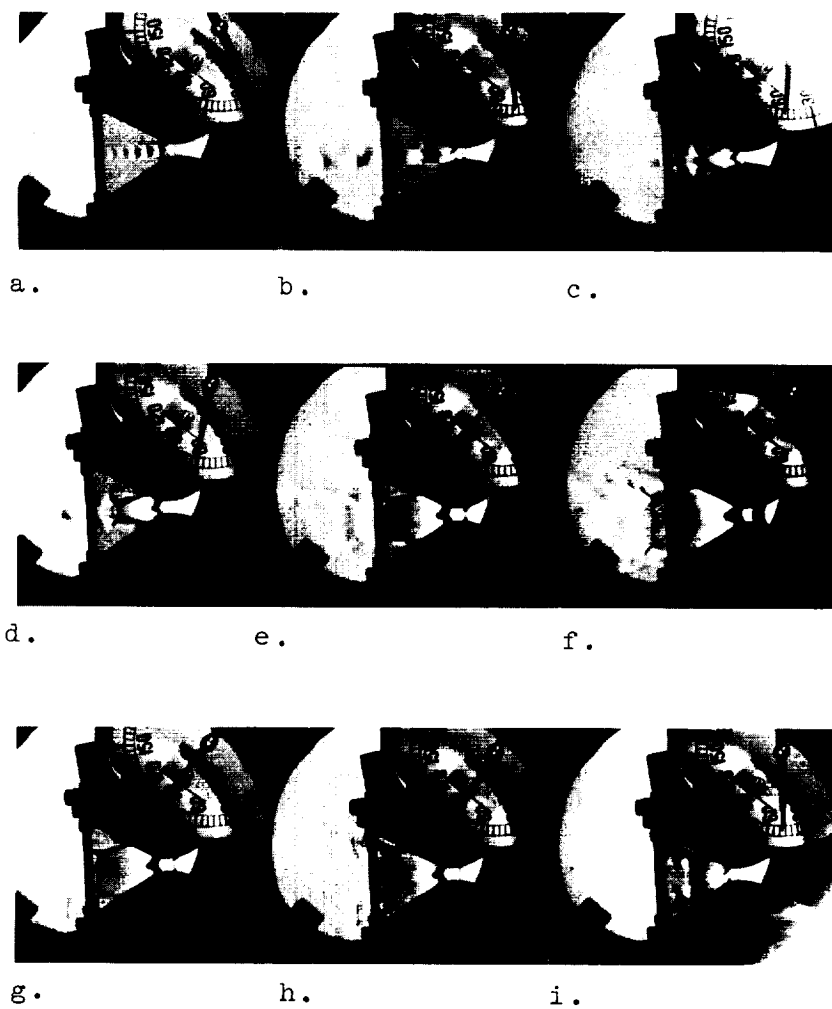


Fig. 18. --Flow patterns; 30-degree,
two-dimensional nozzle.

divergence angle.

For chamber pressures in the range of 0-55 psia (Figure 18a), the flow adjusts to the back pressure through a series of oblique shocks and expansion waves commencing at the sharp corner exit of the throat. There is no apparent attachment of the flow to the walls of the nozzle. As the chamber pressure is raised above this value, the flow separates from the walls with accompanying oblique shocks. Actually, the shock patterns are three-dimensional, and the flow separates from the glass walls as well as from the diverging walls. This effect is indicated by the lighter shading of the photographs upstream of the origin of the separation shocks.

One notes that the two oblique shocks suddenly coalesce to a normal shock. This behavior which is peculiar to the nozzles of wide divergence angle, seems to cause the flow to separate into two supersonic streams separated by a central, subsonic core as indicated in Figure 18e.

A comparison of Figure 18c with 18i and 18d with 18h shows a hysteresis effect in the separation behavior. The photographs in Figures 18c and 18d were made as the chamber pressure was increased; the photographs of 18h and 18i were made as the pressure was decreased. One notes that even though the chamber pressures are lower

in the latter two photographs, the point of separation is appreciably downstream of where it occurred when the pressure was being raised. This type of behavior did not always occur. However, the fact that it did occur seems to indicate that wall effects downstream of separation can influence the upstream flow behavior in the supersonic region.

Figure 19 shows typical pressure profiles for Nozzle D-3a. For chamber pressure ratios (p_c/p_a) lower than approximately 3.65, the static pressure along both walls was a constant value just slightly less than atmospheric. Over the range, $3.6 < p_c/p_a < 5.2$ the wall pressure profiles indicated that the flow was somewhat unsymmetrical, but the effect was a minor one. In general, the jet behavior was symmetrical.

However, it was determined that the jet could be deflected a few degrees off the center line by sliding one of the nozzle blocks laterally so that the corner of the throat of one block was slightly (approximately 0.030 inch) downstream of the other. The deflection of the jet was toward the nozzle block positioned further upstream.

Unsteady flow behavior: Oscillograms of the pressure fluctuations in the 30-degree, two-dimensional nozzle show that the flow is stable over a range of chamber pressures from 0-55 psia. At the pressure of 55 psia the wall-

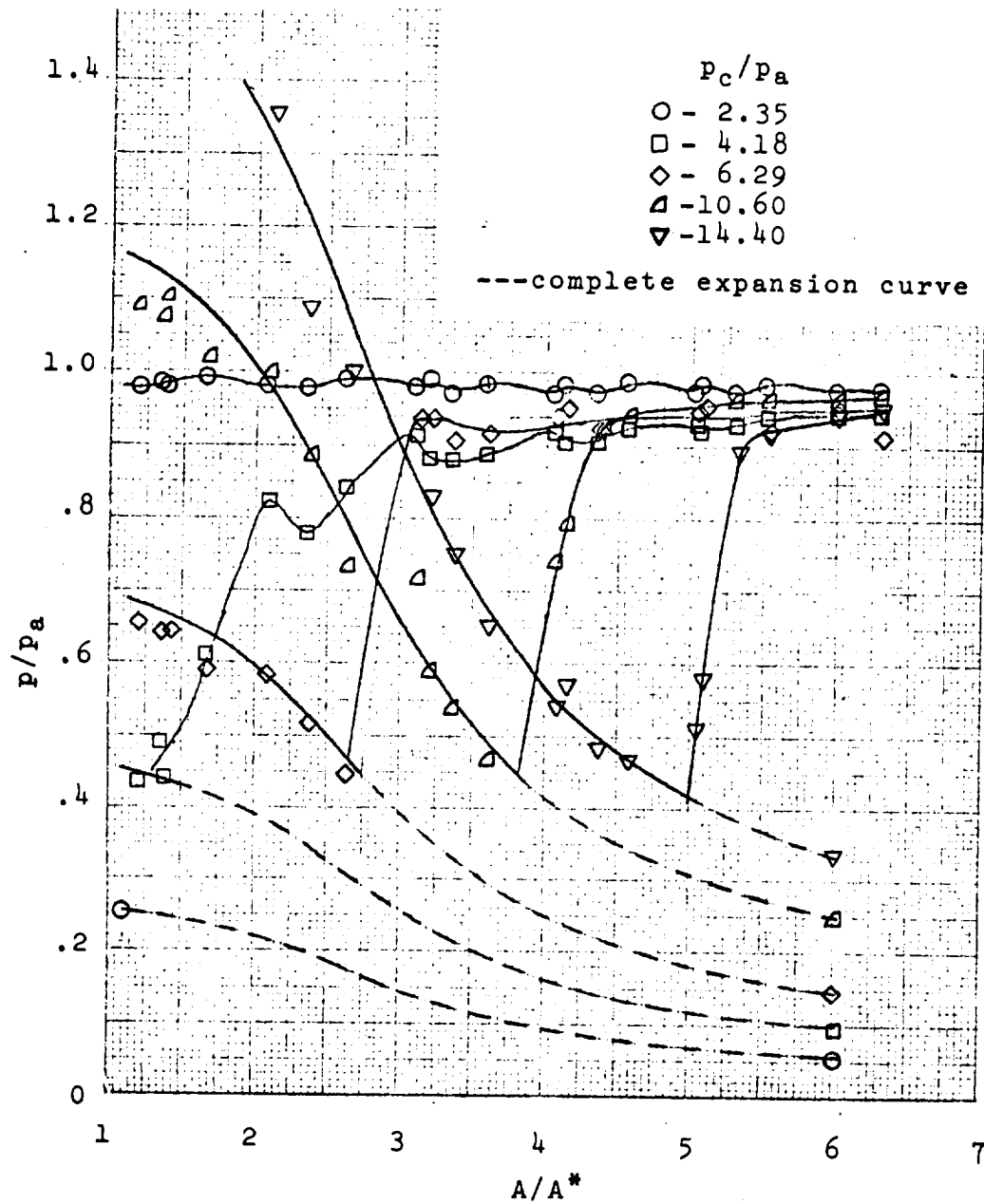


Fig. 19. --Wall static pressures;
30-degree, two dimensional nozzle

static pressures suddenly start to fluctuate in a manner which indicates that the flow switches from one side of the nozzle to the other at a rate of approximately once every 2 to 4 seconds. Actually, the flow tends to favor a particular configuration and the switching is more in the nature of a momentary breakdown from the favored configuration. The duration of the pressure disturbances vary over a range of 0.5 to 3 seconds.

Switching occurs only over a very narrow range of chamber pressures; from 55 to 57 psia. Pressure fluctuations of much smaller magnitude (~ 0.6 psia) and higher frequency (~ 20 oscillations per second) were observed for chamber pressures up to 70 psia. No fluctuations occurred for chamber pressures greater than this value.

The three-dimensional nature of the nozzle was also manifested in the behavior of the flow during switching, as evidenced by the fact that only one of the two rows of pressure taps on one side of the nozzle transmitted pressures which were out of phase with the opposite side. The pressure fluctuations from the second row were in phase with those of the opposite side. It should be noted that all of the pressure tap locations were downstream of separation, and the pressures recorded were those in the region of secondary circulation.

High-speed motion pictures revealed a steady flow

behavior up to the threshold chamber pressure of 55 psia. In this range, the intersection of the expansion waves originating at the throat progressively moved downstream as the chamber pressure was increased. At a chamber pressure of 55 psia, a strong, unstable disturbance appeared across the jet at the point where the downstream edge of the expansion fan intersected the jet boundary. This disturbance appeared to be rather like the rapid disintegration and reformation of a star-shaped shock, and is well represented in Figure 18b.

As was the case for the 10-degree nozzle, the fluctuations in the positions of the oblique shock waves were particularly severe. These fluctuations also occurred with a frequency of approximately 600-700 oscillations per second. The flow tended to spread laterally downstream of the disturbance, fluctuated irregularly, and occasionally (from the reference point of the time slowing provided by high-speed motion pictures taken at 5000 pps) tended to attach to one wall or the other for brief instants.

30-Degree Nozzle With Straight Extension (D-3b)

After observing the flow patterns in the 30-degree nozzle, the author speculated that if the relatively-large-divergence-angle section of a nozzle was followed by a section of relatively small divergence angle (which is the basic type of configuration of a contoured nozzle),

the spreading of the jet downstream of separation in the section of large divergence angle would intercept the wall in the section of narrow divergence angle. As a result, a "dead-air" space would be formed, air would be entrained from this space by the high-speed jet, and the pressure in this space would be reduced. The low pressure would, in turn, cause the flow to overexpand to a greater extent before separation occurred. To check this hypothesis, the 30-degree nozzle blocks were slid forward in the nozzle fixture so that a straight section extended downstream of the blocks. Nozzle D-3b of Figure 9 shows the configuration.

Figure 20 shows the types of flow which resulted. Although pressure data were not acquired for this arrangement, careful comparison of these photographs with those for Nozzle D-3a (e.g., Figure 18d compared with Figure 20e) indicate that separation does occur further downstream.

Perhaps of even greater interest is the effect of the extension on the deflection of the jet. The presence of the extension provides a surface toward which the jet can be deflected. Once the deflection occurs, the entrainment of air on the side of the jet toward which it is deflected creates a low pressure region which promotes the deflection.

Figure 20 indicates two types of jet deflection.

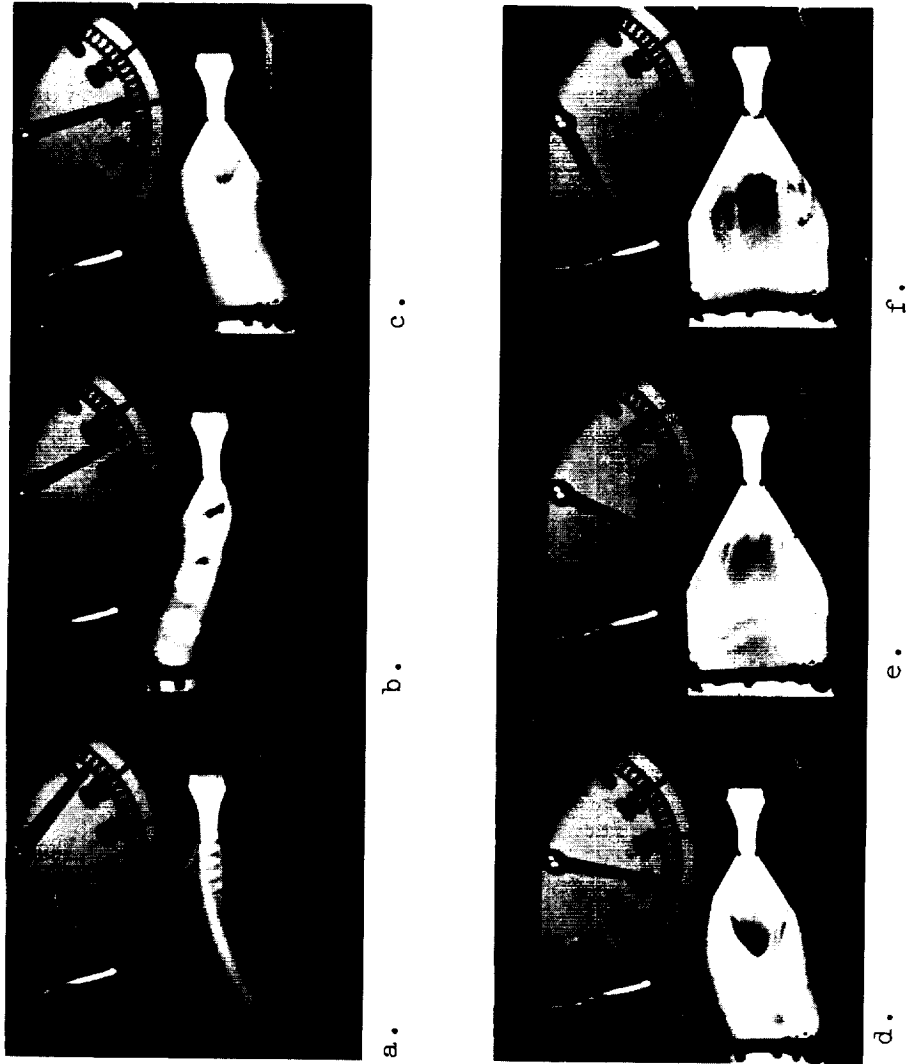


Fig. 20. --Flow patterns; 30-degree nozzle
with straight extension.

The first of these is a uniform bending of the jet due to a transverse pressure gradient across the jet. This effect is most graphically illustrated by Figures 20a and 20b. The second type of deflection is the flow turning caused by shocks associated with different separation positions on opposite sides of the jet. This effect is illustrated by Figures 20c and 20d.

30-Degree Nozzle With Curved Throat Exit (D-3c)

For one test, the orientation of the 30-degree nozzle blocks in the fixture was reversed so that the surface immediately downstream of the throat was curved. The arrangement is D-3c of Figure 9. Figure 21 shows the resulting flow patterns.

The primary point of interest is that normal shocks in the center of the flow stream did not occur, as they did when the throat exit was a sharp corner. Consequently, the flow structure is quite different. This difference can be observed by comparing Figures 21 and 18, (in making the comparison it should be noted that positions of the nozzle blocks relative to the fixture are slightly different for the two cases). With the curved throat exit, the jet remains compact after separation instead of being split as for the case of the sharp-corner exit.

Although pressure data were not acquired for this configuration, general observations revealed that the flow

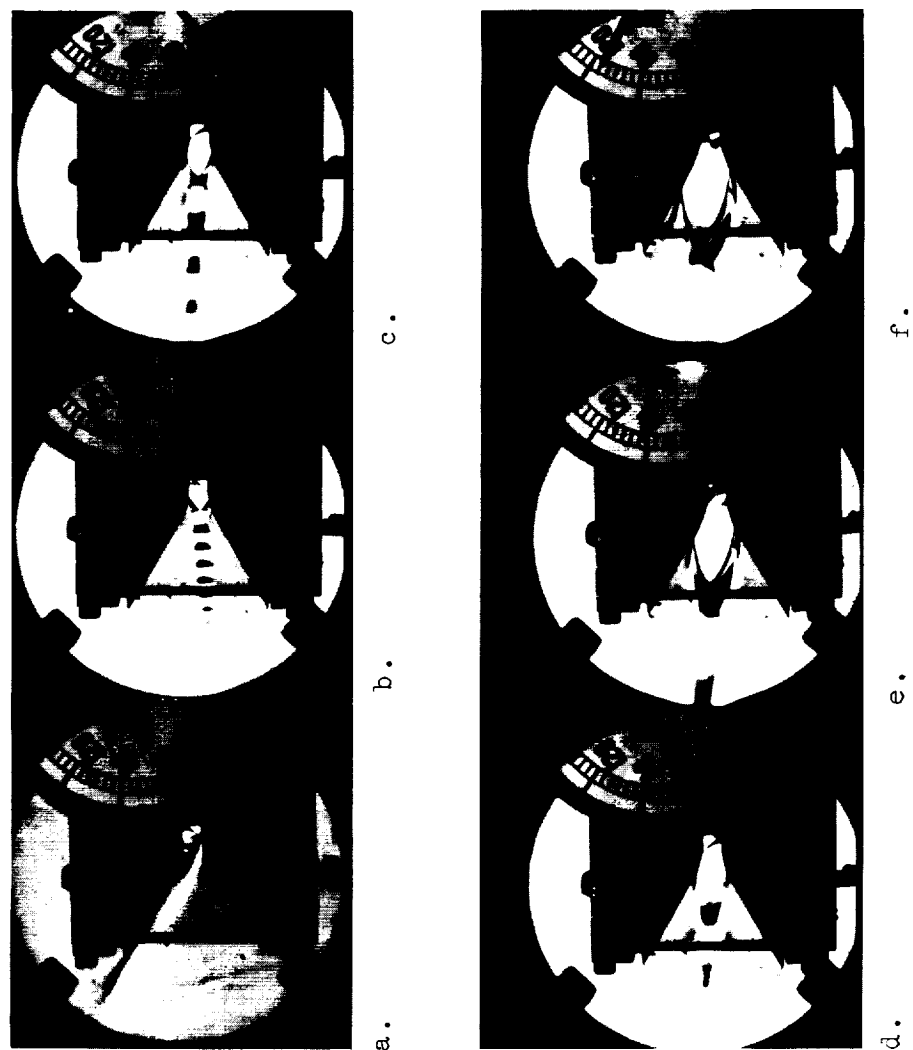


Fig. 21. -- Flow patterns; 30-degree nozzle
with curved throat exit.

behavior was much smoother than for the case of the sharp-corner exit. This result is attributed to the absence of interference between separation shocks and expansion waves from the throat exit. However, as a result of observing the flow with the schlieren system, the impression was formed that the separation shocks fluctuated at high speed when the chamber pressure was in the region of 80 psia. The blurred quality of the separation shocks pictured in Figure 21d tends to support this conclusion. If fluctuations did occur, there was no noticeable effect on the flow behavior.

Contoured Nozzle With Large Initial Divergence Angle (D-4)

Figure 22 shows the flow pattern in Nozzle D-4. The streaks emanating from the sides of the nozzle are Mach waves which originated on small ridges on the surface of the nozzle blocks. These ridges were the result of the technique used to machine the blocks. The surfaces were later ground to continuous 5-inch radii as mentioned in Chapter III. The Mach waves then disappeared, but otherwise there were no differences in the flow behavior. The two diverging lines which originate on the downstream edges of the throat, and then cross to the opposite nozzle block are the limiting Mach waves arising from the sharp-corner expansion. If the nozzle had been fabricated exactly to the theoretical specifications - with due allowance for boundary layer build-up - and if

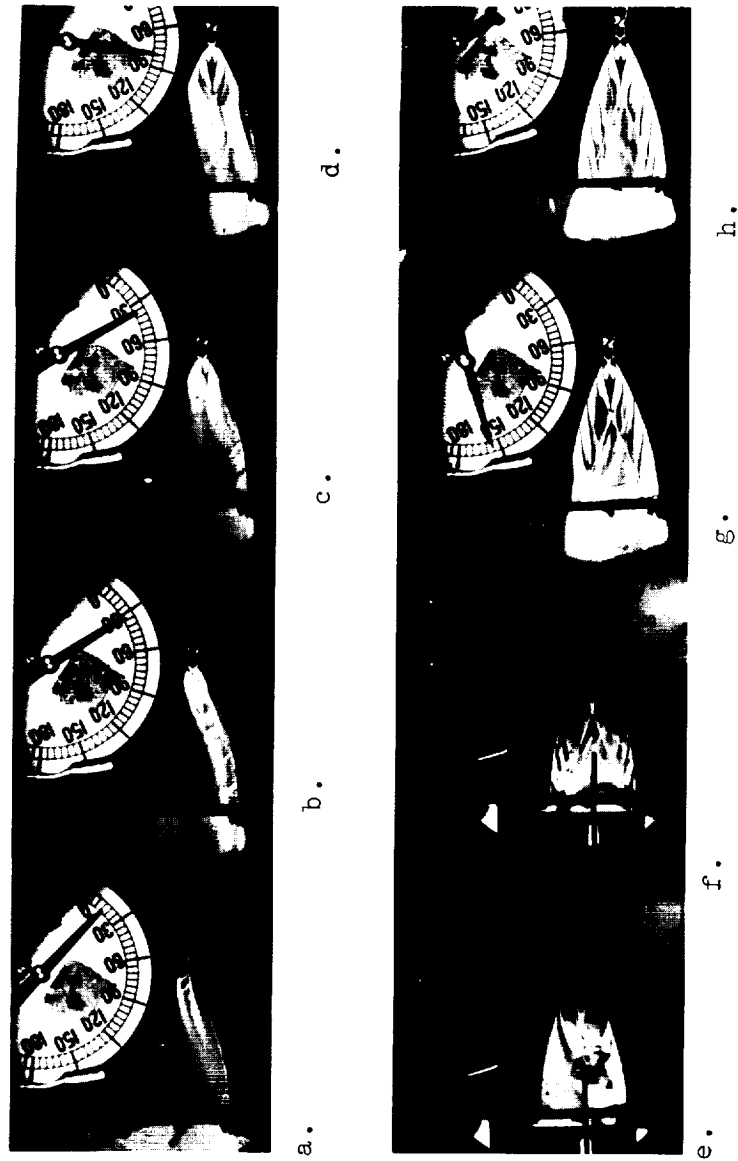


Fig. 22. --Flow patterns; contoured nozzle
with large throat exit angle (D-4).

there were no viscous effects in the flow field, the Mach waves would have intersected the nozzle blocks just at the exit edges.

In many important respects, the flow characteristics seem to be quite similar to those for the 30-degree nozzle with the straight extension. Specifically; the flow is deflected toward one wall, it undergoes the same type of unstable behavior in the region of 50 psia, and the oblique separation shocks coalesce into a normal shock.

Figures 22b and 22c show the difference in the flow structure just before and just after the transition point where instability occurs. Inspection of these and other photographs indicates that at the point of instability, oblique shock waves accompanying separation occur in the same space as the expansion waves from the throat. As a result, an interaction is produced in the flow stream in the region where the expansion waves intersect. This interaction seems to terminate the supersonic flow field, and the flow-tends to spread out beyond the region of the interaction.

As the chamber pressure is increased further, the separation shocks move downstream of the expansion waves from the throat corners, and the flow becomes stable. However, the oblique separation shocks are joined by a normal shock which produces a subsonic zone in the center

of the flow. Figures 22e and 22f are photographs made with a total pressure probe inserted in the flow stream. The total pressure (psig) is indicated by the small gage in the bottom of each photograph. In Figures 22e the probe is downstream of the normal shock. The ratio of probe total pressure to chamber pressure corresponds to the pressure ratio across a normal shock at approximately Mach 2.1. In Figure 22f the probe is in the supersonic region, as indicated by the conical shock emanating from the tip. The ratio of probe total pressure to chamber pressure corresponds to that for a normal shock at approximately Mach 3.4; a value which agrees very well with the design value for the nozzle.

Figures 22g and 22h show separation of the flow into two supersonic streams due to the effects of the normal shock. The appearance of the normal shock in the flow stream outside the nozzle in Figure 22h is particularly interesting because the static pressure at the exit plane of the nozzle is less than the atmospheric pressure. According to classical theory, this condition would result in the formation of oblique shock waves at the nozzle exit and an inward turning of the flow just downstream of the exit. Obviously, this is not the case in Figure 22d. It is known, however, that separation occurred from one of the glass windows and this effect may have contributed to the appearance of the normal

shocks in the exit flow.

Figure 23 shows the static pressure profiles for Nozzle D-4. Figure 23a is the characteristic pressure distribution corresponding to the type of flow shown in Figure 22a and 22b. The rise in static pressure above atmospheric is caused by the jet impinging on one wall of the nozzle near the exit. Figure 23b shows the pressure distribution corresponding to the type of flow shown in Figure 22c. The primary characteristic is a gradual increase in static pressure. Figure 23c shows the type of pressure distribution which occurred over most of the range of chamber pressure variation. This type of distribution is typical for flows such as those shown in Figures 22d, 22e, 22f, and 22g. The sudden pressure rise is typical of separation. In the case of Figure 23d, flow almost filled the nozzle exit, with separation occurring just upstream of the exit.

Contoured Nozzle With Small Initial Divergence Angle (D-5)

Figure 24 shows the flow patterns in Nozzle D-5, which is the contoured nozzle with a small initial divergence angle. The narrow divergence angle at the throat required that the overall area ratio of the nozzle be small in order to avoid the formation of compression shocks on the turning contour of the nozzle walls. Therefore, to obtain a nozzle of reasonable size for photographic purposes, the height of the throat was selected

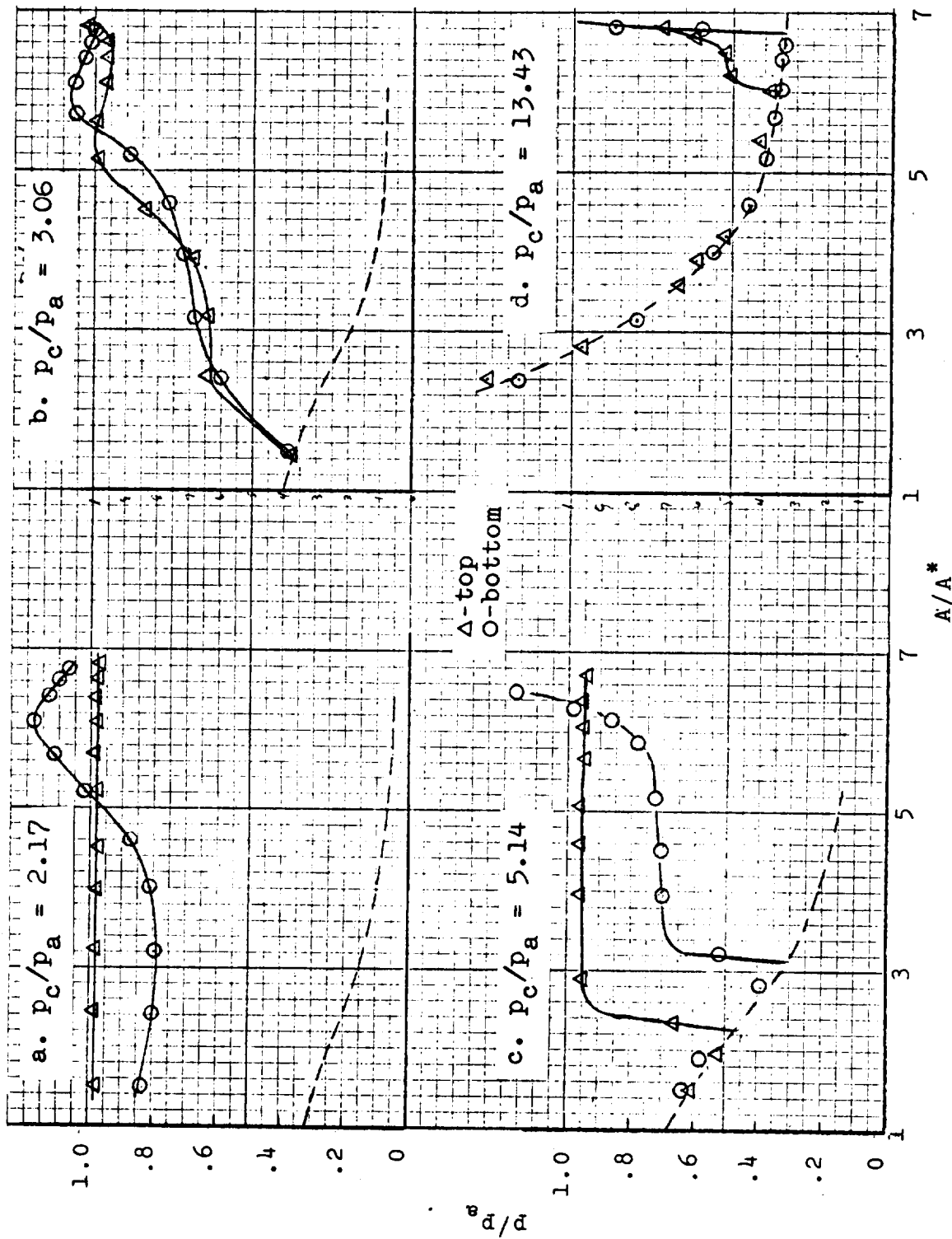


Fig. 23. --Wall static pressures; contoured nozzle, D-4.

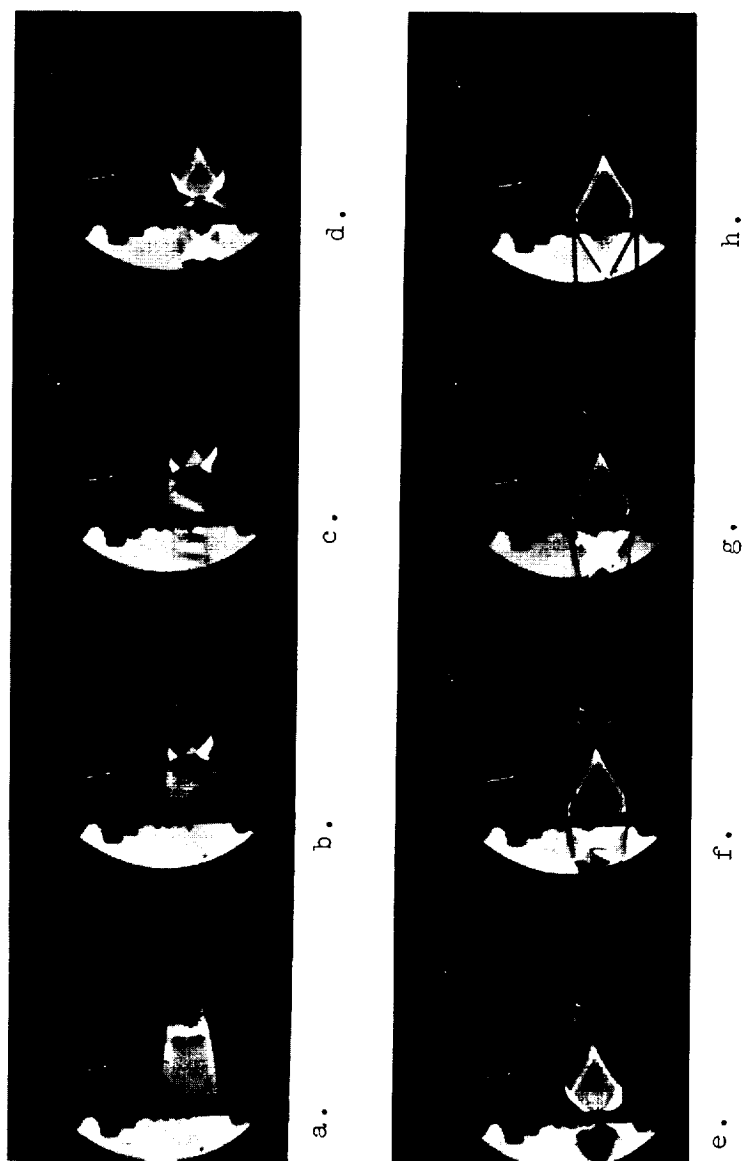


Fig. 24. --Flow patterns; contoured nozzle
with small throat exit angle (D-5).

to be 0.5 inch; a value which is twice as large as for the nozzles discussed previously.

One notes that the mechanism of flow adjustment at low chamber pressures appears to be by means of a normal shock (Figure 24a). However, as the pressure is increased slightly, the normal shock is seen to bridge two oblique separation shocks in the center of the flow stream (Figure 24b). As the point of separation moves further downstream, the proportion of the total shock structure which is normal becomes less (Figures 24c, 24d, 24e). After the flow fills the nozzle, the adjustment to atmospheric pressure at the exit plane is by means of oblique shocks in the manner to be expected from classical theory (Figures 24f, 24g, 24h). One notes a small normal shock in the exit stream (Figure 24f) which disappears as the pressure is raised (Figures 24g, 24h).

Static pressure profiles were also obtained for this nozzle. Their appearance is similar to the profiles presented in Figure 23.

V. EXPERIMENTAL RESULTS; AXISYMMETRIC NOZZLES

9-Degree Conical Nozzle (A-1)

General behavior: The general nature of the flow in this nozzle can be summarized by the following classification of behavior as a function of chamber pressure.

<u>p_c/p_a</u>	<u>behavior</u>
< 1.5	symmetrical - stable
1.5-1.9	symmetrical - slight instability
1.9-2.7	unsymmetrical - flow switching
2.7-3.7	unsymmetrical - essentially stable
> 3.7	symmetrical - stable

Figure 25 shows typical static-pressure distributions along the nozzle wall for various chamber pressures. The pressure distribution for $p_c/p_a = 3.62$ is only one portion of an unsymmetrical distribution. The other profiles are symmetrical. The curve drawn through the minima provides an indirect correlation of separation pressure ratio with Mach number, since the Mach number increases as the area ratio increases in the supersonic regime.

For values of $p_c/p_a < 3.7$ the exhaust stream appeared to be subsonic. When the chamber pressure ratio reached 3.7 there was a sharp transition in the position of the mercury columns in the manometers and the appearance of a supersonic

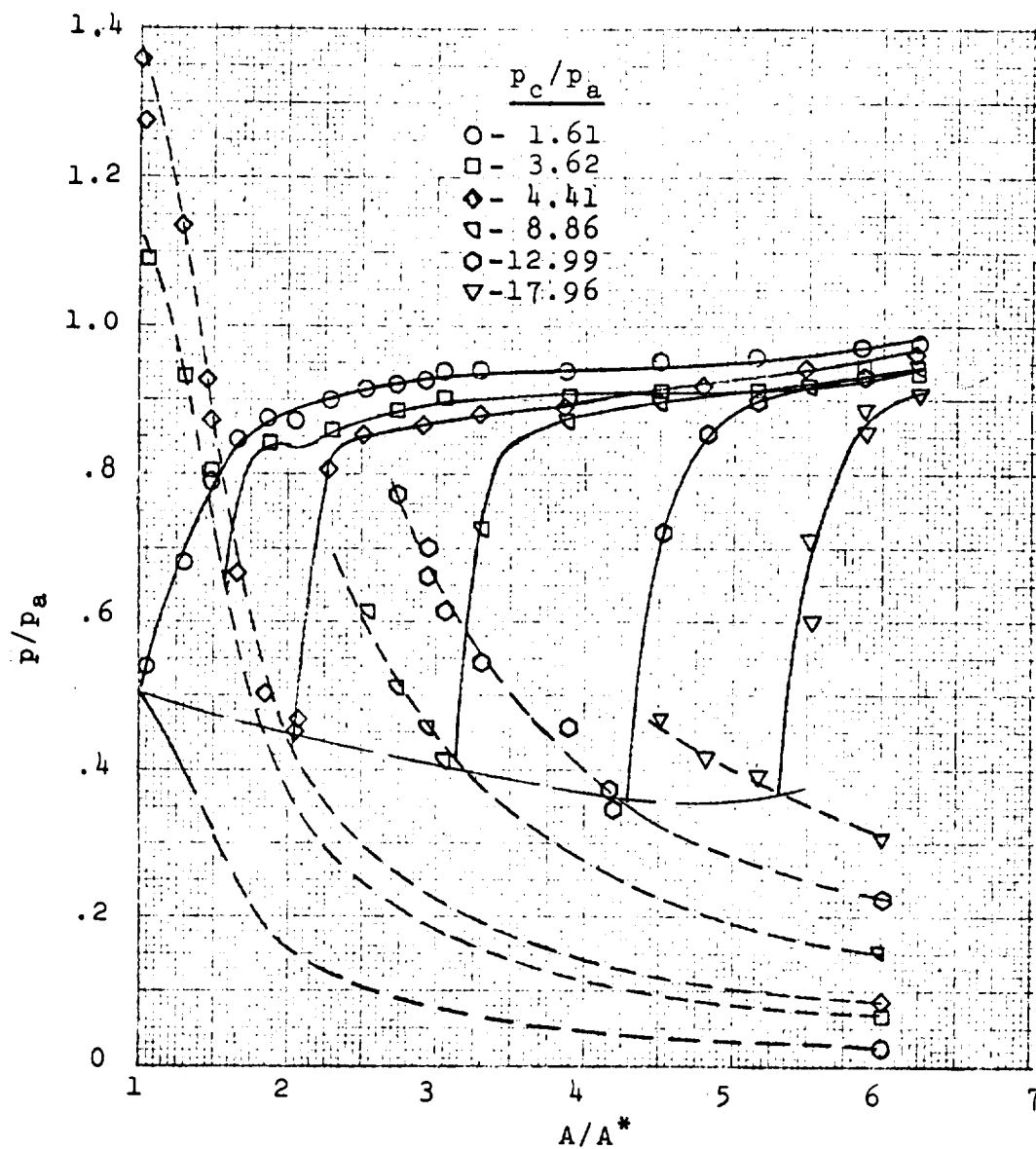


Fig.25. -- Wall static pressures;
9-degree, conical nozzle (A-1)

jet in the center of the exit area was evident. Also, there was a noticeable change in the tonal quality of the sound from the nozzle when this transition occurred. For values of $p_c/p_a < 3.7$, the tonal quality was smooth as if the amplitude of the sound waves were of constant magnitude - except for the audible effects of switching when $1.9 < p_c/p_a < 2.7$. For chamber pressures above the transition point, the tonal quality was much rougher. A microphone and tape recorder were used to monitor the sound of the nozzle on one occasion. It was found that most of the sound energy occurred at a frequency which was varied but was approximately 3000-Hz. However, above the transition point, other low-frequency components were present, but most of the sound energy continued to be concentrated in the 3000-Hz.region.

As a result of these observations, the conclusion is reached that for chamber pressures below the transition point, the flow undergoes normal shocks. These shocks are not necessarily the original cause of separation, but may appear in the stream after separation and cause the flow to spread rapidly and nearly fill the nozzle before it reaches the exit. For chamber pressures above the transition point, the jet exhibits the customary separated, supersonic-jet behavior.

Unsymmetrical behavior: Figures 26 and 27 show typical pressure profiles which illustrate the unsymmetrical flow behavior and how it contrasts with the symmetrical behavior. The pressures along four rows of taps spaced 90-degrees apart

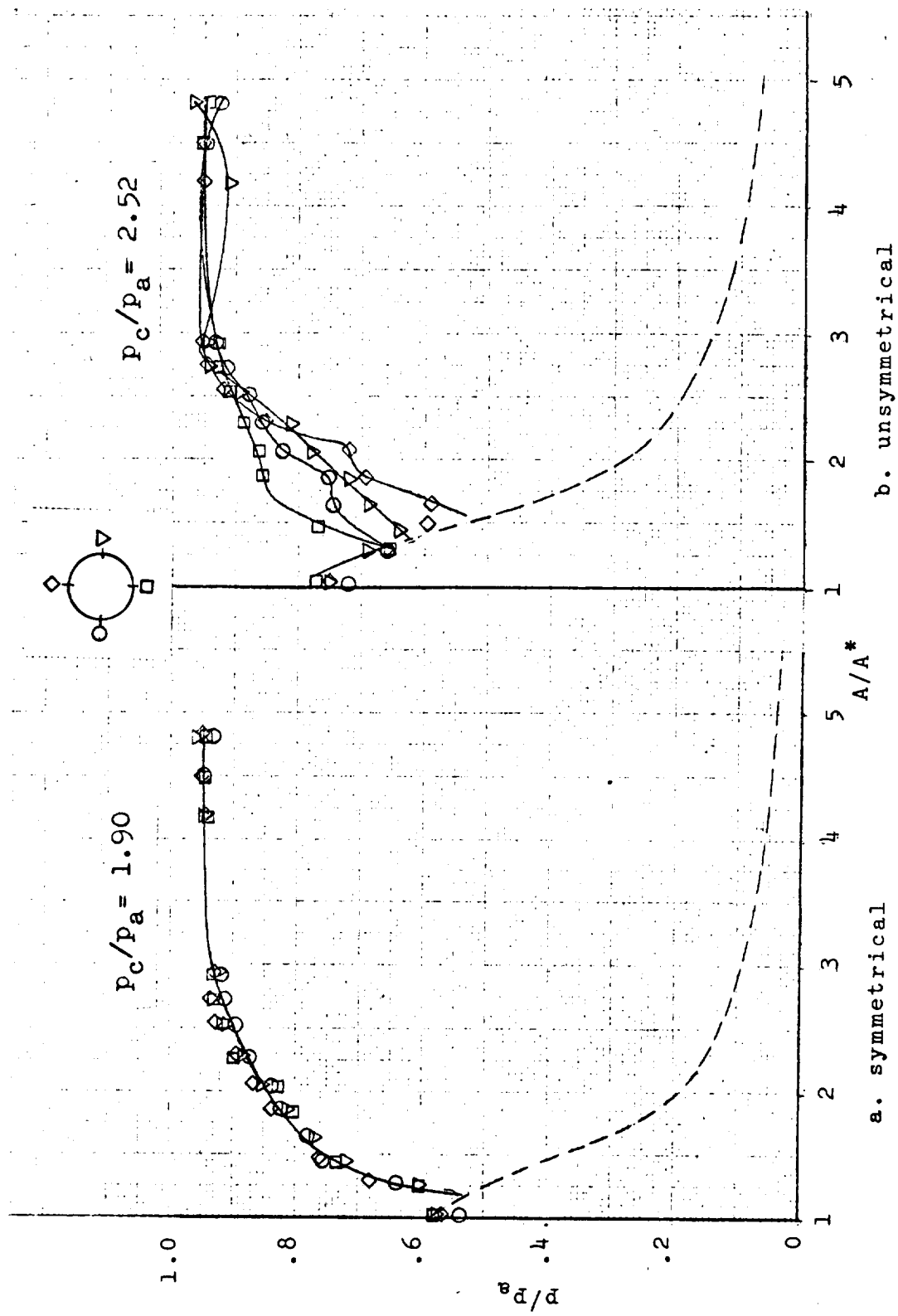


Fig. 26. --Flow symmetry for 9-degree, conical nozzle - lower pressures.

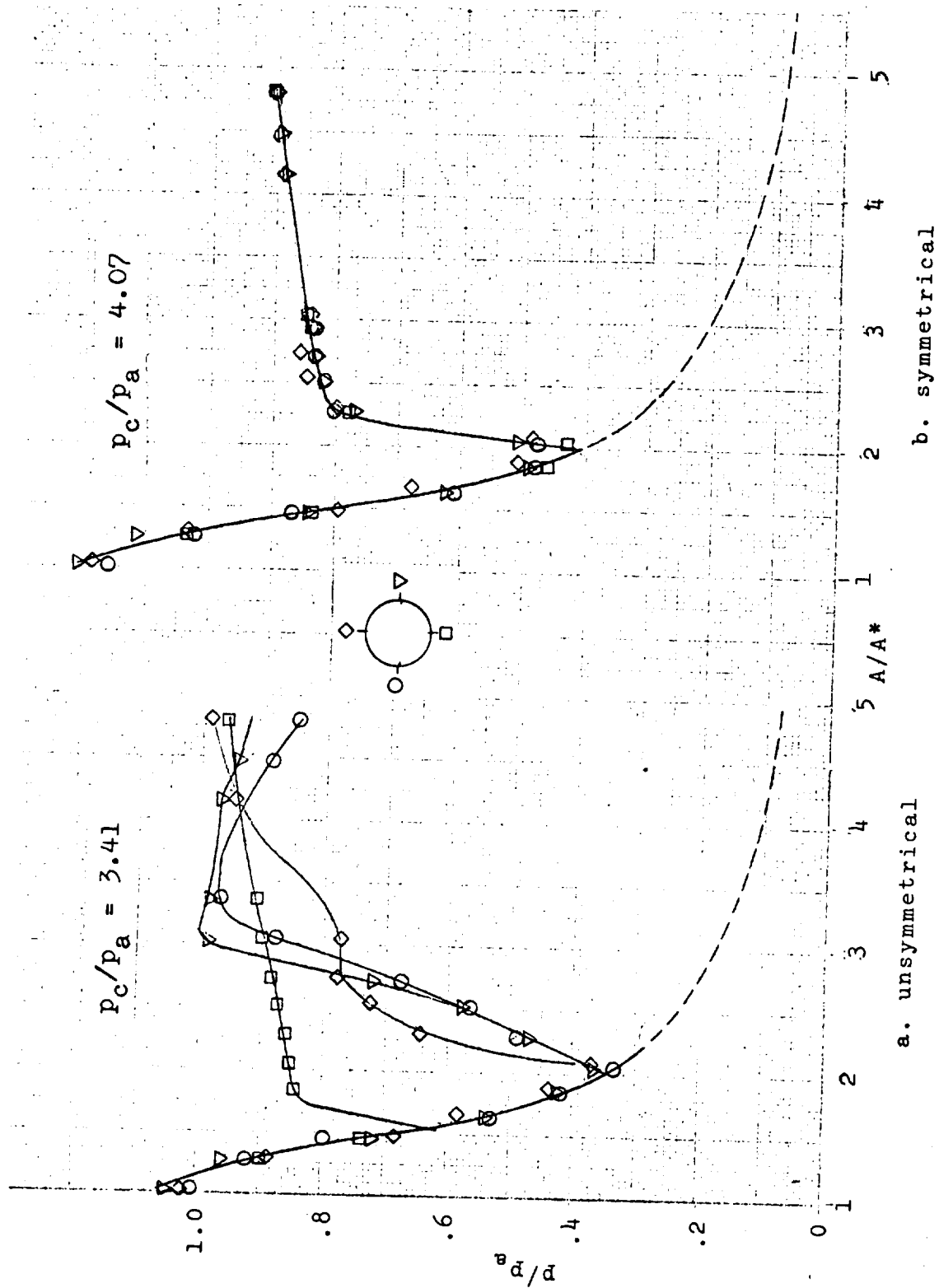


Fig. 27. --Flow symmetry for 9-degree, conical nozzle - higher pressures.

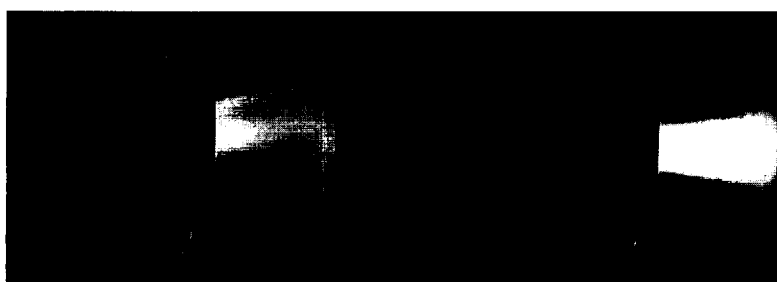
are represented. The relative locations of these rows as viewed from the nozzle exit are indicated in the figures.

Figure 26 shows the transition from symmetrical to unsymmetrical flow which occurred as the chamber pressure was raised. The fact that the pressure rise commenced at a lower value of minimum wall pressure for the symmetrical case of Figure 26a than for the unsymmetrical case of Figure 26b while the chamber pressure increased, suggests that the cause of the pressure rise may have been different for the two cases.

Figure 27 indicates the nature of the transition from unsymmetrical to symmetrical flow. Pressure profiles for other chamber pressures in the unsymmetrical regime were intermediate to those shown in Figures 26b and 27a.

Figure 27a and to a lesser extent, Figure 26b, indicates that the flow separates from one side of the nozzle (as indicated by the square symbols) while it continues to expand along the other sides to a lower pressure before a pressure adjustment occurs. This behavior is somewhat similar to that for the 10-degree, two-dimensional nozzle. The physical picture accompanying this behavior is postulated to be that separation causes the flow to break away from approximately one quadrant of the nozzle wall. The resulting flow stream tends to adhere to the other three quadrants of the nozzle wall and undergoes successive shocks which tends to spread the flow en route to the exit.

Figure 28 shows photographs of the flow just before,



a. unsymmetrical

b. symmetrical

Fig.28. -- Exhaust appearance for symmetrical
and unsymmetrical flow in conical nozzle

and just after the transition from the unsymmetrical to the symmetrical configuration. In order to obtain photographs of the unsymmetrical flow, the schlieren system had to be adjusted so that it was quite sensitive. However, the flow was readily visualized with only nominal sensitivity after transition occurred. This experience provides further evidence that the flow was nearly subsonic at the exit before transition occurred.

Unstable Flow Behavior: When the chamber pressure was in the range of approximately 30 to 40 psia, audible fluctuations in the flow could be discerned. One could stand behind the nozzle and feel that the exhaust stream discharged from one side at an angle approximately equal to the nozzle divergence angle. The direction of the flow would switch with a frequency in the order of once every few seconds. The switching appeared to be to and from a preferred orientation to two or three alternate positions; one of which was that of a symmetrical jet.

Figure 29 shows a section of an oscillograph record of the switching which occurred at a chamber pressure of 35 psia. As shown in Figure 29, major fluctuations occurred every 4 to 6 seconds and lasted for 1 to 2 seconds. However, these numbers are representative only. On some occasions, switching would occur approximately once every three seconds and last for an equal period. The oscillograph records were scrutinized for signs of upstream or downstream pressure changes which could trigger the switching action but none

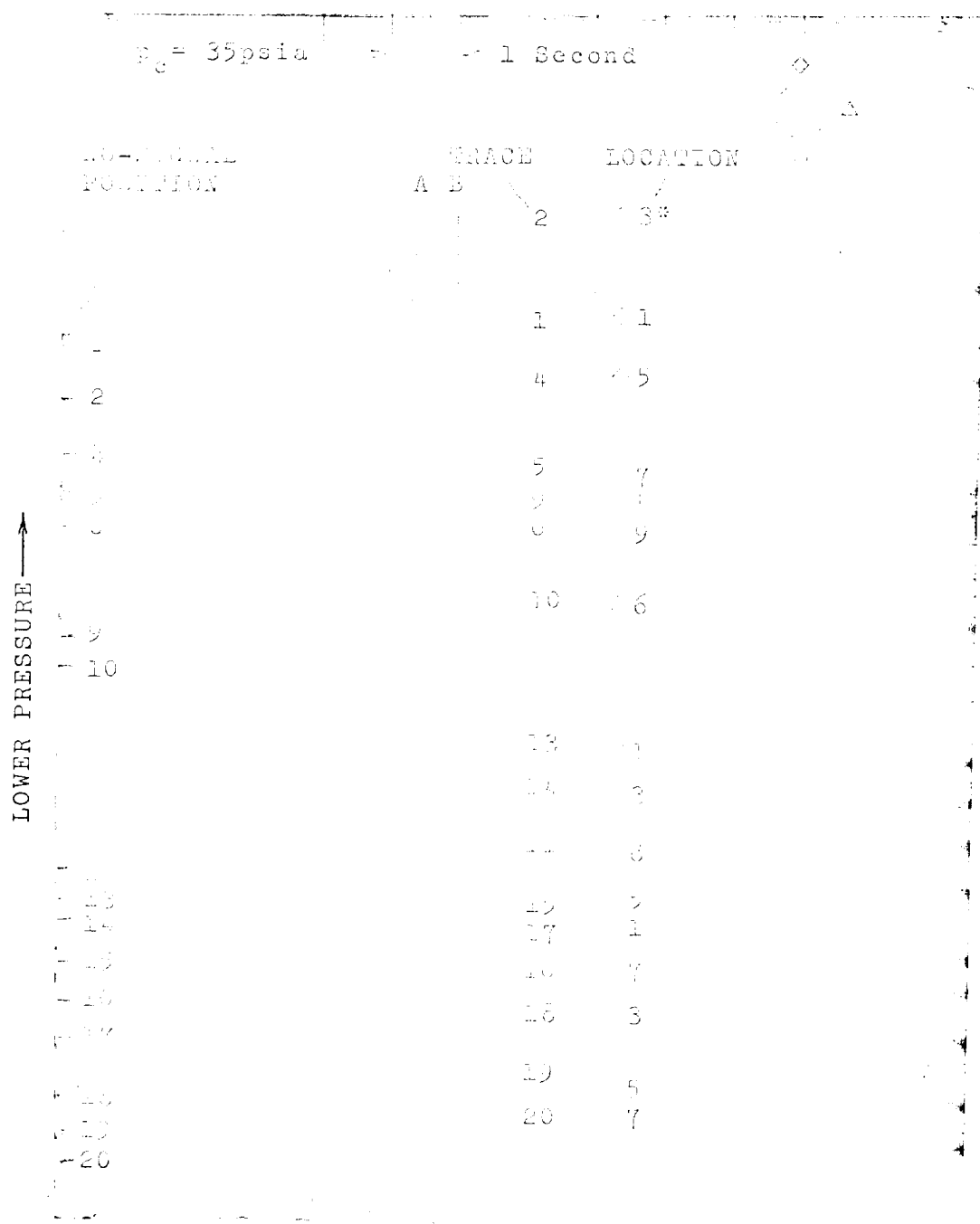


Fig.29. --Oscillograph record of flow switching

were found.

Figure 30 shows the pressure distributions representing both extremes of the fluctuation taken at times A and B indicated in Figure 29. The orientation of the side forces is also indicated. Other orientations of the fluctuating forces also occurred. The magnitude of the fluctuating side forces were somewhat less, but comparable to those described previously for steady, unsymmetrical flow.

Ventilated Flow: Due to the fact that there were more pressure taps in the 9-degree, conical nozzle than there were available manometers, only two rows of taps were used to acquire data for that portion of the symmetrical regime for $p_c/p_a \gtrsim 7.0$. For the first set of data acquired with only two rows of taps, the pressure tubes in the two rows not being used were simply left uncovered and ventilated to the atmosphere.

As a consequence of this arrangement, the flow exhibited instabilities which were not present otherwise. For example, severe switching of the flow from one wall of the nozzle to another occurred at a chamber pressure of 90 psia. Strong oscillations were also observed at a chamber pressure of 170 psia, but wall-to-wall switching did not occur. The switching action could be stopped by plugging the pressure tubes on one side of the nozzle.

Also, by plugging pressure tubes on one side of the nozzle only, the jet could be made to deflect substantially off the axis at chamber pressures as great as 135 psia.

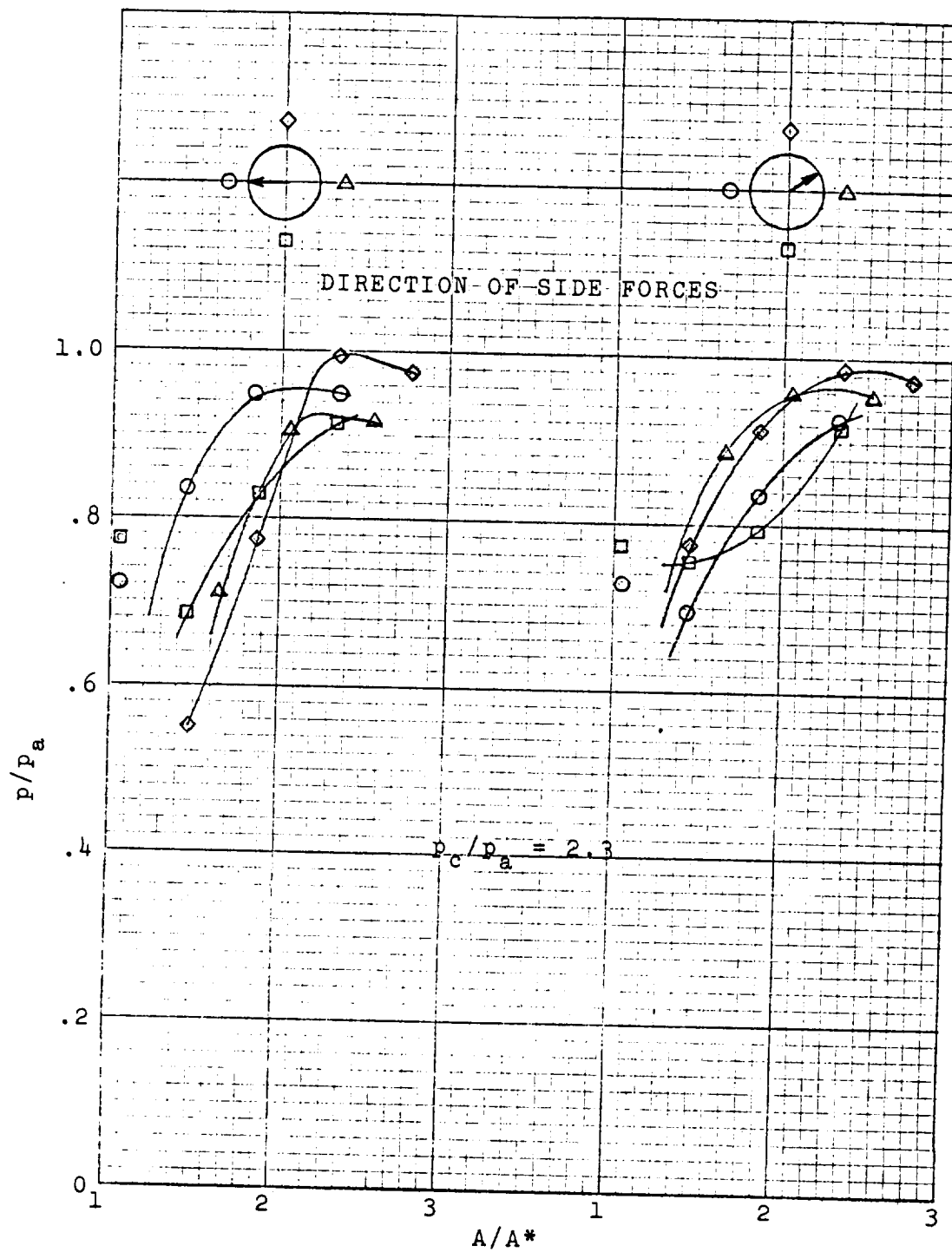


Fig.30. -- Fluctuating pressure distributions
in 9-degree, conical nozzle

After this behavior had been observed, tests were made to see how many of the ventilated tubes on one side of the nozzle could be closed off and still maintain the deflection. It was found that ventilation of only two tubes (located at $A/A^* = 2.78$ and 3.04) was sufficient to cause a steady deflection of the jet at 135 psia. When either of these tubes was closed off, the jet straightened out. Figure 31 shows the wall-pressure distributions for the case of the deflected jet mentioned above. The jet could not be severely deflected at chamber pressures greater than 135 psia.

The foregoing results have obvious implications related to fluid-switching devices and thrust-vector control.

15-Degree Nozzle; (A-2)

Tests were made with the same nozzle employed by Moore (19). Moore attached an ejector to his nozzle to reduce the back pressure, whereas in this study the nozzle exhausted directly to the atmosphere. It appears that this difference may have been responsible for some differences in the experimental results.

The general nature of the flow behavior was quite similar to that for the 9-degree nozzle. The type of behavior can be roughly categorized as follows:

<u>p_c/p_a</u>	<u>type behavior</u>
< 2.4	stable, symmetrical
~ 2.4-3.0	flow switching
2.4-4.0	stable, unsymmetrical
> 4.0	stable, symmetrical

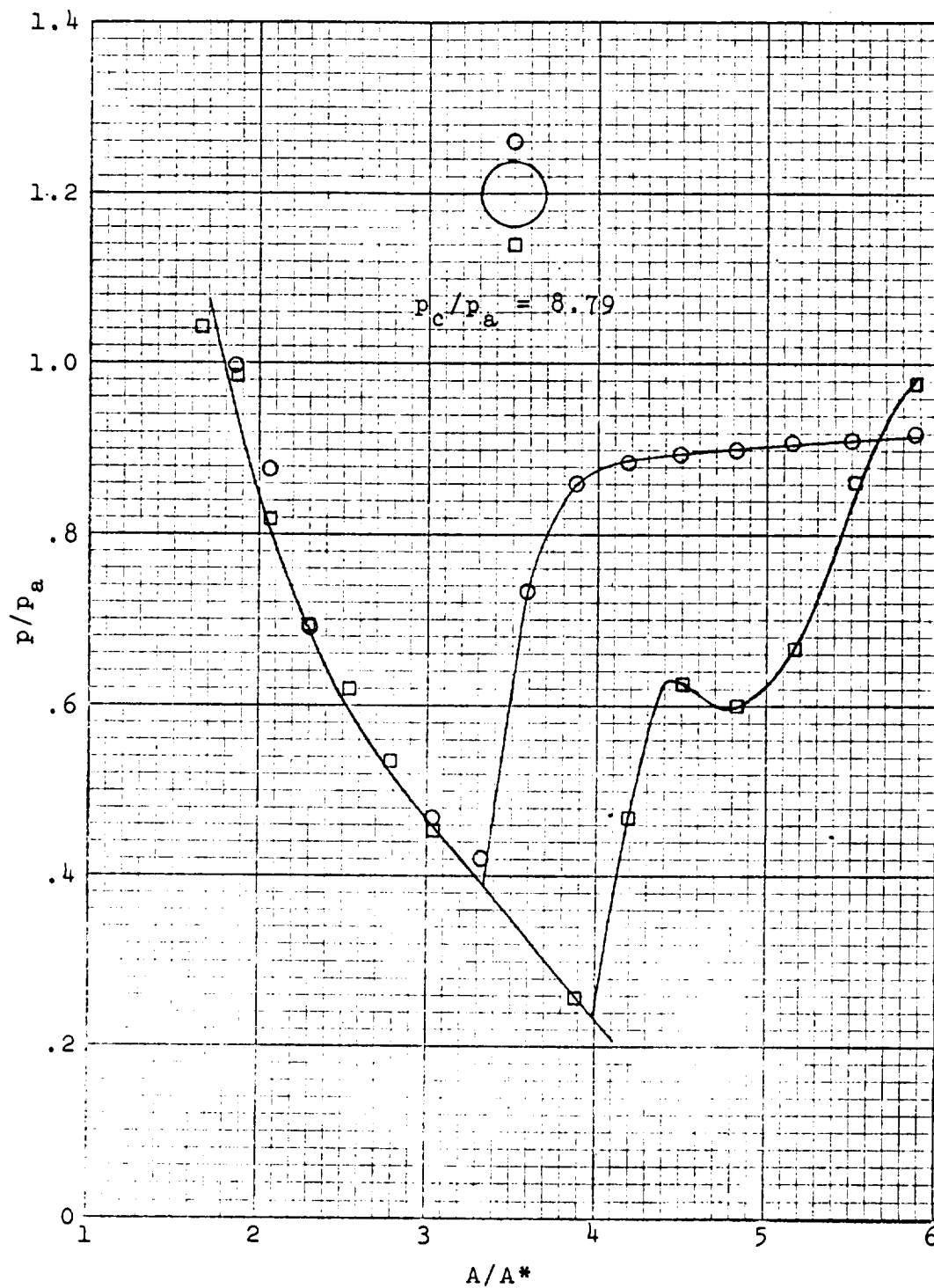


Fig.31 -- Pressure distributions for deflected jet in ventilated, 9-degree conical nozzle

Fiber tufts taped at 45-degree intervals around the periphery of the nozzle exit provided an indication of the flow directions adjacent to the wall. For chamber pressure greater than 60 psia, the ends of all of the tufts were uniformly sucked into the nozzle; thereby indicating that no portion of the exhaust was adhering to the wall. This observation was supported by the uniform appearance of the wall pressure profiles. This type of flow was regarded as symmetrical.

As the chamber pressure was lowered to approximately 60 psia, the ends of one of the tufts extended out of the nozzle; thereby indicating an outward flow along a small segment of the wall. A further reduction in chamber pressure caused progressively more of the adjacent tufts to extend outward. In the region of 45-50 psia, five of the tufts extended outward and three were sucked inward. At this point, the flow was definitely attached to one sector of the nozzle.

When the chamber pressure was reduced to 45 psia, switching of the type described for the 9-degree nozzle abruptly commenced. Switching seemed to be most predominant for a chamber pressure of 45 psia, but also occurred throughout the range of chamber pressures between 35 to 45 psia. At lower chamber pressures, the flow had a rough quality but appeared to fill the nozzle exit.

Figure 32 shows typical pressure profiles in the symmetrical flow regimes. The unsymmetrical pressure profiles are similar to those for the 9-degree conical nozzle.

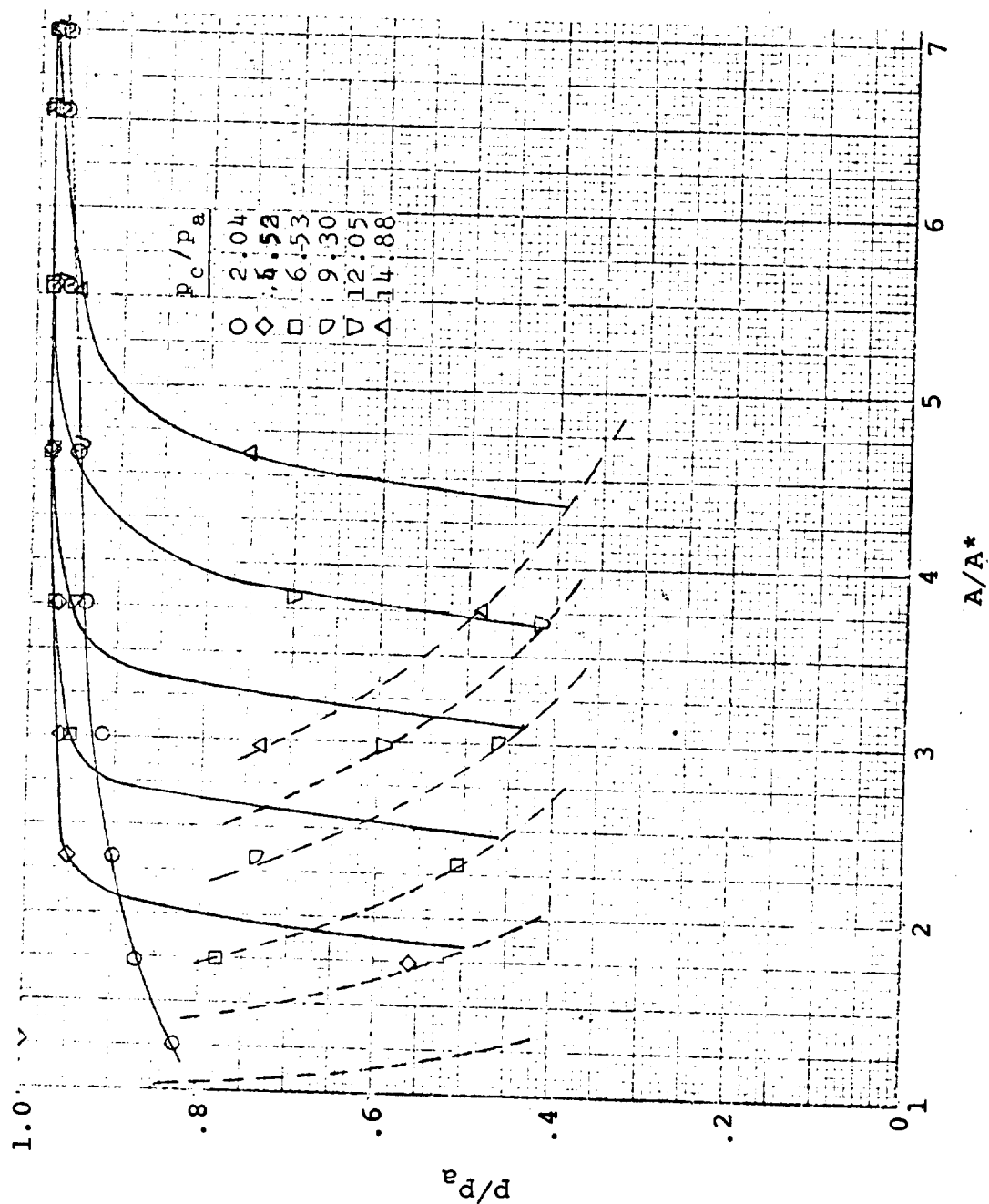


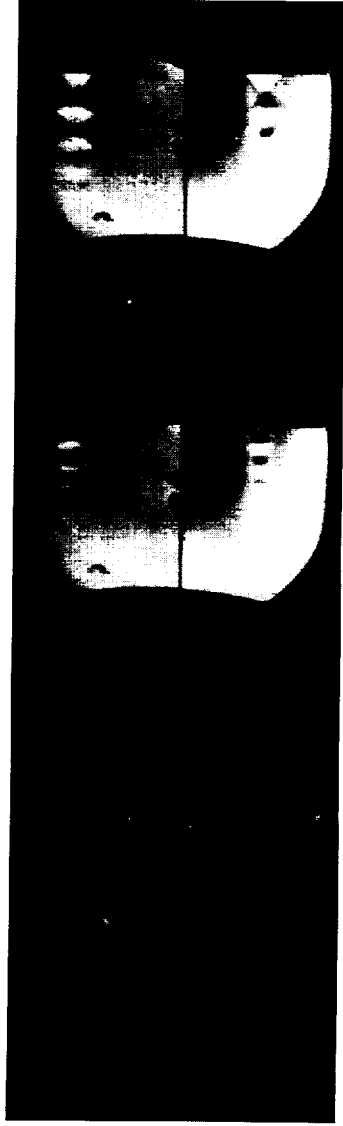
Fig. 32. --Wall static pressures; 15-degree conical nozzle (A-2)

The optical system shown in Figure 13c was used to simultaneously observe the orientation of the exhaust in two mutually perpendicular planes. Figure 33 shows typical photographs of the exhaust stream. Good resolution of the exhaust pattern for unsymmetrical flow at pressures less than 50 psia was not obtained with the crossed-axis system. However, the photograph of Figure 28, which was made with the two-mirror system represented in Figure 13a, shows the appearance in one dimension.

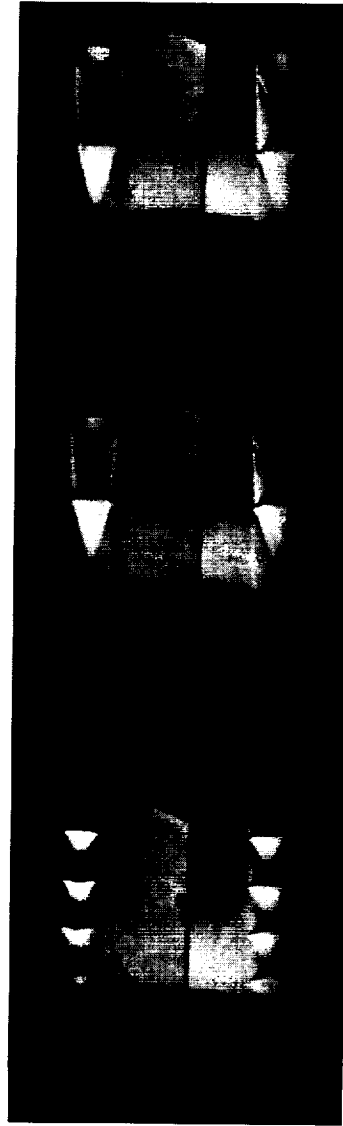
Numerous measurements were made of the inclinations of the center lines of the exhaust jets with respect to the axis of the nozzle from photographs such as those shown in Figure 33. These measurements indicated that the jet was usually aligned very closely with the nozzle axis. In some instances, deflections of 1 to 2 degrees were determined, but such deflections were comparable in magnitude with the uncertainty of the measurement.

In this regard, it should be mentioned that Moore (19) observed unsymmetrical behavior for values of p_c/p_a as great as 8.5. Since the present investigation shows little evidence of any significant unsymmetrical behavior above $p_c/p_a \gtrsim 4.0$, it is suspected that either the lower back pressures or some other effect resulting from the use of ejectors is responsible for the difference.

Motion pictures showed a fluctuation in the width and texture of the exhaust stream at a chamber pressure of 45 psia. The exhaust remained centered on the axis during



a. $p_c = 45\text{psia}$ b. $p_c = 48\text{psia}$ c. $p_c = 57\text{psia}$



d. $p_c = 66\text{psia}$ e. $p_c = 169\text{psia}$ f. $p_c = 193\text{psia}$

Fig.33. --Exhaust patterns for 15-degree, conical nozzle (A-2)

these fluctuations.

30-Degree Nozzle, 0.190-inch Throat Diameter. (A-3)

A series of tests with nozzle A-3 of Figure 11 provided one of the more interesting highlights of the study. The throat diameter of this nozzle was so small that relatively high chamber pressures would yield only relatively low values of momentum flux. This characteristic was reflected in the behavior of the flow. For chamber pressures between 57 and 115 psia, the flow spontaneously adhered to one side of the nozzle wall. It was found that the sector of the wall to which the flow adhered could be influenced by inserting a small probe adjacent to the wall in the region of separation.

When the chamber pressure was increased above 115 psia, the flow would straighten out and was resistant to attempts to deflect it by means of a probe. As the chamber pressure was lowered from values greater than 115 psia, the flow would usually remain axial until a pressure of 92 psia was reached. At this pressure the flow would spontaneously attach to a wall of the nozzle. With continued reduction in chamber pressure, the flow would again become axial at a value of 45 psia. At chamber pressures below this value attempts to switch the flow to a wall by perturbing it were unsuccessful.

Figure 34 shows the pressure distribution corresponding to the maximum value of chamber pressure for which the

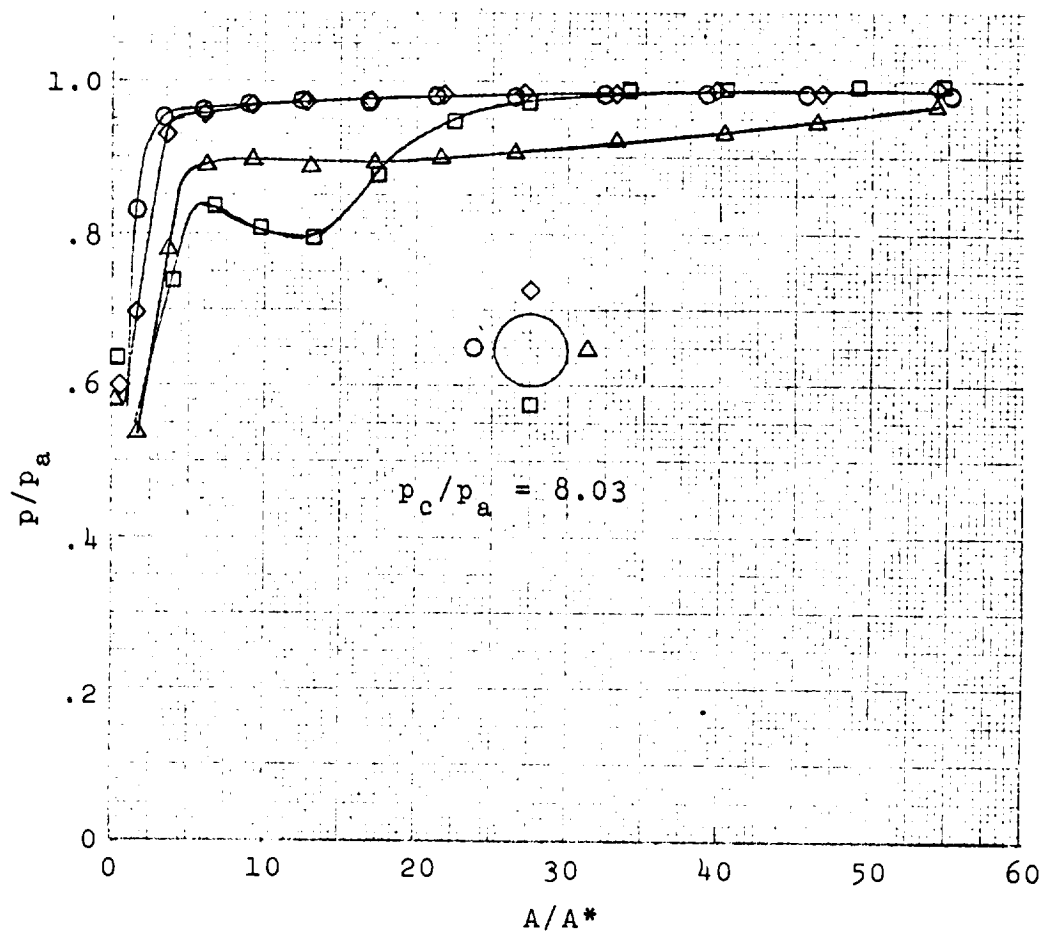


Fig.34. -- Unsymmetrical pressure distributions; 30-degree, conical nozzle with .190-inch throat diameter (A-3)

flow would adhere to the nozzle wall. The deflected momentum flux ($\dot{w}\bar{u}_\infty$) associated with this condition is approximately 4.2 lbf.

30-Degree Conical Nozzle; 0.390-Inch Throat Diameter
(A-4a)

Figure 35 shows the pressure distribution for symmetrical flow in Nozzle A-4a. The pressure distributions were unsymmetrical for $3.0 < p_c/p_a < 6.0$ and symmetrical outside this range. Switching did not occur, but slight pressure fluctuations were measured when the chamber pressure was between 55 and 65 psia.

30-Degree Conical Nozzle with Extensions (A-4b,c)

Straight extensions were added to Nozzle A-4a to approximate the configuration of a contoured nozzle. This arrangement was the axi-symmetric equivalent of Nozzle D-3b discussed in the preceding chapter.

Figure 36 shows the pressure profiles for the nozzle with the long extension (A-4b). A comparison between Figures 35 and 36 readily reveals that the separation pressures and the pressures immediately downstream of separation were lower when the extension was attached. Results intermediate between those of Figure 35 and 36 were obtained when the shorter extension (A-4c, Figure 11) was used.

Strong fluctuations in the flow occurred when the extension was added. The oscillograph records for this test showed "square-wave type" pressure fluctuations with a

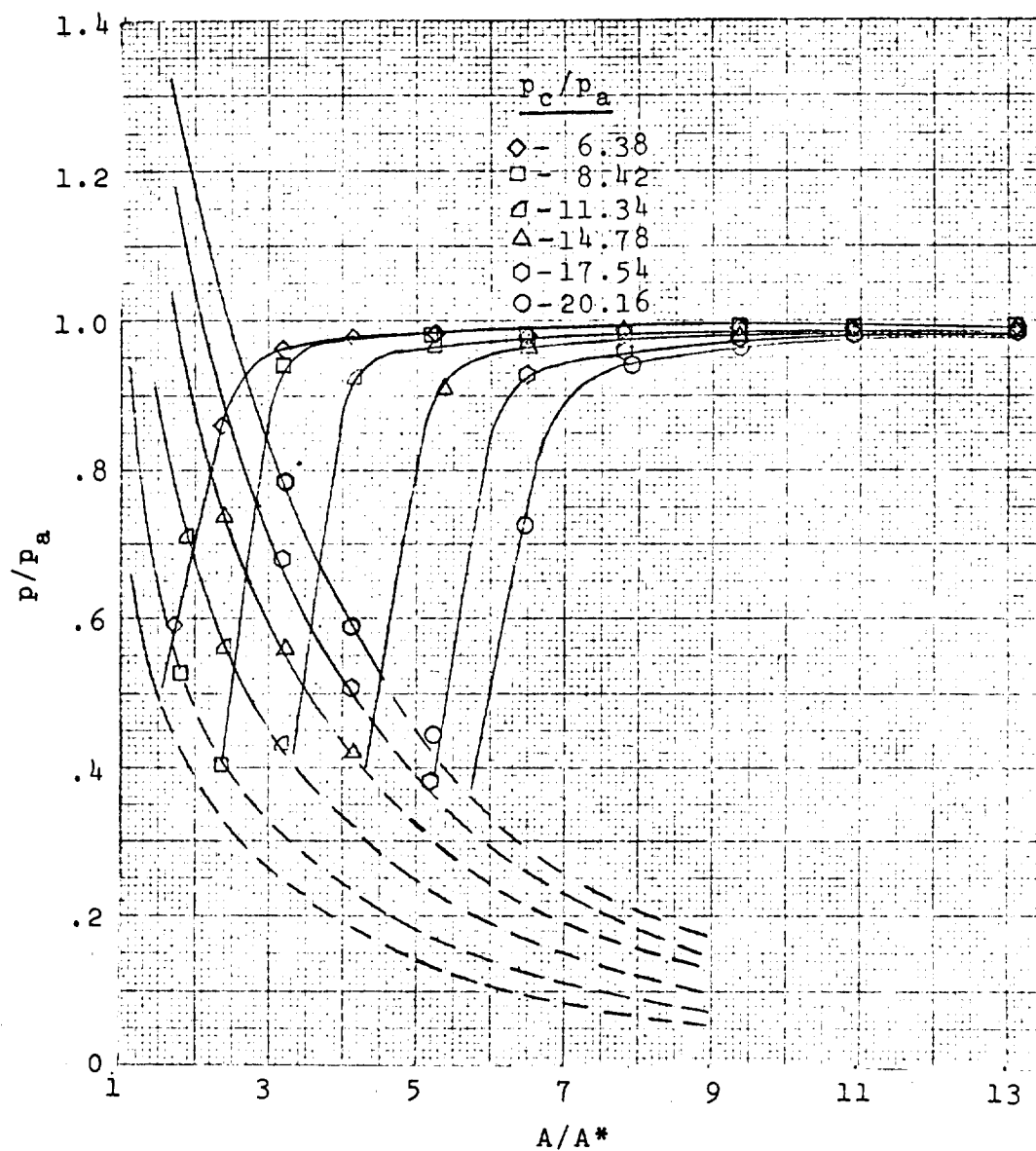


Fig.35. -- Wall static pressures; 30-degree, conical nozzle with .390-inch throat diameter ($A-4_a$)

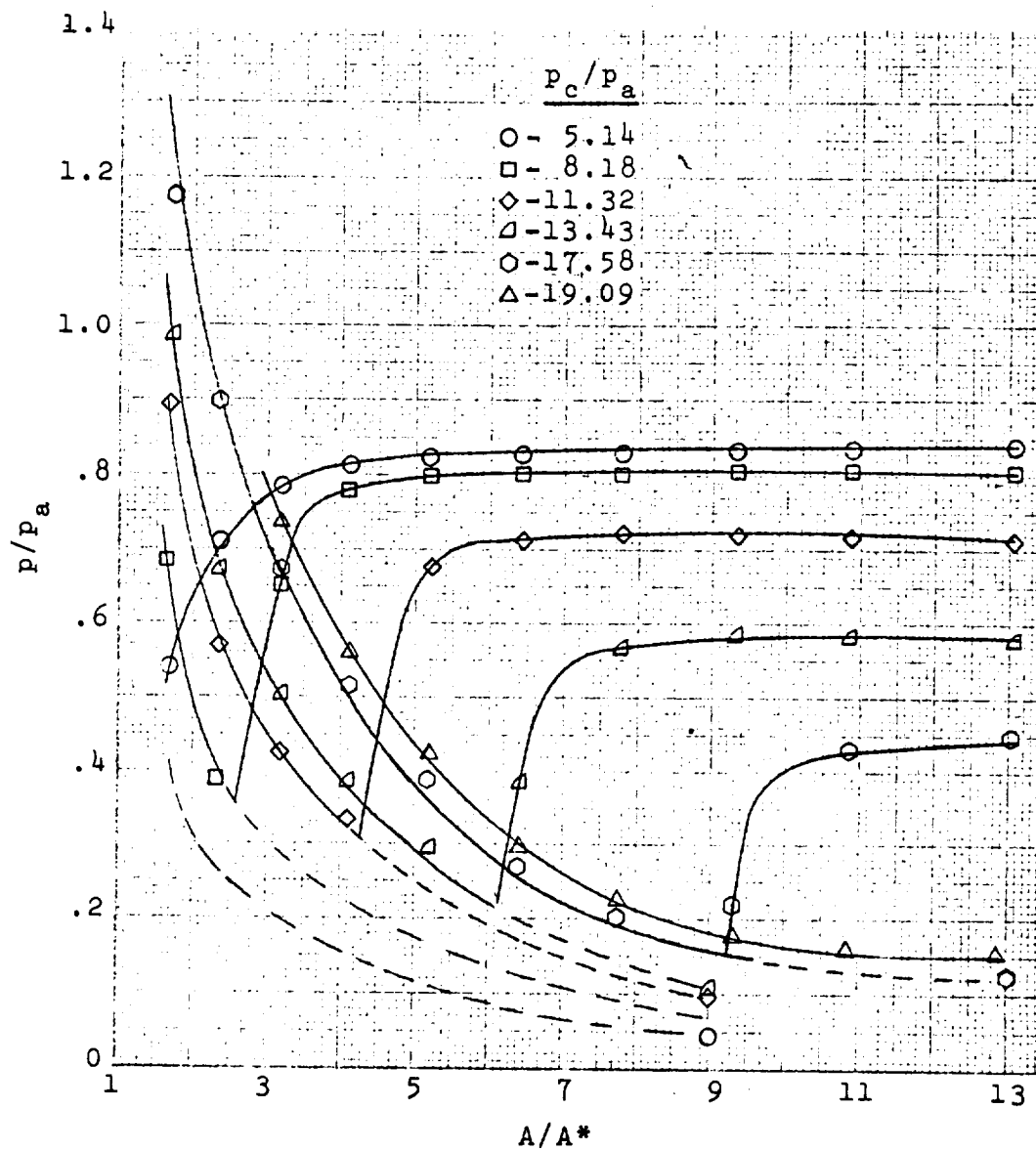


Fig.36. -- Wall static pressures; 30-degree, conical nozzle with straight extension ($A-4_b$)

frequency of approximately once per second when the chamber pressure was 65 psia. The disturbance appeared to be more in the nature of a uniform pressure fluctuation along all four rows of pressure taps, rather than a switching action.

Mach-4, Contoured Nozzle (A-5a,b,c)

These were made with three different lengths of Nozzle A-5, as indicated by the sectional view in Figure 11. By successively truncating the nozzle, it was hoped that the effects of nozzle length on separation could be discerned from the effects of upstream supersonic flow structure. This nozzle was equipped with only two rows of pressure taps spaced 180-degrees apart.

Figure 37 shows the wall pressures for the longest configuration (A-5a). The symbols represent only one of the two rows of pressure taps - but for all values of $p_c/p_a > 1.9$, the pressure profiles for both rows of taps were virtually identical. The bumps in the full-flow portions of the curves for $p_c/p_a = 13.43$ and 21.51 were caused by flow disturbances due to a depression in the wall of the nozzle which was the result of a machining error. One sees that despite the disturbance, separation occurs at progressively lower values of wall pressure as the chamber pressure is raised.

Although data were acquired for the shorter configurations A-5b and A-5c, they are not presented here because the important points are effectively represented by the data for Nozzle A-6 (groove-free) which are presented next.

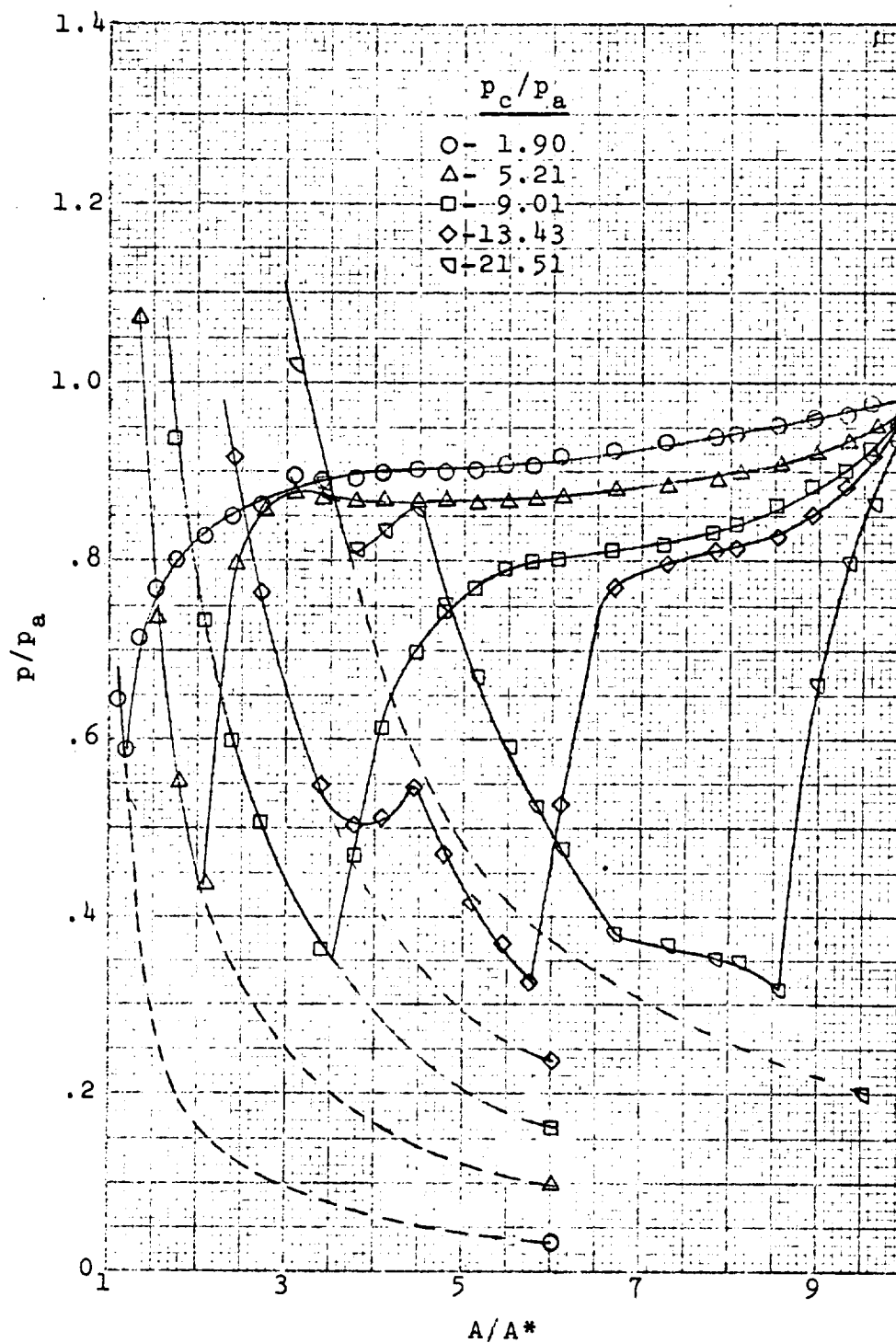


Fig.37. -- Wall static pressures;
Mach-4, contoured nozzle (A-5_a)

Mach-5 Contoured Nozzle (A-6a,b,c,d)

Figure 38 shows the wall-pressure profiles for the longest (A-6a) and the shortest (A-6d) configurations of the Mach-5 nozzle. The results for configurations A-6b and A-6c were intermediate to those shown in Figure 38. The chamber pressures for the two sets of curves are very similar. Thus, the effect of the nozzle length on pressure distribution can be observed directly by comparing curves having the same plotting symbol.

The important characteristic which is clearly demonstrated by the data shown in Figure 38 is that the longer nozzle length causes a reduction in the separation pressure and thereby forces an appreciably greater degree of over-expansion before separation occurs. It is also quite apparent that the pressure plateaus downstream of separation are lower in the long nozzle. It will be shown in Chapter VI that it is the latter effect which is responsible for much of the disagreement in separation correlations for conical and contoured nozzles.

Unsymmetrical flow behavior in the Mach-5 nozzle was detected by the use of tufts taped around the exit of the nozzle. In the range of chamber pressures between 28 and 70 psia ($1.8 < p_c/p_a < 4.7$) various degrees of asymmetry and instability were observed in the shorter Mach-5 nozzle (A-6d). At chamber pressures less than 28 psia the flow appeared to uniformly fill the exit, but the tufts would simultaneously fluctuate in and out of the nozzle at a

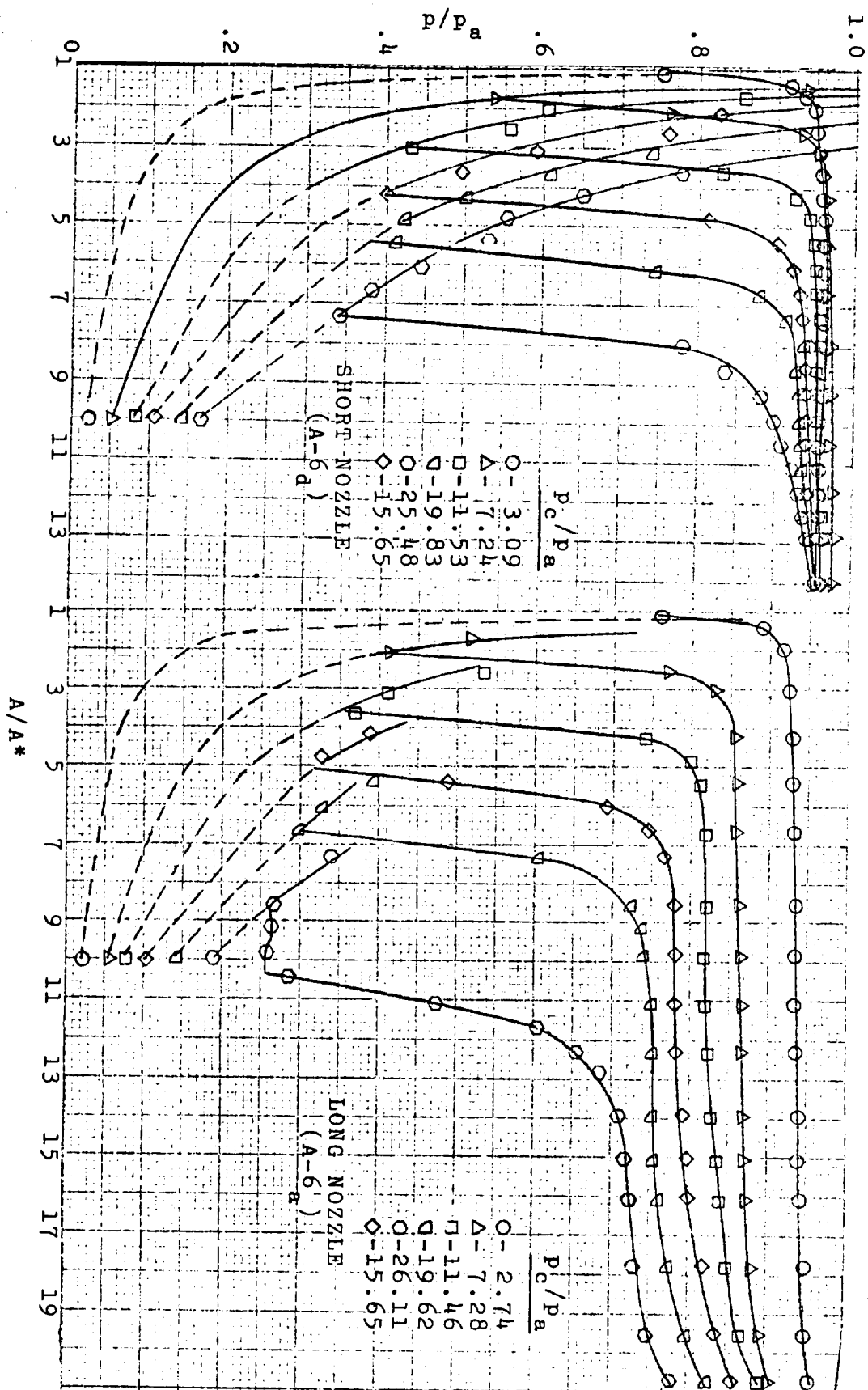


Fig. 38. -- Wall static pressures; Mach 5, contoured nozzle

rapid rate. When the chamber pressure reached 28 psia the flow was adjacent to the nozzle wall over approximately 55 per cent of the exit periphery. This percentage was steadily reduced as the pressure was raised. Throughout this range, fluctuations occurred, but switching from side to side occurred only for chamber pressures between 37 and 50 psia. The switching was most pronounced at a chamber pressure of 37 psia.

Oscillograph records for the contoured nozzle show pressure fluctuations of approximately 40-60 Hz downstream of the separation point over the entire range of chamber pressure from 0 to 365 psia. At various chamber pressures there are quiet zones in which the fluctuations are minimal. As the length of the nozzle increased, the amplitude of the fluctuations greatly increased. In some instances one can discern that the 30-60 Hz signal is modulated by a 5-10 Hz fluctuation of larger amplitude. Switching occurs with varied periodicity ranging from 2 per second to 1 per 6 seconds.

The data presented in this and the preceding chapter are representative of a much larger quantity of information gathered during the program. Approximately 2000 feet of movie film, numerous oscillograph records, and several hundred pressure-distribution curves form the basis for the representative information.

VI. ANALYSIS

Separation Pressure Ratios

Conventional correlation.-Figure 39 shows representative separation pressure ratios, (p_s/p_a) , for some of the axi-symmetric nozzles. Data for two-dimensional nozzles is presented in the next section. Figure 39 is the conventional method of presentation. The uncertainty associated with the separation pressure ratios for small chamber pressure ratios (p_c/p_a) is relatively high because the wall static-pressure gradient was large and because unsymmetrical flow occurred in this pressure regime. When separation pressure ratios are presented for unsymmetrical flow, the separation pressure ratio for the side of the nozzle for which separation first occurred is indicated.

Figure 39 shows that separation in the long Mach-5, contoured nozzle occurred at lower chamber pressures than in the 9 and 30-degree nozzles. In fact, the data correspond rather closely to those for the "longest contoured nozzles" of Figure 5 over the range of chamber pressures utilized. As mentioned previously, this effect is thought to be due to the production of a lower effective pressure downstream of separation which is caused by entrainment of air from the secondary-circulation region. On the other hand, the separation pressure ratios for the short, Mach-5 nozzle are greater

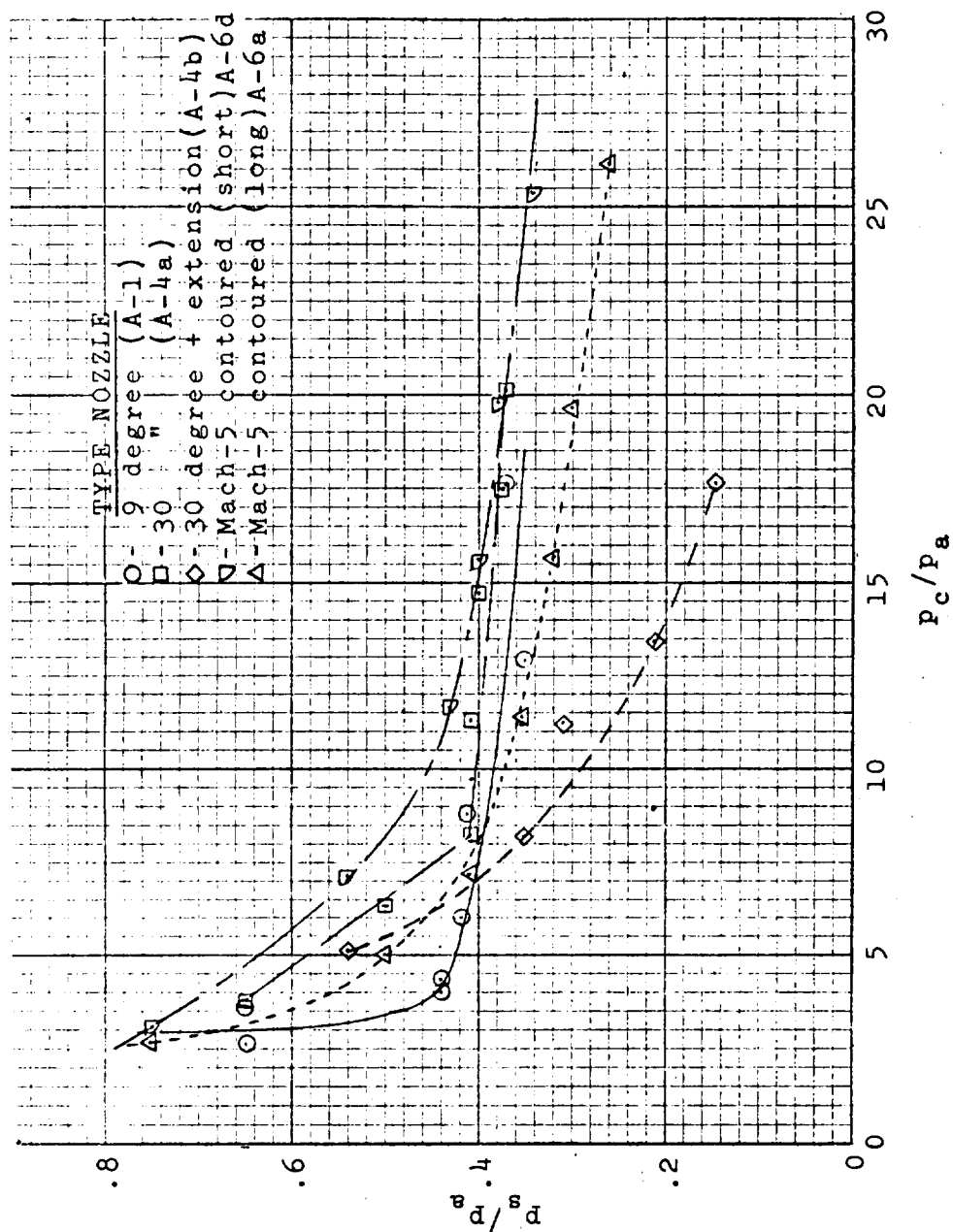


Fig. 39. --Separation correlation based on pressure ratio

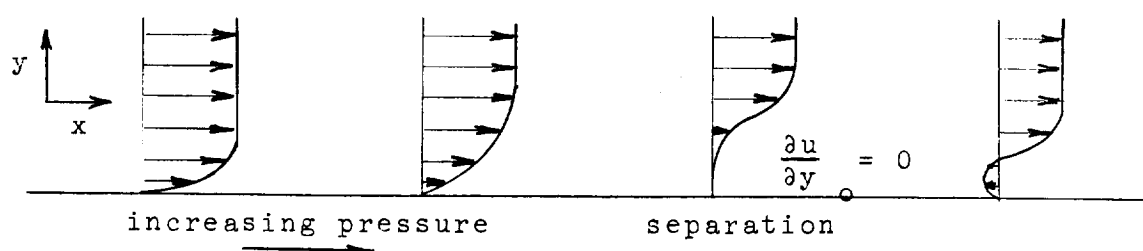
than for the conical nozzles. This result is in contrast with the data of Figure 5, but agrees qualitatively with the information presented in Reference 27.

Perhaps the major significance of Figure 39 is that it illustrates how poor the correlation between p_s/p_a and p_c/p_a can be. Clearly, a correlation which is based on the controlling physical factors is required.

Thermodynamic approach.-In seeking the proper physical model, two different approaches to the problem can be visualized. In the first approach, one would attempt to determine if an alternate solution to the flow problem other than the normal shock solution existed. In such an approach, one might assume that repetitive oblique shocks occur, and then attempt to develop a solution which conforms to a general law of nature - for example; such as determining the shock system which would satisfy the pressure constraints and at the same time, minimize the availability or some other appropriate thermodynamic variable. One of the discouraging factors about attempting a solution of this type, however, is the difficulty in formulating a model which would properly account for the known effects of the boundary layer - for example, such as the demonstrated effects of boundary layer suction in converting from an oblique to a normal shock pattern (29).

Boundary-layer-separation approach.-The second approach which is suggested by evidence such as that just mentioned is, of course, to regard the problem as being one of

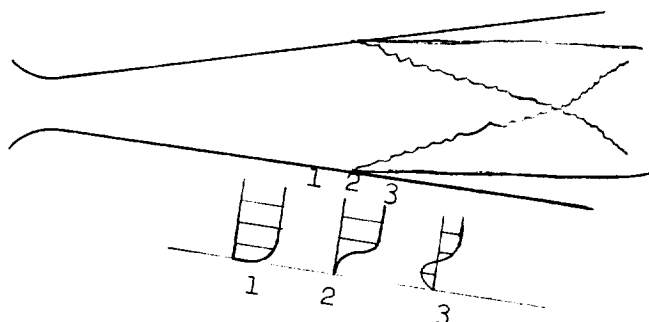
boundary-layer separation. In the usual separation problem, separation can occur if the flow encounters a positive pressure gradient. The velocity profile in the boundary layer gradually changes in the manner shown below. The point at which separation occurs



is defined by the point at which $\left(\frac{\partial u}{\partial y}\right)_{y=0} = 0$. In general, the

larger the free stream Reynolds number the blunter the velocity profile and the greater must be the adverse pressure gradient to cause separation.

For the case of separation in a nozzle, the problem is somewhat different because there is a discontinuity in pressure across the separation shock. The situation is illustrated below:



The fact that the pressure rise is for practical purposes, discontinuous, poses a problem in predicting the point of

separation from the boundary-layer equations since conventional techniques (32) require specification of a pressure gradient. Another factor of concern is that p_2 is not the pressure at the point of separation; nor is p_s , used previously.

In any event, when the separation process is viewed from the standpoint of the boundary layer, the important variables would seem to be the pressures in the immediate vicinity of the boundary layer on either side of the discontinuity, and the velocity profiles immediately before and after the discontinuity. The fact that it is the pressure just downstream of the discontinuity which is important is emphasized because, as has been shown previously, this pressure can differ significantly from the ambient pressure or the pressure at the exit plane of the nozzle.

As mentioned in Section 2, several models have been proposed to explain shock-boundary layer separation on flat plates. A rather successful semi-analytical procedure developed by Reshotko and Tucker (14) is based fundamentally on the fact that for supersonic speeds, the free-stream Mach number has a pronounced effect on the velocity profile in the boundary layer. Consequently, relationship between the Mach number and the velocity profile can be established and then the Mach number ratio (M_2/M_1) across a discontinuity can be determined as a function of the equivalent form factors, $H_i = \delta_i^*/\theta_i$, for incompressible turbulent boundary layers before and at the point of separation. The procedure is an

outgrowth of previous studies by Cohen and Reshotko (33), Stewartson (34), and Howarth (35). The objective is to transform the compressible boundary layer equations to the same form as the incompressible equations, and then utilize information for the separation of incompressible boundary layers to determine the appropriate form factors. The method is outlined below:

The compressible boundary layer equations are:

$$(1) \quad \frac{\partial(\rho u)}{\partial x} + \frac{\partial(\rho v)}{\partial y} = 0$$

$$(2) \quad \rho u \frac{\partial u}{\partial x} + \rho v \frac{\partial v}{\partial x} = - \frac{\partial p}{\partial x}$$

The friction term is not included specifically in the equations, but empirical velocity profiles which are the result of friction terms will be used later.

The stream function is defined as:

$$(3) \quad \psi_y = \frac{\rho u}{\rho_0}$$

$$(4) \quad \psi_x = - \frac{\rho v}{\rho_0}$$

and the coordinates are transformed following the method of Stewartson (34) to:

$$(5) \quad dX = \frac{c_\infty}{c} \frac{p_\infty}{p_0} dx$$

$$(6) \quad dY = \frac{c_\infty}{c_0} \frac{\rho}{\rho_0} dy$$

Where X and Y represent transformed coordinates such that

$$(7) \quad U = \psi_Y$$

$$(8) \quad V = \psi_X$$

U and V are the transformed velocities, c is the speed of sound, the subscript ∞ refers to the free stream value external to the boundary layer, and o refers to the stagnation value. By applying equations 3 through 7 to the momentum equation and employing the first law for adiabatic flow in differential form to the potential flow,

$$\frac{\partial h_o}{\partial x} = 0 = \frac{\partial}{\partial x} \left(h + \frac{u_\infty^2}{2} \right)$$

the transformed continuity and momentum equations become:

$$(10) \quad U_X + V_Y = 0$$

$$(11) \quad UU_X + VU_Y = U_\infty U_{\infty X}$$

These equations are the same as for incompressible flow. Thus, U , V , X , and Y can be regarded as incompressible coordinates. In a similar fashion, the momentum and displacement thicknesses,

$$(12) \quad \theta = \int_0^\delta \frac{\rho u}{\rho_e u_e} \left(1 - \frac{u}{u_\infty} \right) dy$$

and

$$(13) \quad \delta^* = \int_0^\delta \left(1 - \frac{\rho u}{\rho_\infty u_\infty} \right) dy$$

are transformed to:

$$(14) \quad \theta_i = \int_0^{\delta_i} \frac{U}{U_\infty} \left(1 - \frac{U}{U_\infty}\right) dY$$

and $(15) \quad \delta_i^* = \int_0^{\delta_i} \left(1 - \frac{U}{U_\infty}\right) dY$

where the subscript i refers to the transformed variable which corresponds to the incompressible case. In the development of the transformed displacement thickness, the Crocco relationship for the static temperature distribution in the boundary layer is employed, and is

$$(16) \quad \frac{t}{t_\infty} = \frac{t_s}{t_o} \left(1 + \frac{\gamma-1}{2} M^2\right) - \frac{\gamma-1}{2} M^2 \left(\frac{u}{u_\infty}\right)^2,$$

where t_s is the stagnation temperature corresponding to the static temperature t , Equation 16, and the assumption of constant pressure across the boundary layer, is used to eliminate the density terms from Equation 13.

The original and transformed form factors are:

$$(17) \quad H = \delta^* / \theta$$

and

$$(18) \quad H_i = \delta_i^* / \theta_i$$

Consequently, the relationship between these factors becomes:

$$(19) \quad H = H_i \left(1 + \frac{\gamma-1}{2} M^2\right) + \frac{\gamma-1}{2} M^2$$

The transformed continuity and momentum equations can be

manipulated into the following form:

$$(20) \quad [U(U_\infty - U)]_X - [V(U_\infty - U)]_Y + U_\infty X (U_\infty - U) = 0,$$

where $[\quad]_X$ indicates differentiation with respect to the indicated variable.

When Equation 20 is multiplied by Y and integrated with respect to Y across the transformed boundary layer, there results:

$$(21) \quad dH_i = - \frac{dU_\infty}{U_\infty} \frac{H_i (H_i^2 - 1) (H_i + 1)}{2}$$

It can be shown that this relation is also valid for axisymmetric flow.

Fortunately, the equation is separable, and when U_∞ is transformed to Mach number, M , and Equation 21 is integrated, the following equation results:

$$(22) \quad M = \frac{k H_i^2 e^{1/(H_i + 1)}}{(H_i^2 - 1)^{1/2} (H_i + 1)} = k f(H_i) \quad \begin{array}{l} \text{where:} \\ k = \text{integration} \\ \text{constant} \end{array}$$

Thus, a relationship is developed between Mach number and the form factor for incompressible flow. Knowledge of the upstream form factor $(H_{i,1})$ and the form factor at separation $(H_{i,2})$ then permits one to determine the ratio of Mach numbers across the discontinuity; i.e.,

$$\frac{M_2}{M_1} = \frac{f(H_{i,2})}{f(H_{i,1})}$$

Once the Mach number ratio is known, the static pressure ratio across the shock producing the discontinuity can be determined from the two-dimensional shock relations (36)

$$(24) \quad \frac{p_2}{p_1} = \frac{-M_1^2(\gamma+1)(B^2-1)/[2B^2M_1^2(\gamma-1)+4] \pm \{M_1^4(\gamma+1)(B^2-1)^2 + 4[BM_1^2(\gamma-1)+2][M_1^2(\gamma-1)+2]\}^{1/2}}{2B^2M_1^2(\gamma-1)+4}$$

Where $B = M_2/M_1$.

For turbulent boundary layers with zero pressure gradient, the form factor $H_{i,1}$, generally lies in the range from 1.22 $\left[\frac{u}{u_\infty} = (y/\delta)^{1/9} @ Re_L \approx 10^8 \right]$ to 1.40 $\left[\frac{u}{u_\infty} = (y/\delta)^{1/5} @ Re_L \approx 10^5 \right]$.

With a negative pressure gradient such as is encountered in nozzles, the form factor, $H_{i,1}$, would be somewhat lower than for flow with zero pressure gradient. The form factors at separation (defined as the location where $\left(\frac{\partial u}{\partial y}\right)_{y=0} = 0$) generally lie between 1.8 and 2.8 (37, 38, 39). Since we are interested in conditions downstream of separation, it is reasonable to assume that the effective form factor will be at the high end of this range or greater. However, the exact numerical value of $H_{i,2}$ is of small consequence because:

$$1.0 < \frac{f(H_{i,2})}{k} < 1.03 \text{ for } H_i > 2.6. \text{ (from Equation 22).}$$

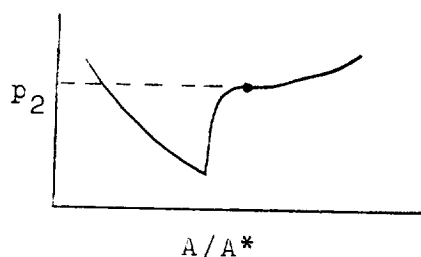
That is, the Mach number corresponding to the form factor is about the same for all $H_i > 2.6$

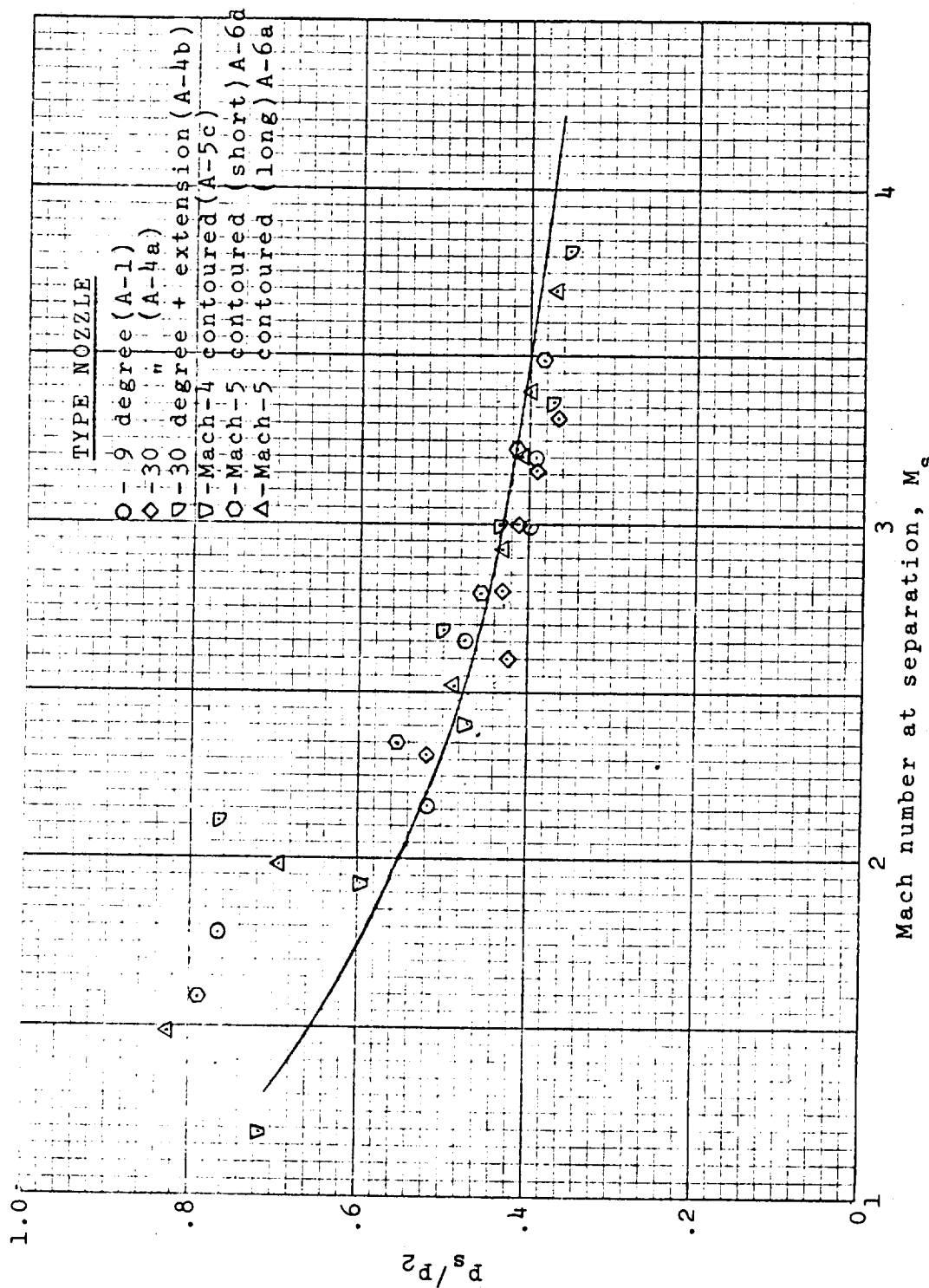
If it is supposed that $\frac{(H_{i,2})}{k} = 1.015$ then the following Mach number ratios across a discontinuity result from Equation 23.

$H_{i,1}$	M_2/M_1
1.1	0.495
1.2	0.650
1.3	0.741
1.4	0.805

Thus, a value of $0.650 \leq \frac{M_2}{M_1} \leq 0.805$ would be reasonable. Love (40) correlated the peak pressure rise downstream of separation of a turbulent boundary layer on flat plates with Reynolds Numbers of about 10^7 quite well with a value of $M_2/M_1 = 0.762$. The values of Re_L for much of the experimental data of this report was approximately 10^6 , so a value of $H_{i,1} \approx 1.4$ and $M_2/M_1 \approx 0.8$ would be reasonable.

Agreement between experimental data and separation model.—Figure 40 shows the ratio p_s/p_2 as a function of the Mach number at separation, M_s . Here, p_2 , is the pressure immediately downstream of the discontinuity (shock) and is taken to be the value just downstream of the knee in the pressure rise in the plots of p/p_a vs A/A^* as indicated below.





This value is somewhat arbitrary, but in most instances there was reasonable confidence that the downstream pressures could be distinguished from the pressures in the shock-boundary layer interaction zone. The Mach number at separation, M_s , corresponds to the Mach number in the stream tube just outside the boundary layer. This value was determined from the isentropic flow relation:

$$M_s = \left\{ \frac{2}{\gamma-1} \left[\left(\frac{p_s}{p_o} \right)^{\frac{1-\gamma}{\gamma}} - 1 \right] \right\}^{\frac{1}{2}}$$

where p_s and p_o were measured values.

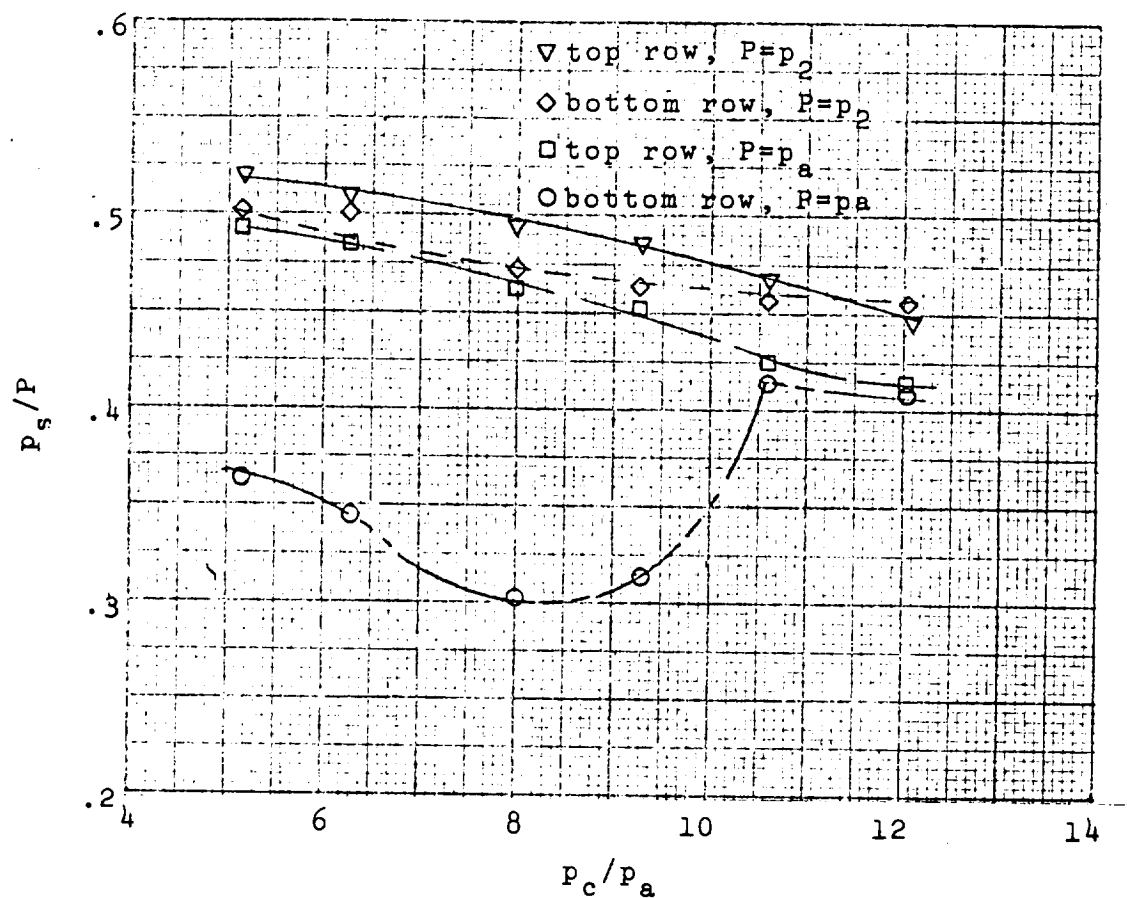
The analytical values of the separation pressure ratios determined from Equation 24 for $M_2/M_s = 0.8$ are also shown in Figure 40. The agreement seems to be amazingly good except at the lower Mach numbers which occur just downstream of the throat and lie in the unstable and unsymmetrical flow regime. There is a tendency for the points to fall below the curve as the Mach number increases. However, this behavior is compatible with the fact that the Reynolds number increases with distance down the nozzle and the initial boundary layer velocity distribution becomes blunter and more resistant to separation.

One is led to the conclusion that the same factors which govern separation of boundary layers on flat plates also govern the separation of boundary layers in nozzles. It follows that the nozzle contour is not an important factor except as it affects the x pressure gradient and the

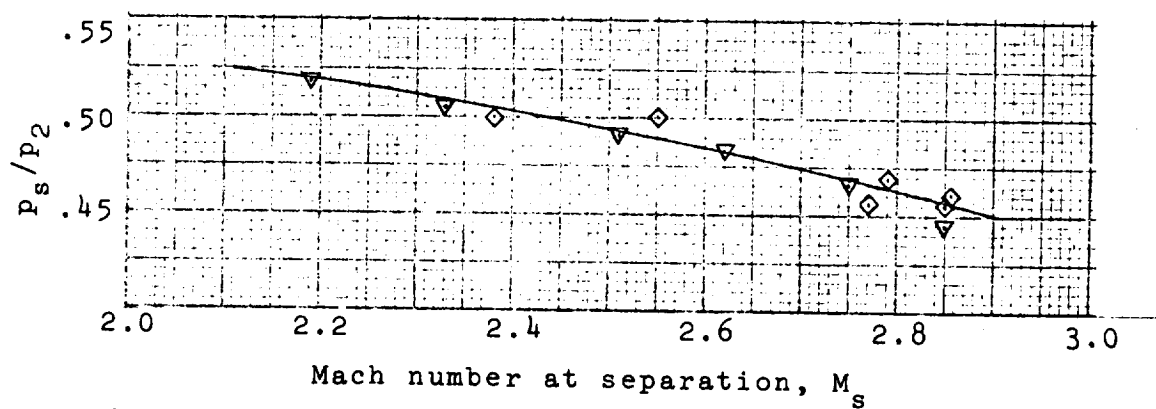
freestream Reynolds and Mach numbers adjacent to the boundary layer. Also, one must know the static pressure in the secondary circulation region just downstream of separation. Knowledge of this pressure requires a solution to the entrainment problem which is dependent on the characteristics of the jet and the nozzle contour downstream of separation.

Correlation for 10-degree, two-dimensional nozzle.-

As a further test of the concept that the pressure immediately downstream of separation is a controlling influence on the separation location, the same type of correlation employed for the axi-symmetric nozzles in Figure 40 was applied to separation on both sides of the 10-degree, two-dimensional nozzle. Figure 41 shows the results. This application is considered to be a rather severe test because, as indicated in Figures 14 and 15, the separation positions and pressures were quite different on the opposite walls over most of the range of chamber pressures because the flow attached to one wall. This condition is reflected by the circular and square plotting symbols in Figure 41a. The diamond and triangular plotting symbols in Figure 41a show a greatly improved correlation when the pressure just downstream of separation is used as the criterion, and Figure 41b shows a further improvement when Mach number is employed as the independent variable. These values correspond very well with the separation correlation presented in Figure 40. The separation behavior in the other two-dimensional nozzles is in general accord with these findings.



a. based on chamber-pressure ratio



b. based on Mach number

Fig. 41. --Separation correlations for 10-degree, two-dimensional nozzle

In addition to providing greater confidence in the separation model, the correlation between separation Mach number and pressure ratio across the separation shock could be useful in understanding the behavior of some types of supersonic fluid switches. In switch applications in which supersonic flow fills the entire channel before adhering to one of the walls, the mechanics of the flow deflection would be governed by separation considerations. With an established relation between separation Mach number and pressure ratio across the separation shock, the problem is essentially reduced to determining the pressure just downstream of separation. Thus, such factors, as the effect of back loading and the rate at which control flow must be introduced into the pocket just downstream of separation to cause switching, become more tractable.

Two-Dimensional Flow Structure

It is of interest to determine how well the shock and flow angles which can be observed from schlieren photographs of the two-dimensional nozzles agree with those which are predicted from the separation model. Figure 42 shows the shock angles predicted for the separation model, and those measured for the 10 and 30-degree nozzles. The shocks in the wide-angle, contoured nozzle (D-4) were characterized by substantial curvature near the wall. Thus, there was considerable uncertainty associated with the measurement of the shock angles. Because of this uncertainty, numerical data is not

90

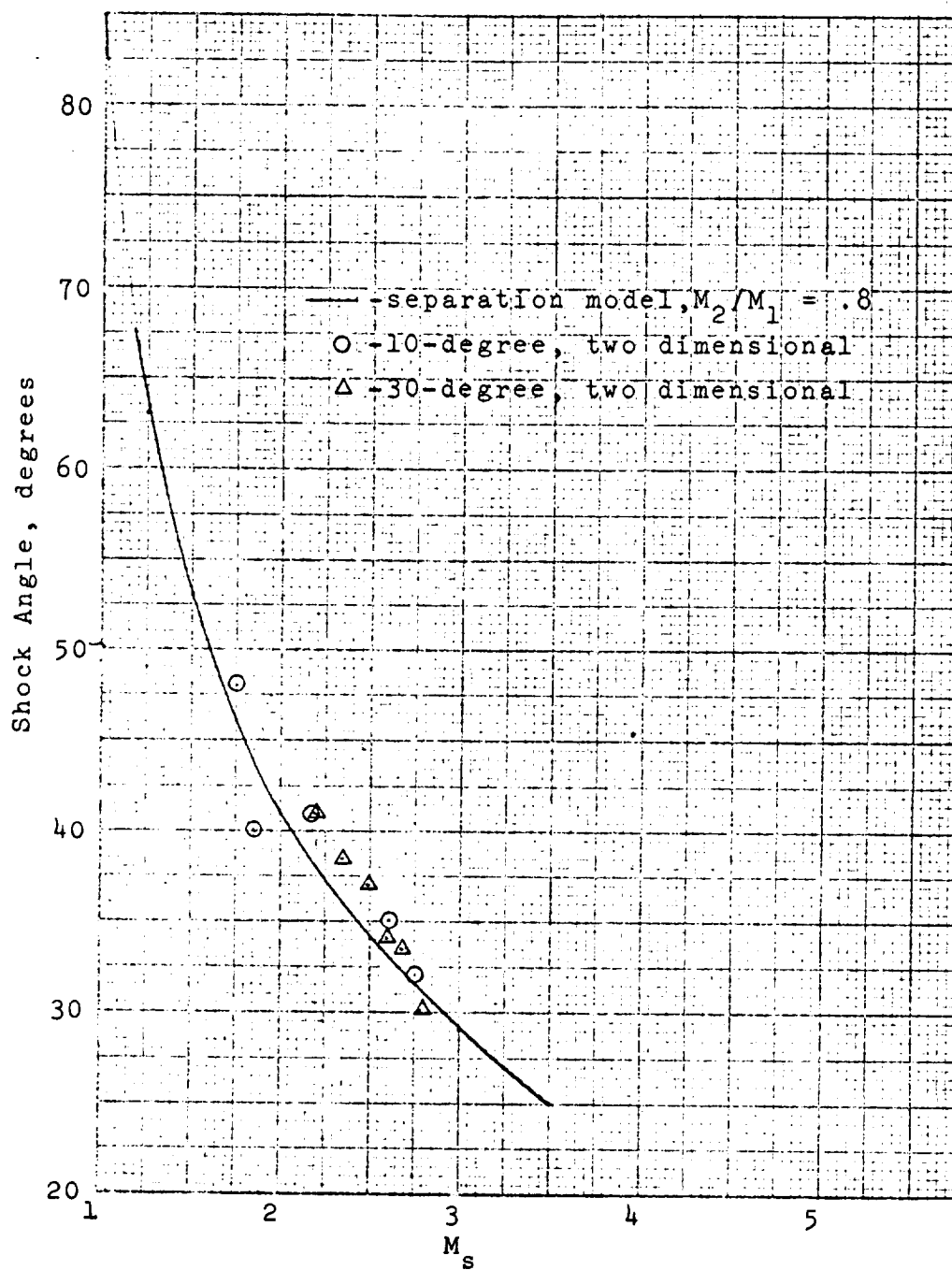


Fig. 42 --Separation-shock angles

presented. However, the angles were judged to be about the same as or perhaps somewhat greater than those for the 30-degree nozzle. From the data of Figure 42, the conclusion is reached that the visible evidence of the flow structure is in moderately good accord with the separation model.

A direct comparison of the flow turning angles was also desired. However, the edge of the flow field is difficult to determine precisely from schlieren photographs, and there is uncertainty associated with which part of a photograph represents a region of subsonic mixing and which part is supersonic flow. Consequently, no attempt is made to display such data.

Another aspect of the two-dimensional flow worth noting is the flow behavior for sharp-cornered nozzles at low chamber pressures. When the throat exit is a sharp corner, the flow will discharge from the throat as an underexpanded or overpressured supersonic jet without attaching to the nozzle walls until a certain value of chamber pressure is reached. For the 30-degree and the Mach-5 nozzles, this pressure could be approximately determined by assuming that the static pressure on the wall just downstream of the throat at attachment was $0.45 p_a$. This value is somewhat lower than that required by the separation relationship for separation at the Mach number corresponding to the Prandtl-Meyer expansion for the throat angle. As an example of determining the chamber pressure ratio for attachment, the Mach number corresponding to the throat expansion associated with the

30-degree nozzle is 2.13. The ratio of static to stagnation pressure at this Mach number is $\frac{p}{p_o} = 0.104$. Therefore:

$$p_o/p_a = \frac{p/p_a}{p/p_o} = \frac{0.45}{0.104} = 4.33$$

The measured value was approximately 4.0.

The foregoing is offered only as an approximation. The physical circumstances are that the flow from the throat behaves as an underexpanded jet discharging into a region of lower pressure until the expansion angle associated with this type of flow approaches that of the wall. Probably, entrainment causes a reduction in pressure experienced by the jet very close to the throat, and this reduced pressure forces further expansion. As indicated by the curve for $p_c/p_a = 4.18$ in Figure 19, and by similar curves for other nozzles, the nature of the pressure recovery is different than for the conventional boundary layer separation. As mentioned previously, a strong disturbance occurs in the stream which causes it to break up and become unstable just at the value of chamber pressure where the flow attaches to the wall. The ensuing mixing action downstream causes a gradual pressure rise along the nozzle wall.

Unstable and Unsymmetrical Behavior

General model.—To a certain extent, the unsymmetrical flow structure in the axi-symmetric nozzles can be surmised from the pressure profiles such as represented in

Figure 26b and 27a, and from the appearance of the exhaust. Figure 43 shows the flow pattern surmised from this evidence. The flow structure is quite similar to that for the two-dimensional nozzles except that oblique events become conical events in the axi-symmetric nozzle. In the unsymmetrical regime, separation first occurs only in a small region of the nozzle. A conical separation shock emanates from the point of separation and appears as in sectional view A-A₁ of Figure 43. If the pressure disturbance causing separation occurs over a substantial area of the periphery rather than at a point, the shock appearance will be more like that shown in the sectional view, A-A₂. The flow is turned in the same manner as the shock but through a smaller angle.

Separation from the opposite side of the nozzle is delayed because the downstream pressure is lower due to greater entrainment caused by the flow being in closer proximity to the wall on that side of the nozzle. This concept, that the local point of separation is determined by the local downstream back pressure, is important to understanding unsymmetrical and unstable flow behavior. The validity of this conclusion tends to be supported by the fact that pressure rises indicated by the diamond plotting symbols in Figures 26a and 27a agree with the separation pressure correlations presented previously.

In arriving at the conclusion that the unsymmetrical

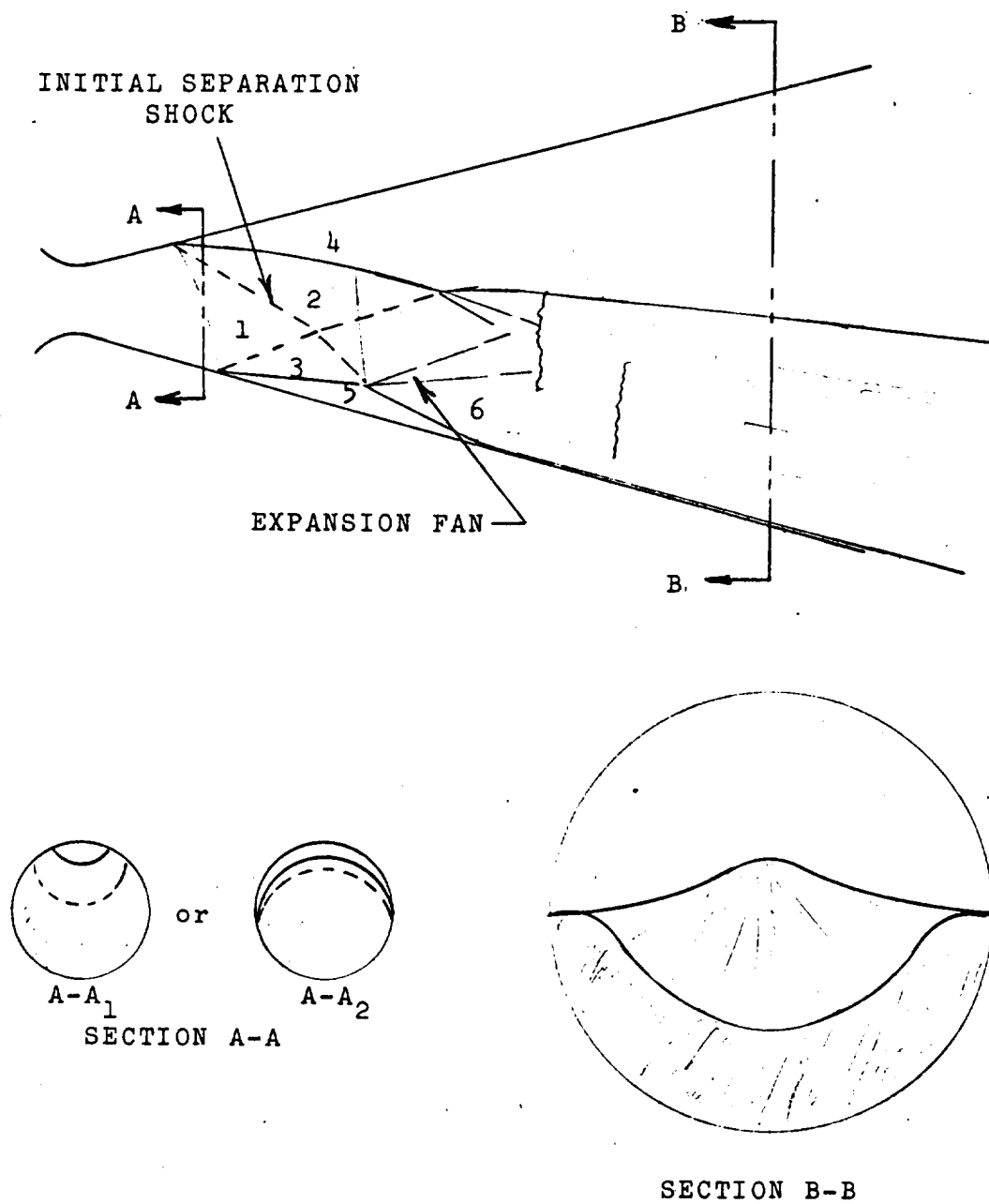


Fig. 43. --Flow structure in axis-symmetric nozzles

flow behavior is a separation phenomena of the type described above, some other possibilities had to be eliminated. One of these possibilities is that normal shocks occur and the flow downstream of the shocks becomes subsonic and attaches to a side of the nozzle. The fact that the flow follows the complete expansion curve on three sides of the nozzle after a pressure rise occurs on the other side (See Figure 27) tends to eliminate this possibility. But a better indication is the fact that the pressure rise downstream of the initial disturbance is much less than that which would be produced by a normal shock at the Mach number associated with the static pressure at separation.

Possibility of double solution.-A second possibility which is of particular concern to the stability problem is that the flow equations may have a double solution over a range of chamber pressures. Specifically, it is of interest to determine if there is more than one position in the nozzle for a given chamber pressure which will satisfy the separation criteria. Such a condition could result if the functional relationship between the ratio of local static wall pressure to back pressure p/p_a and free stream Mach number established by the nozzle flow equations satisfies the separation-pressure-ratio relationship of Figure 41 for more than one value of Mach number. If one assumed that the flow is isentropic in the stream tube just outside the boundary layer, then for that stream tube:

$$p/p_o = (1 + \frac{\gamma-1}{2} M^2)^{\frac{\gamma}{1-\gamma}}$$

for all nozzle shapes. Thus,

$$p/p_2 = (p_o/p_2) \left(\frac{p}{p_o} \right) \approx \frac{p_c}{p_2} \left(1 + \frac{\gamma-1}{2} M^2 \right)^{\frac{\gamma}{1-\gamma}}$$

Figure 44 shows this relationship for several values of p_c/p_2 . Also shown, is the separation correlation determined previously and a correlation of typical pressure ratios for separation of laminar boundary layers.

The major significance of Figure 44 is that, if the boundary layer is either wholly laminar or wholly turbulent throughout the nozzle, there is only one separation position for a given chamber pressure (the point where the curves intersect). However, this conclusion is valid only if the pressure downstream of separation is the same on all sides of the nozzle.

Effect of boundary layer transition.—On the other hand, if there is a transition from laminar to turbulent flow within the nozzle, a slight asymmetry in the transition (which could be caused by variations in local roughness) could cause unsymmetrical flow even if the pressure is uniform around the periphery of the jet just downstream of separation.

It is hazardous to apply a simple mathematical criterion such as Reynolds number to determine the point of transition in a nozzle. In general, the favorable pressure gradient will tend to stabilize the boundary layer whether it is laminar or turbulent. Bartz (41) showed that because of the favorable pressure gradient in the subsonic portion of the nozzle, the boundary layer is very thin near the throat

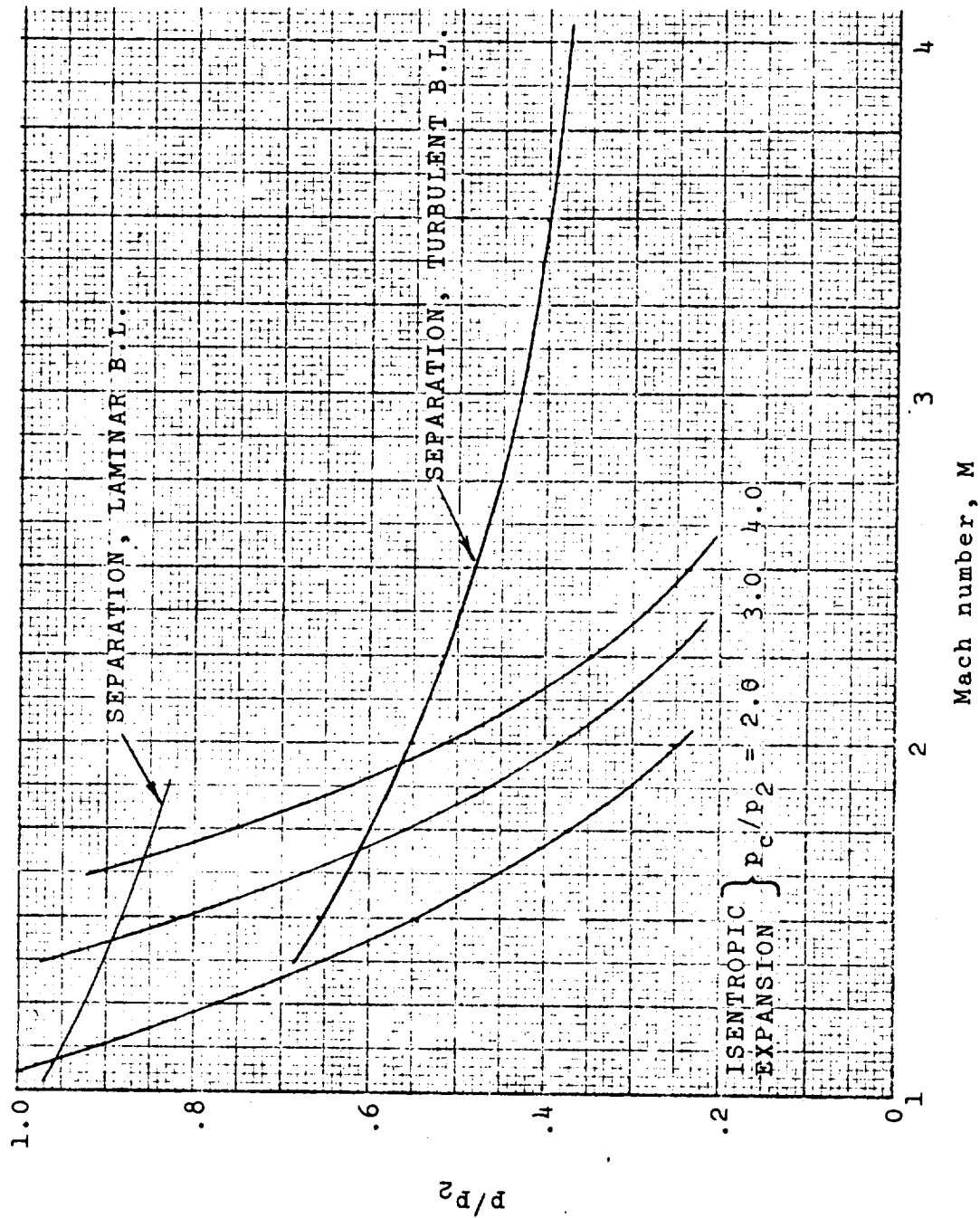


Fig. 44. --Illustration of the possibility of a double solution to the nozzle-flow and separation equations

regardless of the boundary-layer conditions upstream of the throat. Consequently, the assumption that the boundary layer starts to grow at the throat is not a bad one. However, Bartz's analysis is based on a developed turbulent boundary layer throughout the nozzle, so his results really are not applicable to the transition problem. A more valid approach, suggested by Kays (42) is to assume that a laminar boundary layer starts to grow at some point upstream of the throat and then compute the momentum displacement thickness as a function of position. The suggested criterion for transition is that $\frac{u_{\infty} \theta}{\nu} = 320$.

Despite the pitfalls which may be involved, it was of interest to determine the separation pressure ratios as a function of Reynolds number. Reynolds number based on both length and diameter were computed. For length Reynolds numbers, the assumption was made that the origin of coordinates was the location of the minimum throat diameter. Figure 45 shows a plot of the pressure rise coefficient, P , as a function of length Reynolds number, Re_L , where:

$$\frac{p_2 - p_s}{\frac{1}{2} \rho_s \bar{u}_{\infty s}^2} = \frac{p_2/p_o - 1}{\frac{1}{2} \gamma M_s^2}$$

The straight lines are correlations given by Shapiro (43) for separation of turbulent and laminar boundary layers. The laminar line is based on the "foot" pressure rise which is associated with the separation of laminar boundary layers.

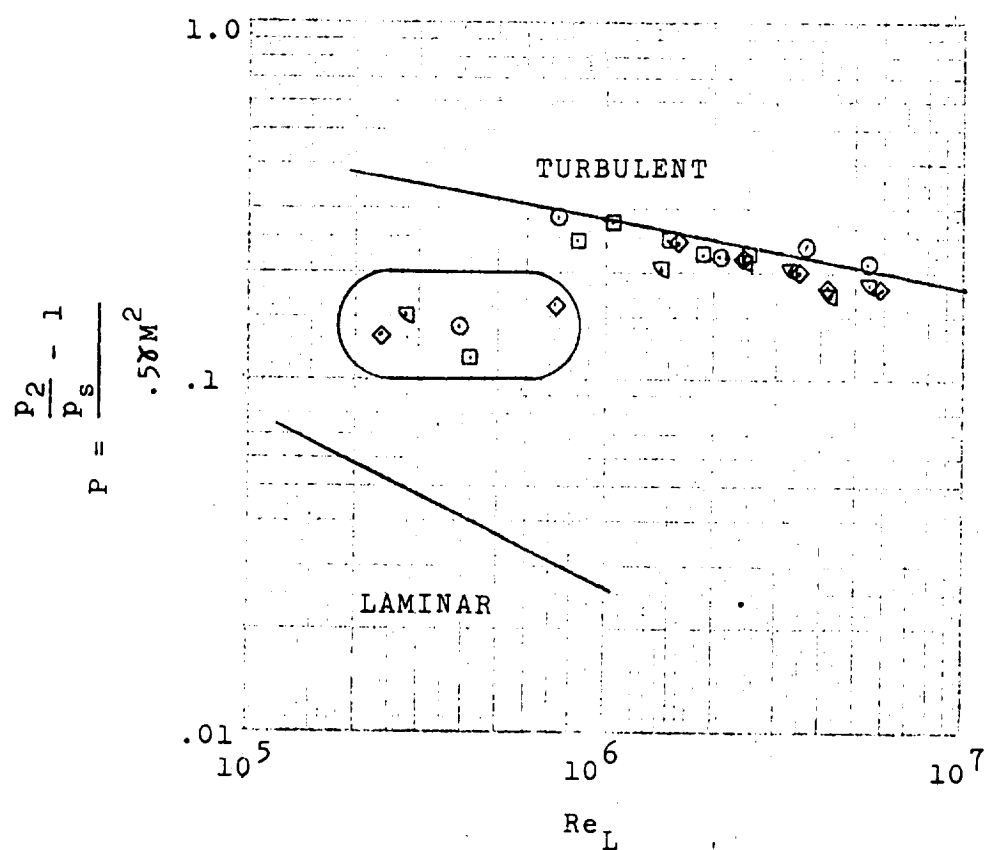


Fig. 45. --Separation correlation based on Reynolds number [after Shapiro(44)]

This pressure rise is lower than the pressure-rise across the compression shock caused by the thickening of the boundary layer. The pressure-rise coefficient based on peak pressure more nearly corresponds to the pressure rise across the separation shocks. This value is approximately 0.1 and is moderately independent of Reynolds number up to a value of approximately 10^6 where transition to a turbulent boundary layer usually occurs on a flat plate with no velocity gradient in the x direction.

The encircled points all correspond to unsymmetrical flow conditions, and the other points correspond to symmetrical flow. Consequently, this representation provides some evidence that the unsymmetrical separation may have been triggered by the transition from a laminar to a turbulent boundary layer.

As a further check on this matter, the inside surface of some of the plastic nozzles was coated with a volatile oil (oil of cloves) to provide a visible indication of boundary layer transition. The principle of operation was that in the region of the turbulent boundary layer, the oil would be evaporated from the surface in a relatively short period of time, while very little evaporation would occur in the laminar region. The results were inconclusive. For chamber pressures just above those associated with unsymmetrical flow, evaporation appeared to occur uniformly and rapidly downstream of the throat, but did not evaporate upstream of the throat. When the chamber pressure was lowered

to that of the unsymmetrical flow regime, evaporation did not occur either upstream or downstream of the throat. If there is any conclusion from the test, it is that transition occurred at the throat when the chamber pressure was above the unsymmetrical flow regime and that the flow was laminar to the point of separation in the unsymmetrical regime. However the evidence is considered to be too questionable to serve as a basis for definite conclusions.

Another check that was made was to investigate the symmetry of flow in a nozzle having an appreciably larger throat diameter than employed for the previous tests. Since the Reynolds number based on length can be expressed as

$$Re_L = \frac{\dot{w}}{\mu} \frac{A^*}{A} x$$

and because \dot{w}/A^* depends only on the upstream stagnation pressure and temperature, the value of Re_L will be greater in the large nozzle than in the small nozzle at the same value of chamber pressure because the value of x will be greater at the same A/A^* . Consequently, if unsymmetrical flow is associated with boundary layer transition, the conversion from unsymmetrical to symmetrical flow should occur at a lower pressure in the larger nozzle. This is what occurred. The larger nozzle had a throat diameter of 1.070 inches as compared to 0.4 to 0.6 inches for the nozzle discussed previously, a diverging half angle of 13 degrees, and

an overall area ratio of 3.6 as compared to 7.3 for the 9 and 15-degree conical nozzles. For values of $p_c/p_a < 1.4$, the flow was unstable in much the same manner as described previously. Above this value, the flow stabilized and appeared to be symmetrical. It will be recalled that unstable and unsymmetrical flow occurred for $1.5 \leq p_c/p_a \leq 3.7$ for the nozzles of smaller throat diameter.

Further evidence to the effect that boundary layer transition may have been associated with the flow behavior at low chamber pressures is provided by the shadowgraphs of flow in the 10-degree, two-dimensional nozzle shown in Figure 46. The exposure time was in the order of 20 microseconds, and was sufficiently short to resolve action which had previously registered as blurs in longer-exposure photographs. These photographs cover values of p_s/p_a ranging from 1.88 to 3.72. Over most of this range of chamber pressures, the high-speed motion pictures revealed rapid movement of the separation shocks, as described previously. The flow became steady when the chamber pressure reached approximately 55 psia.

The shadowgraphs provide additional insight regarding the shock and flow structure associated with this behavior. One observes that numerous compression waves precede the point of separation and that the turning angle of the flow is relatively small at low values of p_c/p_a . The "gradual-type" of separation is typical of laminar boundary layers; particularly in transonic flow (47). The first



a. $p_c = 30$ psia

b. $p_c = 34$ psia



c. $p_c = 45$ psia

d. $p_c = 55$ psia

Fig. 46. --Shadowgraphs of flow in 10-degree,
two-dimensional nozzle

normal shock downstream of separation in Figure 46b occurs at approximately the correct position for the pressure rise across the shock to be from the isentropic expansion value to atmospheric. The formation of normal shocks across the detached supersonic stream has a destabilizing effect because greater turbulent mixing downstream of the shocks causes greater entrainment and enhances the opportunity for downstream pressure fluctuations. When the pressure becomes 55psia, the separation shocks occur at a single location, the turning angle becomes greater, and the shocks become more sharply defined, in a manner which is more characteristic of the separation of a turbulent boundary layer.

Flow deflection as a normal consequence of the interaction between separation and entrainment.—Although there is considerable evidence to the effect that unsymmetrical and unstable flow in the axi-symmetric nozzles was a consequence of separation of a laminar or transitional boundary layer, a case can also be built for unsymmetrical and unstable flow behavior due to separation of purely turbulent boundary layers. The influence of Mach number on the form factor of the compressible, turbulent boundary layer is such that the pressure rise required for separation progressively decreases as the Mach number decreases. Consequently, the turning angle of the flow as it traverses the shock also decreases as the Mach number decreases. From two-dimensional shock theory, the turning angle is:

$$\Delta = \tan^{-1} \left\{ \frac{\xi - 1}{\gamma M_s^2 - \xi + 1} \left[\frac{2\gamma M_s^2 - (\gamma - 1) - \xi(\gamma + 1)}{\xi(\gamma + 1) + \gamma - 1} \right]^{\frac{1}{2}} \right\}$$

where: $\xi = p_2/p_s$

Figure 47a shows the dependence of turning angle, Δ , on Mach number for values of ξ based on an assumed Mach number ratio across the separation shock, $M_2/M_s = 0.8$. This relationship becomes more significant when chamber-pressure ratio, p_c/p_a is the independent variable. Such a relationship follows from:

$$(1) \quad p_s/p_2 = f\{M_s(M_2/M_s)\}$$

Figure 42

$$(2) \quad p_o/p_s = \left(1 + \frac{\gamma - 1}{2} M_s^2\right)^{\frac{\gamma}{\gamma - 1}}$$

isentropic flow

$$(3) \quad p_o/p_2 = (p_o/p_2)(p_s/p_2) \approx p_c/p_2$$

Figure 47b shows the relationship between flow turning angle and p_c/p_2 . In many instances $p_c/p_2 \approx p_c/p_a$. This relationship, perhaps more than any other, reveals the reason for the flow peculiarities at low chamber pressures, because it demonstrates that a small change in the value of p_c/p_2 can greatly alter the flow turning angle at low values of chamber pressure. Therefore, relatively small differences in the value of p_2 on opposite sides of the jet can cause relatively large differences in turning angle on opposite sides of the jet when the value of p_c/p_a is small.

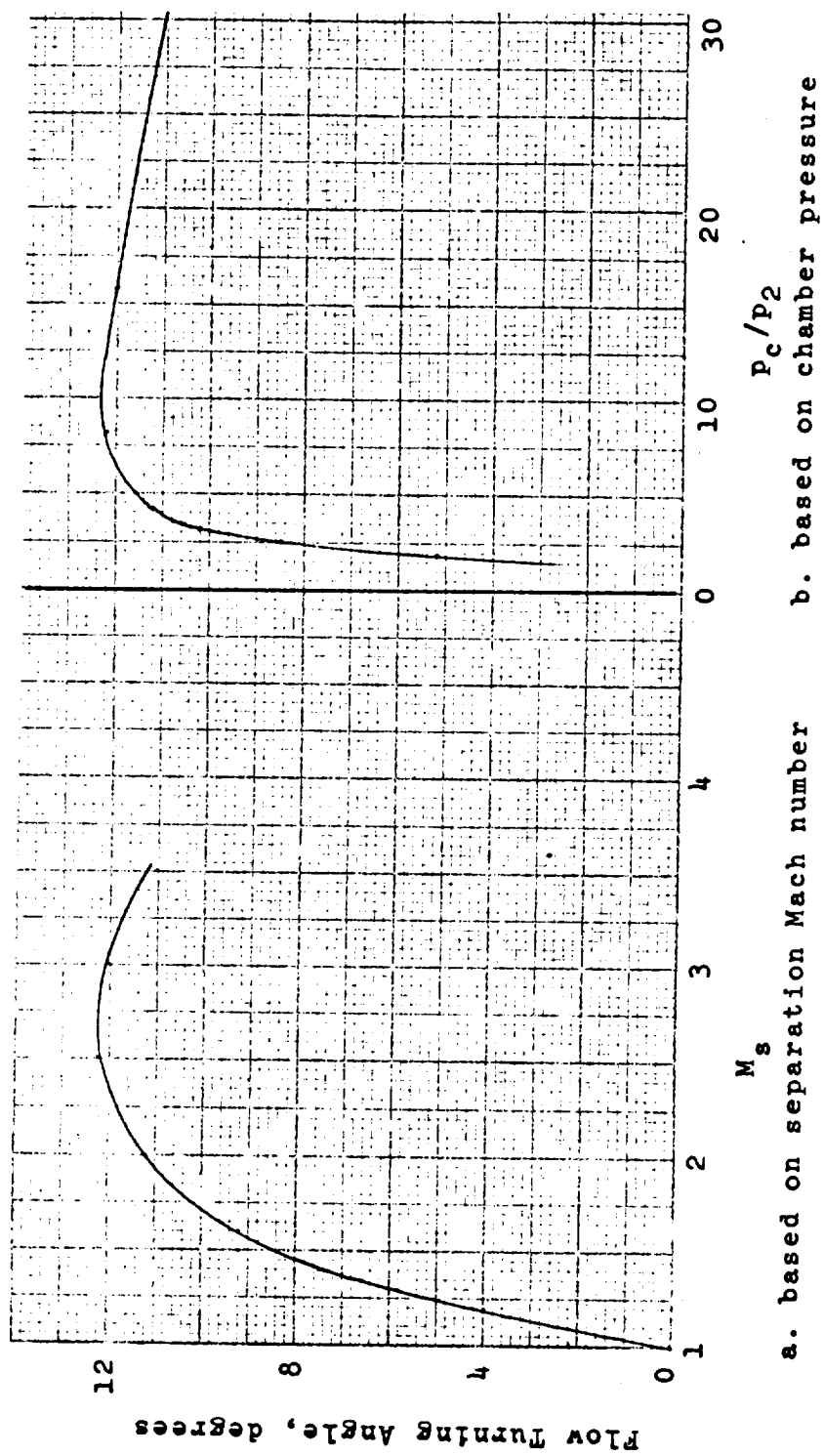


Fig. 47. --Flow turning angle at separation

When the wedge angle between the jet and the wall is small, as it is for low values of chamber pressure, the ratio of surface area for entrainment (jet surface area) to the cross-sectional area for secondary flow becomes large, and this causes a reduction in the pressure in the secondary circulation region. A deflection of the jet away from the axis causes a change in this ratio which then causes a reinforcing pressure differential across the jet which, in turn, tends to produce a further increase in the deflection. Once the lower pressure on one side of the secondary circulation region occurs, the supersonic flow is forced to expand further on that side before separating than on the high-pressure side. The resulting shock structure causes a net deflection of the flow toward the low-pressure side. The small wedge angles are also the probable cause of the flow instabilities because the flow can satisfy two conditions. One condition is that of separating "upstream" with a small turning angle and the other is the reduced pressure causing separation further downstream at a higher Mach number and larger flow turning angles. Since the occurrence of the second condition tends to destroy the circumstances which caused it there is a tendency for the flow to switch from one condition to the other.

Intuitively, one suspects that for a given nozzle, there is a maximum flow rate that can be deflected in this manner before the momentum flux in the jet exceeds the pressure differential available to cause deflection. A proper

analysis of the problem would involve a two-step iteration of which one part would consist of determining the supersonic flow field downstream of the shock-boundary layer interactions for assumed values of static pressures downstream of the interaction. The second part would be to solve the jet entrainment problem for the resulting configuration of the supersonic jet to determine what the pressures downstream of separation should be. The pressures would then be modified and the process would be repeated until there is agreement between the assumed and computed pressures.

The problem can be visualized by reference to Figure 43. With knowledge of the upstream supersonic flow field in region 1 from the nozzle geometry and by assuming the pressures in fields 2 and 3 (which are equal to those in fields 4 and 5), the location of the separation shocks can be determined from the separation pressure ratio correlation of Figure 40. By numerical or graphical techniques, the shock contours and the supersonic flow field downstream of separation could then be determined - at least in principle. But it would be a difficult and time consuming problem even with a high-speed digital computer because of complexities in geometry and the rotational effects downstream of the shocks. The even more complicated problem of jet mixing and entrainment of the surrounding air would then have to be solved to determine the pressures in zones 4 and 5. At present, there is no established technique for solving the latter problem.

It should be noticed that the nature of the entrainment problem may be different on opposite sides of the jet. This difference may arise if the nozzle and shock geometry is such that the jet can intercept the wall of the nozzle at a finite angle. As indicated in Figure 43, the refracted shock waves will be reflected as expansion fans from the jet boundaries. At these locations, the boundaries will be turned outward and the flow may then intercept the wall on one side. If this occurs, a portion of the flow in region 6 will be reduced to zero velocity and its static pressure will rise. This stagnated flow will subsequently be entrained by the jet, and a mass balance between the stagnated flow and the entrained flow will determine the pressure in the pocket thus formed.

The situation is more complex in the case of the axisymmetric than for the two-dimensional jet because of the geometry of the separation shocks and nozzle walls. If the shock waves and the nozzle walls are regarded as barriers against transmission of downstream pressure signals, then the axisymmetric geometry is more conducive to communication of pressure signals around the periphery of the supersonic jet. Because of this type of communication, small stable deflections of axisymmetric jets caused by differential separation effects are not likely to occur. However, if the jet adheres completely to one side of the wall after separation, the flow can then behave somewhat in a

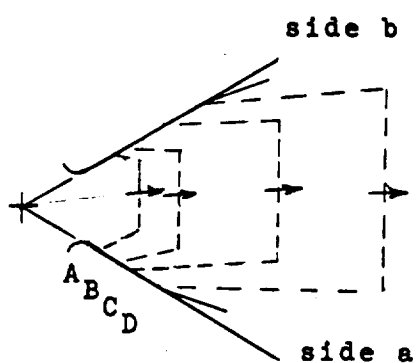
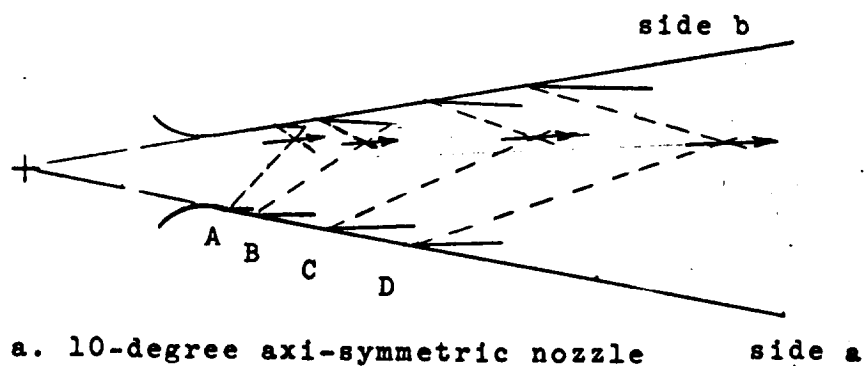
two-dimensional manner. These conclusions are supported by the experimental results of the study which show that when deflection occurs it is usually completely against the wall of the nozzle.

Although an accurate description of the jet behavior requires the complex approach described above, insight regarding the possibilities of flow deflection can be obtained by the following simple approach illustrated in Figure 48, which has the object of showing the effect of pressure differential on the deflection of the jet. For the sake of illustration, a radial supersonic flow field is assumed. A given point on one of the nozzle walls is selected, the area ratio, A/A^* , at this point is determined from the geometry, the Mach number corresponding to this area ratio is determined from the isentropic relationships for one-dimensional flow (actually, a two-dimensional computation is required; but for the sake of illustration, the one-dimensional model is simpler), and the shock and flow deflection angles for separation at this Mach number are determined from the two-dimensional shock relationship pertaining to the separation model developed previously. The shocks are assumed to be straight. Then, to evaluate the effects of different pressures on opposite sides of the nozzle downstream of separation, a pressure difference is assumed. For this particular example, the assumption is made that the downstream pressure on one side of the nozzle is half of the value on the other

side. (i.e. $p_{2a}/p_{2b} = 0.5$). The shock location, shock angle, and flow turning angle can then be determined from the separation and two-dimensional shock relations. A rough idea of the flow deflection is obtained by assuming that the streamline passing through the shock intersection remains undeviated and that the average flow is in the direction of this streamline. Once the average flow direction is determined, one can judge whether the resulting flow deflection is apt to produce the assumed pressure difference.

Figure 48 illustrates the construction for 10-degree and 30-degree axi-symmetric nozzles having approximately the same throat diameter. Figure 48a for the 10-degree nozzle, demonstrates the main point that the average flow deflection decreases as the chamber pressure increases. If one expects, as is reasonable, that the difference in pressures on opposite sides of the jet downstream of separation will diminish as the flow deflection decreases, then dependency of the effect on pressure ratio would be even greater than shown.

Probably, a more important factor is the possibility of forming a closed recirculation pocket on one side of the jet. One sees that at the lower chamber pressures there is a good possibility of this occurring because the shock geometry is such that the position of intersection between the refracted shock wave and the jet boundary downstream of turning by the shock wave is close to the wall; and since the jet must expand outward at this point, the chances of the jet intercepting the wall are good. Also, if this circumstance



	p_c/p_{2a}	$p_{2b} = .5p_{2a}$
--- shocks	A- 2.20	
— flow boundary	B- 3.63	
	C- 8.35	
	D- 15.80	

Fig. 48. --Deflections due to differential pressure

occurs at low pressures, the size of the pocket will be relatively small and may, therefore, effectively seal off both longitudinal and circumferential circulation into this region.

An important difference exists between the flow in nozzles of wide divergence angle as compared to that in nozzles of small divergence angle. The shock angles at the walls are controlled by the shock-boundary layer interaction, and should be the same at the same separation Mach number, regardless of geometry. In wide-angle nozzles, the shocks are more nearly aligned along the axis and this allows greater expansion of the supersonic flow before intercepting the shock. As indicated in Figure 18, normal shocks appear in the flow field of the wide-angle nozzles. The location of these shocks can be explained if the assumption is made that a normal shock will occur whenever the flow in the central stream tube expands to the point that the pressure rise across the shock will be such that the downstream pressure matches the local environmental pressure, p_a . Once the normal shock occurs, the flow originally undergoing the oblique shock will transition from supersonic to subsonic in a shorter distance than otherwise because mixing occurs both interior and exterior to the jet periphery. This action tends to destroy the possibility for the formation of a closed recirculation pocket. Figure 48b shows the normal shock structure for a 30-degree axi-symmetric nozzle. Normal

shocks of this type are not possible for the 10-degree axisymmetric nozzle because the oblique shocks intersect before the flow in the central zone can expand to a sufficiently low pressure to permit matching of the atmospheric pressure through a normal shock.

The formation of a normal shock, or Mach-disc, across the flow stream could also alter the entrainment behavior from that associated with a supersonic jet. This could be important in contoured nozzles of high Mach number which are characterized by large divergence angles.

Side thrust:-The side thrust produced by unsymmetrical separation was determined by evaluating the pressure forces over various sectors of the nozzle surface by the following method: A control volume as shown by the dashed lines in Figure 49 was selected

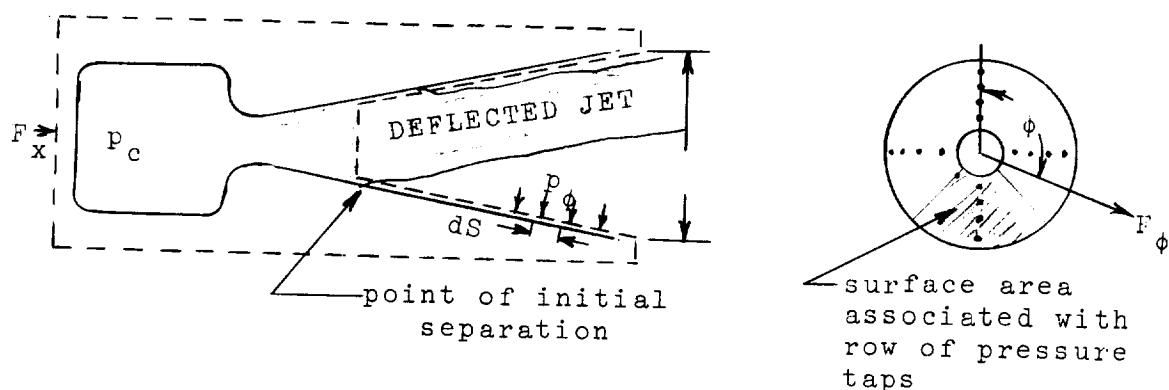


Fig. 49 --Control volume for determination of nozzle forces

The force balances are:

$$(x): \quad (1) \quad F_x + p_a A_e - p_s A_s - \sum_{\phi} \sin \alpha \int_S^e p_{\phi} dS = \dot{w} \bar{u}_{\infty s}$$

$$(\phi): \quad (2) \quad F_{\phi} = \left[\frac{1}{4} \cos \alpha \int_S^e p_{\phi} dS \right] \frac{2\sqrt{2}}{\pi}$$

The assumption is made that the pressures measured along a row of pressure taps are constant over the entire quadrant of the nozzle in which they are centered. The factor outside the brackets in Equation 2 corrects for the average cosine of the angle between the local force direction and the ϕ axis, and:

- F_x = static thrust produced by closed-chamber rocket
- F_{ϕ} = component of side force normal to nozzle axis (one component for each of the four quadrants containing pressure taps)
- p_{ϕ} = measured wall static pressures along each row of pressure taps
- A = nozzle cross-sectional area
- S = nozzle surface area
- \dot{w} = mass flow rate
- \bar{u}_{∞} = average x velocity in free stream
- s = point where separation first occurs
- e = at exit of nozzle

From geometry:

$$dS = \frac{2\pi r dx}{\cos \alpha}, \quad A = \pi r^2, \quad dA = 2\pi r dr, \quad \frac{dr}{dx} = \tan \alpha$$

$$(3) \quad dS = \frac{dA}{\cos \alpha \tan \alpha} = \frac{dA}{\sin \alpha}$$

Then equations 1 and 2 can be expressed as:

$$(4) \quad F_x = \dot{w} \bar{u}_{\infty s} + p_a A^* \sum_{\phi} \int_s^e \frac{p}{p_a} d\left(\frac{A}{A^*}\right) + \frac{p_s}{p_a} \frac{A_s}{A^*} - \frac{A_e}{A^*}$$

and

$$(5) \quad F_{\phi} = \frac{2\sqrt{2}}{\pi} \frac{p_a A^*}{4 \tan \alpha} \int_s^e \frac{p_{\phi}}{p_a} d\left(\frac{A}{A^*}\right)$$

Thus, the integrals are expressed in terms of area ratios. In practice, the integrals were determined by measuring the areas under the pressure profiles.

To determine \dot{w} and $\bar{u}_{\infty s}$ the one-dimensional, isentropic relations for flow of a perfect gas were employed. These relations yield:

$$(6) \quad \dot{w} = \frac{p_o A^*}{\sqrt{T_o}} \left\{ \frac{\gamma}{K} \left(\frac{2}{\gamma+1} \right)^{\frac{\gamma+1}{\gamma-1}} \right\}^{\frac{1}{2}}$$

$$(7) \quad \bar{u}_{\infty s} = \left\{ \frac{2\gamma K T_o}{\gamma-1} \left(1 - \left[\frac{p_s}{p_o} \right]^{\frac{\gamma-1}{\gamma}} \right) \right\}^{\frac{1}{2}}$$

where γ = ratio of specific heats

K = gas constant

T = temperature

()_o = signifies stagnation state

All quantities on the right-hand side of the above equations except for γ and K were measured. Actually, the

chamber pressure p_c , was measured - and a very small (1.005) correction applied to determine p_o . Also, the assumption was made that the discharge coefficient = 1.0.

The static pressure employed in Equation 7 is the measured value at the wall just at the point of separation. Thus, the computed velocity corresponding to this pressure would be inclined to the axis at the angle of the wall, and would not strictly be the x-component of velocity. On the other hand, for sharp-cornered nozzles, the velocities in the center of the stream at the same x location would be greater than the velocity near the wall. In view of these offsetting factors, and the fact that a great deal of accuracy is not required for the purpose at hand, it was considered adequate to utilize the velocity computed from Equation 7 as the average axial velocity.

The application of the foregoing procedure to the data of Figure 26a yields the following results:

$$\dot{w} \bar{u}_{\infty s} = 6.18 \text{ lbf}$$

$$F_x = 3.46 \text{ lbf}$$

$$F_\phi = 0.97 \text{ lbf}$$

$$\phi = 164^\circ$$

$$F_\phi / F_x = 0.281$$

$$F_\phi / \dot{w} \bar{u}_{\infty s} = 0.157$$

One sees that the side force is a substantial fraction of the net static thrust. The orientation of the force appears to be random and would therefore constitute a very severe perturbation if a rocket were required to operate in the unsymmetrical regime for any significant period of time. The performance penalty associated with this operation when the nozzle is overexpanded would also be quite substantial. If the exit area ratio of the nozzle was properly matched for the operating chamber and atmospheric pressures, the static thrust would be $\dot{w}\bar{u}_{\infty s}$. Thus, for the conditions depicted, the actual static thrust is only 55 per cent of the ideal value.

The situation represented here reflects about the maximum value of the momentum flux which was deflected by spontaneous unsymmetrical separation in the 9-degree nozzle. It will be recalled that the flow was symmetrical for values of $p_c/p_a > 3.7$.

VII. CONTROLLED DEFLECTION STUDIES

During the course of the investigation of unstable and unsymmetrical flow, the discovery was made that the jet could be deflected preferentially from one wall to another by inserting a small probe, such as a match stick, along the nozzle wall until the tip of the probe was in the vicinity of the separation region. For cases where the flow was unstable, the insertion of the probe would stabilize the flow. This behavior suggested possibilities for thrust-vector control based upon the separation effects, rather than upon commonly utilized methods which are based on the pressure rise across a shock wave submerged in a supersonic flow field. The separation-type of deflection is capable of deflecting the jet completely to one side of the nozzle and therefore, the deflected momentum constitutes a greater percentage of the total momentum than that usually associated with the submerged shock case. This characteristic may prove advantageous in some applications.

As a preliminary exploration of the possibilities of controlling the separation, tests were made to determine the maximum momentum flux which could be deflected. One of the 0.016-inch diameter holes in the nozzle wall

which held the steel pressure tubing was extended completely through the wall, and the pressure tubing was pushed on through the hole until approximately 1/16 inch of the tube protruded into the flow stream. By trial and error, the hole position located furthest downstream which would cause a steady deflection of the jet was found.

Figure 50a shows the appearance of the deflected jet in two mutually perpendicular planes. The obstruction was at the top of the nozzle as seen in the side-view photographs. The position of the obstruction was somewhat downstream of the location where separation occurred naturally. Thus, as the chamber pressure was raised, the usual unstable and unsymmetrical flow regime occurred and was followed by a symmetrical regime similar to that shown in Figure 27. When the pressure was raised to the value where supersonic flow filled the nozzle to the point where the obstruction was located (at $p_c/p_a \approx 4.0$), unsymmetrical separation recurred and prevailed until a value of $p_c/p_a = 6.51$ was reached. The jet abruptly became straight at this chamber pressure ratio and remained so at higher chamber pressures. Figure 51 shows the static pressure profiles for the deflected jet and after the jet straightened. The maximum deflected jet momentum flux, was $\dot{w}\bar{u}_\infty = 16.2$ lbf.

The sharp pressure increase along one wall of the

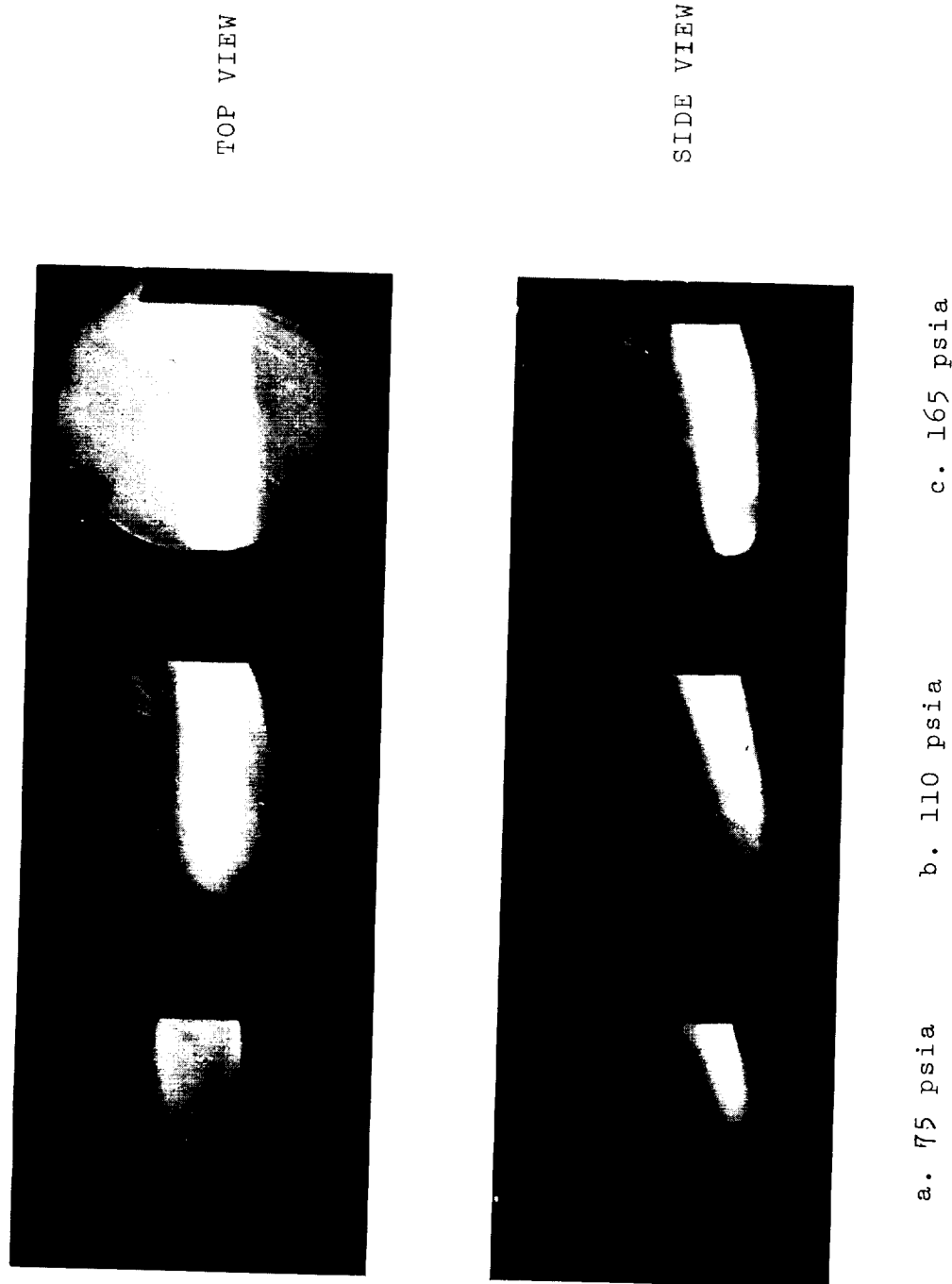


Fig. 50. -- Forced separation in 9-degree conical nozzle

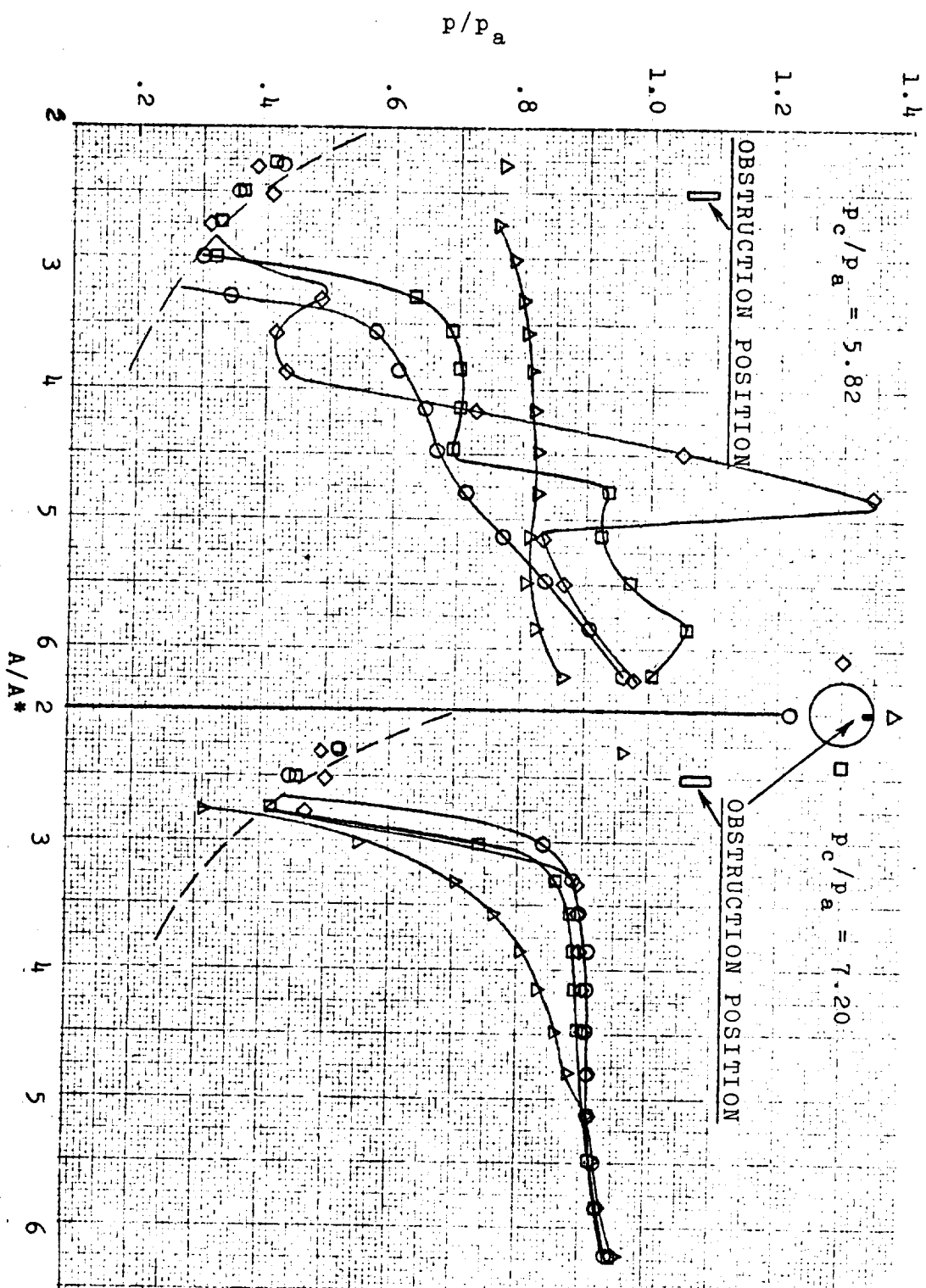


Fig. 51. --Pressure profiles for forced separation

nozzle indicated by the diamond plotting symbols is suggestive of a strong-shock pressure rise and indicates that the main body of the flow was probably adjacent to that wall.

The side represented by the triangular symbols was in the secondary circulation region, and the other two sides were probably in a mixing region between the supersonic and secondary circulation regions.

Tests were also made with the obstruction positioned further upstream. The behavior was expected to be similar to that described above, with the exception that the steady deflection would commence at a lower pressure and terminate at a lower pressure. This indeed was the case; but in addition, stable deflections of the jet were found to occur over other pressure ranges. These pressure ranges were:

<u>Pressure range</u>	<u>Jet character</u>	<u>p_c/p_a</u>
1	steady deflection	3.3 - 5.7
2	straight	5.7 - 8.4
3	steady deflection	7.4 - 10.3
4	straight	10.3 - 11.0
5	steady deflection	11.0 - 13.0
6	diminished deflection	> 13.0

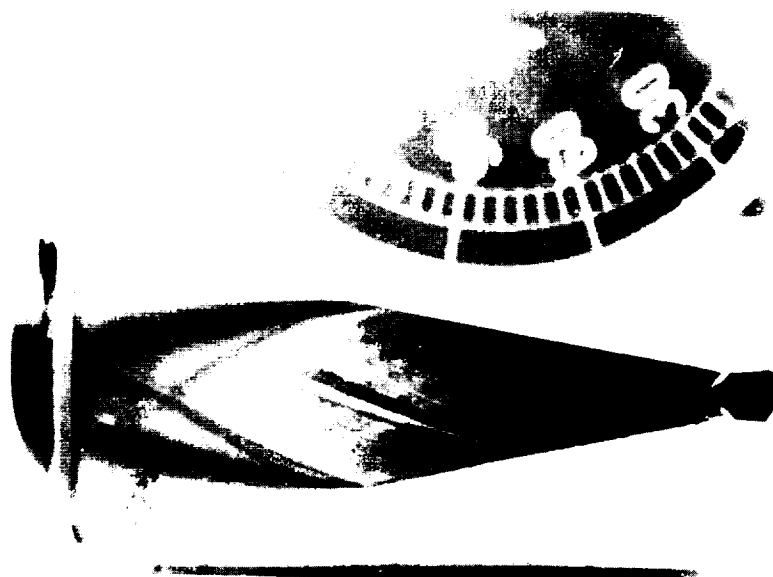
Figure 50b shows the deflection in range 3, and Figure 50c shows the type of deflection in range 5.

Separation commences on the same side of the nozzle for each of the deflection regimes. This behavior

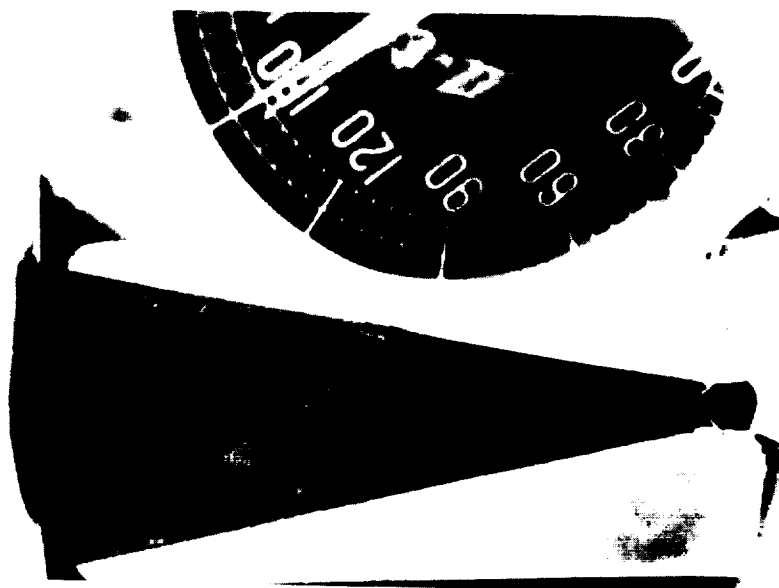
seems to rule out the possibility that reflected shock waves triggered the deflection in the secondary regimes. The cause of the multiple zones has not been determined; however, the fact that they occur seems to be indicative that a larger region for shock-boundary layer interaction around the periphery of the jet may have been involved. This thought is in line with the observation that the maximum momentum flux that could be deflected with the probe in the position furthest downstream was less than that observed in the ventilated nozzle (Figure 31). Thus, a larger interaction area may have been effective in the ventilated nozzle.

Tests of a similar nature were also conducted with the 30-degree axi-symmetric nozzle. Deflections of the type described above were not observed, however non-uniform pressure profiles were measured.

Tests were also made to determine if the flow in the 10-degree, two-dimensional nozzle could be deflected by an obstruction placed across one of the walls. It was found that the flow could be deflected through large angles even at the very high chamber pressures. The effect is shown in Figure 52. The originals of the photographs of Figure 52 are color transparencies. The color scheme reveals that there is a very strong rarefaction between the two shock waves emanating from the obstructions. The first shock wave upstream of the obstruction



a. 160 psia - no obstruction



b. 160 psia - with obstruction

Fig. 52. -- Forced flow deflection in two-dimensional nozzle at high chamber pressure

is believed to originate at the position corresponding to the separation correlation for the pressure in the region just forward of the obstruction. The second shock geometry and location is believed to correspond to the separation correlation for the pressure rise from the local value downstream of the first shock to the value in the secondary circulation region - which is approximately p_a . Thus the flow is turned twice - once by the first shock and once by the second.

If flow filled the nozzle so that the obstruction was buried in the supersonic flow field, a shock similar to the first would occur, and there would be a pressure rise across the shock which would result in a greater net pressure on the obstruction side of the nozzle and thereby create a side force. However, the flow would turn to refill the nozzle downstream of the obstruction. With the obstruction just forward of the normal separation position, there is a net turning of the flow. The side force can be determined approximately by the difference in the pressure - area product on the opposite sides of the nozzle as measured from the point of initial separation on one side of the nozzle to the point of natural separation on the other side. If the nozzle contour downstream is such that the deflected flow can approach a wall and thereby entrain air so as to cause a pressure reduction in the secondary circulation region;

the flow will attach, and the point of separation on the side opposite the obstruction will move further downstream. Thus, the net side force on the nozzle will become greater.

Additional work of this nature is now being conducted by another investigator with specific emphasis being placed on triggering separation with air jets rather than with a solid obstruction.

VIII. SUMMARY OF RESULTS AND CONCLUSIONS

The major conclusions and the results of this study are summarized below:

1. The cause of the apparent differences cited in the literature regarding the separation behavior in nozzles of different geometry; particularly, the differences between conical and contoured nozzles; has been identified as being due to the differences in static pressure in the region of entrainment just downstream of separation. It follows, and is shown, that the usual procedure of basing separation correlations on the pressure at the nozzle exit can not yield a correlation universally applicable to nozzles of different geometry.
2. Arguments for treating separation in nozzles by the same methods generally applied to the discontinuous separation of two-dimensional, supersonic boundary layers have been strengthened considerably by demonstrating that widely differing separation data for widely differing nozzle geometries (Figure 39) can be

brought into agreement by a single correlation based on a boundary-layer separation model, when proper consideration is given to the downstream pressure (Figure 40). The particular separation model employed to demonstrate the general validity of the boundary-layer approach is one in which the Mach-number ratio across the separation shocks is determined by applying knowledge of boundary-layer form factors from incompressible flow in conjunction with compressibility transformations. Two-dimensional shock theory is then applied to determine the pressure rise across the separation shock, and the position of the shock is determined by matching the pressure rise to the upstream and downstream pressures applicable to the nozzle. Consequently, the prime variables which govern the position of separation are the velocity profile in the boundary layer, the Mach number, and the pressure - all just upstream of separation; and the pressure in the entrainment region just downstream of separation. Nozzle geometry is important only as it affects these quantities.

3. Experimental measurements of shock angles in two-dimensional nozzles of narrow and wide divergence angle which generally support the boundary-layer separation model have been made. Conversely, the inter-relationship between boundary-layer separation and the associated shock and flow-turning angles has been shown to have significant effects on the structure of the supersonic flow stream.
4. The specific cause of anomalous separation behavior in contoured nozzles has been identified as being the result of a peculiar entrainment situation in which the flow turning at separation couples with the relatively narrow exit divergence which is characteristic of contoured nozzles, to produce relatively low pressures in the entrainment region downstream of separation. These effects are illustrated in Figure 38.
5. The boundary-layer separation model mentioned in paragraph 2 has been found to be valid even for the case of attached flow in two-dimensional nozzles in which the downstream pressure is governed by mixing effects in a closed recirculation region. Knowledge that

the separation pressures and shock structure conforms to such a relationship may be beneficial to better understanding of the behavior of fluidic devices.

6. Several characteristics of unstable and unsymmetrical flow in two-dimensional and axisymmetric nozzles have been identified -- such as the rapid fluctuation of shocks and flow, the character of the transition between an over-pressured jet and wall-attached flow in two-dimensional nozzles, the nature of the flow switching and unsymmetrical separation in axisymmetric nozzles, and the general magnitude of force perturbations and the jet deflection angles accompanying unsymmetrical separation.
7. The shock and flow-turning angles which are the natural result of compressible boundary layer separation can couple with jet entrainment to cause both unsymmetrical and unstable behavior at low Mach numbers. The transition from a laminar to a turbulent boundary layer in the nozzle can result in unsymmetrical flow.
8. The feasibility of stabilizing flow

fluctuations and controlling the orientation of supersonic jets by means of forcing separation with an obstruction or with bleed air introduced at specific locations has been demonstrated. This type of controlled deflection possesses some potential advantages over conventional techniques and may therefore, have applications in thrust-vector control and in fluidic devices.

IX. RECOMMENDATIONS FOR FUTURE WORK

This work, and the work of others when viewed in retrospect, seems to make a convincing case that separation in nozzles is merely a specialized case of separation of turbulent boundary layers. Although the evidence indicates that the rationale for determining the Mach-number ratio across the separation shock was satisfactory, a better description of the boundary-layer characteristics just before separation would have been advantageous. Some means of determining the local form factor, δ^*/θ (or some other related parameter) of turbulent boundary layers in the presence of pressure gradients and heat transfer such as occur in nozzles would be desirable. Once such relationships are established, controlled experiments to determine separation parameters in terms of these variables could be made. The effect of high heat-transfer rates to the nozzle walls would be particularly interesting.

The anomalous flow behavior which can result when transition from a laminar to a turbulent boundary layer occurs at low Mach numbers prompts an interest in the general problem of boundary layer transition in nozzles. A systematic, analytical and experimental study of the

conditions of boundary-layer transition in the presence of negative pressure gradients, heat transfer, and carefully controlled stream turbulence levels may be rewarding. Also, an investigation of separation in nozzles subject to laminar conditions throughout could be worthwhile.

The importance of downstream pressure in the secondary circulation region has been emphasized in this study. The determination of these pressures requires the solution of a jet entrainment problem which differs from the customary ejector problem because the direction of entrained flow is opposite to that of the main jet. The entire problem poses some interesting technical questions and is worthy of further consideration.

The potentiality for deflecting supersonic jets through large angles by means of a disturbance upstream of separation has been indicated. This matter is worthy of further study.

Additional studies related to the deflection of jets in two-dimensional nozzles as a function of deflected momentum flux and nozzle divergence angle, with particular emphasis on the factors contributing to the pressure in the closed recirculation region are also recommended.

APPENDIX A

LIST OF SYMBOLS

A	Local cross-sectional area of nozzle
A*	Throat area of nozzle where $M=1.0$
B	Mach-number ratio across discontinuity, M_2/M_1
c	Speed of sound
F	Force
H	Boundary-layer form factor, δ^*/θ
h	Enthalpy
K	Gas constant
L	Length of nozzle from throat to exit
M	Mach number
M*	Dimensionless velocity ratio defined in Appendix B
P	Pressure-rise coefficient
p	pressure
R	Radius of curvature of two-dimensional, contoured nozzle
Re _L	Reynolds number based on length
r	Cross-sectional radius of axi-symmetric nozzle
S	Inside surface area of nozzle
t	Temperature
U	Transformed velocity component parallel to wall
u	Velocity component parallel to wall

LIST OF SYMBOLS (continued)

u_s^*	Characteristic velocity in the boundary layer
\bar{u}_∞	Average free-stream velocity along nozzle axis
V	Transformed velocity component perpendicular to wall
v	Velocity component perpendicular to wall
\dot{w}	Mass flow rate
X	Transformed coordinate parallel to wall
x	Coordinate parallel to wall, or along x axis, as appropriate
Y	Transformed coordinate perpendicular to wall
y	Coordinate perpendicular to wall, or half-width of two-dimensional nozzle, as appropriate

Greek Symbols

α	Divergence half-angle for straight-walled nozzles
β	Throat exit half-angle for contoured nozzles
Δ	Flow turning angle across separation shock
δ	Boundary-layer thickness
δ^*	Boundary-layer displacement thickness
γ	Specific-heat ratio
μ	Dynamic viscosity
ν	Kinematic viscosity
ω	$f(M^*)$, given in Appendix B
ϕ	Angular direction measured about nozzle centerline
ρ	Density

LIST OF SYMBOLS (continued)

Ψ	Transformed stream function
ψ	Stream function
σ	Shock angle
θ	Momentum displacement thickness
ξ	Pressure rise across discontinuity, p_2/p_s
II	Identification for left-running characteristic
I	Identification for right-running characteristic

Subscripts

1	Just upstream of separation
2	Just downstream of separation
a	Atmospheric value
b	Back pressure at nozzle exit
c	Chamber
e	At nozzle exit
i	Incompressible case
o	Stagnation value
s	Separation value or value at location of minimum pressure in nozzle in which separation occurs
t	At nozzle throat
∞	In free stream

APPENDIX B

TWO-DIMENSIONAL CONTOURED NOZZLES

The computation of the flow fields and wall contours for the sharp-cornered, two-dimensional nozzles was based on standard, method-of-characteristics techniques as described in Reference 29. The hodograph coordinates for the flow field resulting from an abrupt corner expansion were determined from the relationships:

$$(1) \quad \theta + \omega + \beta = 2I$$

$$(2) \quad \theta - \omega + \beta = 2II$$

$$(3) \quad \omega = \left(\frac{\gamma+1}{\gamma-1} \right)^{\frac{1}{2}} \tan^{-1} \left\{ \frac{M^{*2}-1}{\frac{\gamma+1}{\gamma-1} - M^{*2}} \right\}^{\frac{1}{2}} \\ - \tan^{-1} \left\{ \frac{M^{*2}-1}{1 - \frac{\gamma-1}{\gamma+1} M^{*2}} \right\}$$

$$(4) \quad M^{*2} = \frac{\left(\frac{\gamma+1}{2} \right) M^2}{1 - \frac{\gamma-1}{2} M^2}$$

where:

β = flow angle with respect to nozzle plane of symmetry

I = right running characteristic, looking downstream

II = left running characteristic, looking downstream

For nozzles having wall contours shaped to cancel the incident expansion waves, the entire hodograph plane can be mapped without prior knowledge of flow geometry except for the initial turning angles. In this instance, one-degree increments in turning angle at the corner were employed.

Once the hodograph map was completed, the geometry of the flow field was established by computing the locations of the intersections of the right and left running characteristics (Mach waves). This was a sequential process commencing with the determination of the intersections of the Mach waves emanating from the throat with the axis and then with the first Mach wave from the opposite throat corner. The process was then carried downstream. The direction of the Mach wave between two adjacent flow fields was taken to be the average of the Mach angles associated with each field.

The coordinates of the nozzle contours associated with initial turning angles were determined from the intersections of the flow streamlines with the Mach waves from the opposite throat corner (i.e., with the left running characteristics).

The Fortran program for these computations follows. As written, the program computes the flow field and wall contours for initial turning angles of 1 to 30 degrees, in one-degree increments. With the alteration of only

TABLE 4.--Data for two-dimensional,
sharp-cornered, perfect nozzles

centerline		$\beta = 7^\circ$				$\beta = 14^\circ$				$\beta = 21^\circ$				$\beta = 28^\circ$			
β°	x_b	p_b/p_o	x_w	y_w	p_w/p_o	x_w	y_w	p_w/p_o	x_w	y_w	p_w/p_o	x_w	y_w	p_w/p_o	x_w	y_w	p_w/p_o
1	.207	.528	.898	1.110	.346	1.038	1.259	.246	1.160	1.445	.172	1.283	1.682	.117			
2	.529	.450	1.419	1.165	.330	1.637	1.397	.234	1.838	1.692	.163	2.045	2.070	.110			
3	.663	.403	1.670	1.187	.314	1.929	1.459	.222	2.177	1.809	.154	2.438	2.262	.104			
4	.778	.364	1.893	1.203	.299	2.191	1.510	.211	2.486	1.909	.146	2.804	2.433	.098			
5	.885	.330	2.106	1.214	.285	2.444	1.555	.201	2.789	2.002	.138	3.167	2.595	.092			
6	.990	.299	2.316	1.221	.271	2.696	1.595	.191	3.094	2.089	.131	3.540	2.753	.087			
7	1.095	.271	2.526	1.225	.258	2.951	1.630	.181	3.408	2.173	.123	4.010	3.036	.076			
8	1.202	.246	$M_e = 1.57$.246	3.214	1.663	.172	3.735	2.255	.117	4.339	3.067	.076			
9	1.312	.222				3.485	1.691	.163	4.076	2.334	.110	4.773	3.225	.072			
10	1.427	.201				3.768	1.716	.154	4.436	2.410	.104	5.237	3.385	.067			
11	1.547	.181				4.063	1.737	.146	4.816	2.484	.098	5.732	3.546	.063			
12	1.674	.163				4.372	1.753	.138	5.219	2.555	.092	6.264	3.708	.059			
13	1.809	.146				4.697	1.764	.131	5.648	2.623	.087	6.836	3.872	.055			
14	1.953	.131				5.039	1.770	.123	6.104	2.687	.081	7.452	4.038	.052			
15	2.108	.117				$M_e = 2.06$.116	6.590	2.747	.076	8.117	4.203	.048			
16	2.276	.104							7.110	2.801	.072	8.837	4.369	.045			
17	2.457	.092							7.666	2.850	.067	9.615	4.535	.042			
18	2.655	.081							8.261	2.892	.063	10.459	4.699	.039			
19	2.872	.072							8.899	2.925	.059	11.374	4.860	.036			
20	3.110	.063							9.585	2.949	.055	12.368	5.018	.034			
21	3.372	.055							10.321	2.962	.052	13.449	5.170	.031			
22	3.664	.048							$M_e = 2.63$.048	14.626	5.314	.029			
23	3.988	.042										15.908	5.449	.027			
24	4.351	.036										17.307	5.571	.025			
25	4.759	.031										18.834	5.678	.023			
26	5.218	.027										20.503	5.766	.021			
27	5.740	.023										22.328	5.829	.019			
28	6.334	.019										24.328	5.864	.018			
29	7.015	.016										$M_e = 3.35$.016			
30	7.798	.014															

ΔJOB,ME412,RAL,5
ΔFTN,L,X

```

C      PROGRAM FOR DETERMINING SHARP-CORNER PERFECT NOZZLE PROFILES

C      PROGRAM PERFECT
C      MEANING OF SYMBOLS
C      DELT=INCREMENT OF TURNING ANGLE IN EXPANSION FAN (DEGREES)
C      MENO OF INCREMENTS OF TURNING ANGLE
C      GAM=SPECIFIC HEAT RATIO
C      Y0=Y COORDINATE OF CORNER ,X0=X COORDINATE=0.0)
C      AM(I,J)=MACH NO IN FIELD I,J
C      W(I,J)=SHAPIRO OMEGA=FUNCTION OF MACH NO
C      AL(I,J)=MACH WAVE ANGLE,ALPHA
C      TH(I,J)=ANGLE OF VELOCITY VECTOR WITH RESPECT TO X AXIS
C      PL(I,J)=GENERALLY POSITIVE CHARACTERISTIC=ALPHA+THETA
C      SUB(I,J)=GENERALLY NEGATIVE CHARACTERISTIC ANGLE=THETA-ALPHA
C      Y(I)=LEFT RUNNING CHARACTERISTIC IN HODAGRAPH PLANE
C      X(I)=RT.  RUNNING CHARACTERISTIC IN HODAGRAPH PLANE
C      K=SUBSCRIPT TO RELATE MACH NO AS FUNCTION OF OMEGA IN TABULAR FORM
C      PRATIO(I,J)=LOCAL RATIO OF STATIC TO STAGIATION PRESSURE
C      DZ(I,J)=AVERAGE DOWN CHARACTERISTIC ANGLE BORDERING FIELD I,J ON
C      TOP
C      UZ(I,J)=TANGENT OF AVERAGE UP CHARACTERISTIC ANGLE BORDERING FIELD
C      ON RIGHT (BETWEEN FIELD I,J AND I,J+1)
C      XX=X COORDINATE OF TOP RIGHT FIELD BOUNDARY
C      YY(I,J)=Y COORDINATE OF TOP RIGHT FIELD BOUNDARY
C      HR(I,J)=X COORDINATE OF WALL CONTOUR WHICH WILL TURN FLOW TO THE
C      ANGLE IN FIELD I,J WITHOUT COMPRESSION WAVES
C      SS(I,J)=Y COORDINATE AS FOR ABOVE
C      DIMENSION BB(99) ,AM(31,31),W(31,31),AL(31,31),TH(31,31),
1      SUB(31,31),Y(50),X(50),PRATIO(31,31),DOWN(31,31),
2      DZ(31,31),UP(31,31),UZ(31,31),YY(31,31),XX(31,31),PL(31,31) ,
3      RRR(31,31),SS(31,31)

```

```

DATA ((BB(K), K=1,99)= 1.0818,1.1326,1.1769,1.2177,1.2565,
11.2938,1.3300,1.3655,1.4004,1.4349, 1.4692,1.5032,1.5371,1.5709,
21.6047, 1.6385,1.6725,1.7065,1.7406,1.7750, 1.8095,1.8443,1.87
393,1.9146,1.9503, 1.9862,2.0226,2.0593,2.0964,2.1339,2.1718,
42.2103,2.2492,2.2887,2.3287, 2.3693,2.4105,2.4523,2.4947,2.5378,
5 2.5816,2.6261,2.6714,2.7176,2.7644, 2.8122,2.8609,2.9105,
62.9610,3.0126,3.0652,3.1189,3.1738,3.2298,3.2871,3.3457,3.4056,
73.4669,3.5297,3.5940,3.6600,3.7276,3.7969,3.8681,3.9412,4.0163,
84.0936,4.1730,4.2546,4.3390,4.4258,4.5152,4.6076,4.7029,4.8014,
94.9032,5.0085,5.1176,5.2306,5.3479,6.0064,6.8190,7.8509,9.2105)
DELT=1.0
M = 31
GAM=1.4
Y0=1.0
C CALCULATION OF J=1 FIELD POINTS FROM CORNER EXPANSION
AM(1,1)=1.0
W(1,1)=0.0
AL(1,1)=90.0
TH(1,1)=0.0
PL(1,1)=90.
X(1)=500.
SUB(1,1)=-90.
Y(1)=(1000.-W(1,1)+TH(1,1))/2.
DO 30 I=2,M
A=I
TH(I,1)=(A-1.)*DELT
W(I,1)=1000.+TH(I,1)-Y(1)*2.
X(I)=(1000.+W(I,1)+TH(I,1))/2.
K=W(I,1)+.01
AM(I,1)=BB(K)
AM(2,1)=1.0818

```

```

AL(I,1)=ATANF(1./SQRTF(AM(I,1)*AM(I,1)-1.))*57.2963
PL(I,1)=TH(I,1)+AL(I,1)
SUB(I,1)=TH(I,1)-AL(I,1)
30 CONTINUE
C CALCULATION OF FIELD POINTS ALONG AXIS
DO 40 J=2,M
I=J
TH(I,J)=0.
W(I,J)=2.*X(I)-1000.
Y(J)=(1000.-W(I,J))/2.
K=W(I,J) +.01
AM(I,J)=BB(K)
IF ( K.EQ.0) AM(I,J)=1.0000001
AL(I,J)=ATANF(1./SQRTF(AM(I,J)*AM(I,J)-1.))*57.2963
PL(I,J)= TH(I,J)+AL(I,J)
SUB(I,J)=TH(I,J)-AL(I,J)
40 CONTINUE
C CALCULATION OF INTERNAL FIELD POINTS
MM=M-1
DO 50 J=2,MM
KK=J+1
DO 45 I=KK,M
TH(I,J)=X(I)+Y(J)-1000.
W(I,J)=X(I)-Y(J)
K=W(I,J) +.01
AM(I,J)=BB(K)
IF ( K.EQ.0) AM(I,J)=1.0000001
AL(I,J)=ATANF(1./SQRTF(AM(I,J)*AM(I,J)-1.))*57.2963
PL(I,J)=TH(I,J)+AL(I,J)
SUB(I,J)=TH(I,J)-AL(I,J)
45 CONTINUE

```

```

50 CONTINUE
   DO 60 J=1,M
   DO 55 I=1,M
      PRATIO (I,J)=1./((1.+(GAM-1.)*AM(I,J)*AM(I,J)/2.)**(GAM/(GAM-1.)))
55 CONTINUE
60 CONTINUE

C   CALCULATION OF CHARACTERISTIC AVERAGE ANGLES
   KKK=M-1
   DO 70 J= 1,KKK
   DO 70 I= J,KKK
      DOWN(I,J)=(SUB(I,J)+SUB(I+1,J))/2.0
      DZ(I,J)=TANF(DOWN(I,J)/57.2963)
      UP(I,J)=(PL(I,J)+PL(I,J+1))/2.
      UZ(I,J)=TANF(UP(I,J)/57.2963)
70 CONTINUE

C   CALCULATION OF X,Y COORDINATES
   DO 80 J=1,KKK
   DO 80 I= J,KKK
      INTERSECTION OF FIRST MACH WAVE (CHARACTERISTIC) WITH AXIS
      IF (I-1) 90,90,100
90  YY(1,1)=0.0
      XX(1,1)=-Y0/UZ(1,1)
      GO TO 80

C   DETERMINATION OF CHARACTERISTIC INTERSECTIONS JOINING CORNER
100 IF(J-1) 110,110,120
110 XX(I,J)=(YY(I-1,J)-Y0-XX(I-1,J)*UZ(I,J))/(DZ(I,J)-UZ(I,J))
      YY(I,J)=XX(I,J)*DZ(I,J)+Y0
      ANG=TANF(TH(I,J)/57.2963)
      RR(I,J)=(YY(I-1,J)-Y0-XX(I-1,J)*UZ(I,J))/( ANG -UZ(I,J))
      SS(I,J)=RR(I,J)*ANG +Y0
      GO TO 80

```

```

C      DETERMINATION OF X INTERCEPTS ALONG AXIS
120 IF (I-J) 115,115,125
115 XX(I,J)=XX(I,J-1)-YY(I,J-1)/DZ(I,J)
   YY(I,J)=0.0
   RR(I,J)=0.0
   SS(I,J)=0.0
   GO TO 80

C      DETERMINATION OF CHARACTERISTIC INTERSECTIONS IN GENERAL
125 XX(I,J)=YY(I-1,J)-YY(I,J-1)+XX(I,J-1)*DZ(I,J)-XX(I-1,J)*UZ(I,J)
   XX(I,J)=XX(I,J)/(DZ(I,J)-UZ(I,J))
   YY(I,J)=(XX(I,J)-XX(I,J-1))*DZ(I,J)+YY(I,J-1)
   ANG=TANF(TH(I,J)/57.2963)
   RR(I,J)=YY(I-1,J)-SS(I,J-1)+RR(I,J-1)*ANG   -XX(I-1,J)*UZ(I,J)
   RR(I,J)=RR(I,J)/(ANG-UZ(I,J))
   SS(I,J)=(RR(I,J)-RR(I,J-1))*ANG   +SS(I,J-1)
80 CONTINUE
   DO 210 J=1,M
   PRINT 180,J
180 FORMAT (1H1,* J= *,I3/)
   PRINT 200, (I,I=1,30)
200 FORMAT(*I*//(' 10I8'))
   PRINT 201, (XX(I,J),I=1,30)
201 FORMAT(* XX*//('10F8.3'))
   PRINT 202, (YY(I,J),I=1,30)
202 FORMAT(* YY*//('10F8.3'))
   PRINT 203, (RR(I,J),I=1,30)
203 FORMAT(* RR*//('10F8.3'))
   PRINT 204, (SS(I,J),I=1,30)
204 FORMAT(* SS*//('10F8.3'))
   PRINT 205, (TH(I,J),I=1,30)
205 FORMAT(* TH*//('10F8.3'))

```


ΔJOB,ME412,RAL,5
ΔFTN,L,X

```

C      PROGRAM FOR DETERMINING SHARP-CORNER PERFECT NOZZLE PROFILES

C      PROGRAM PERFECT
C      MEANING OF SYMBOLS
C      DELT=INCREMENT OF TURNING ANGLE IN EXPANSION FAN (DEGREES)
C      M=NO OF INCREMENTS OF TURNING ANGLE
C      GAM=SPECIFIC HEAT RATIO
C      YU=Y COORDINATE OF CORNER ,X0=X COORDINATE=0.0)
C      AM(I,J)=MACH NO IN FIELD I,J
C      W(I,J)=SHAPIRO OMEGA=FUNCTION OF MACH NO
C      AL(I,J)=MACH WAVE ANGLE,ALPHA
C      TH(I,J)=ANGLE OF VELOCITY VECTOR WITH RESPECT TO X AXIS
C      PL(I,J)=GENERALLY POSITIVE CHARACTERISTIC=ALPHA+THETA
C      SUB(I,J)=GENERALLY NEGATIVE CHARACTERISTIC ANGLE=THETA-ALPHA
C      Y(I)=LEFT RUNNING CHARACTERISTIC IN HODAGRAPH PLANE
C      X(I)=RT. RUNNING CHARACTERISTIC IN HODAGRAPH PLANE
C      K=SUBSCRIPT TO RELATE MACH NO AS FUNCTION OF OMEGA IN TABULAR FORM
C      PRATIO(I,J)=LOCAL RATIO OF STATIC TO STAGNATION PRESSURE
C      UZ(I,J)=AVERAGE DOWN CHARACTERISTIC ANGLE BORDERING FIELD I,J ON
C      TOP
C      UZ(I,J)=TANGENT OF AVERAGE UP CHARACTERISTIC ANGLE BORDERING FIELD
C      ON RIGHT (BETWEEN FIELD I,J AND I,J+1)
C      XX=X COORDINATE OF TOP RIGHT FIELD BOUNDARY
C      YY(I,J)=Y COORDINATE OF TOP RIGHT FIELD BOUNDARY
C      XR(I,J)=X COORDINATE OF WALL CONTOUR WHICH WILL TURN FLOW TO THE
C      ANGLE IN FIELD I,J *WITHOUT COMPRESSION WAVES
C      SS(I,J)=Y COORDINATE AS FOR ABOVE
C      DIMENSION RB(99) ,AM(31,31),W(31,31),AL(31,31),TH(31,31),
1      SUB(31,31),Y(50),X(50),PRATIO(31,31),DOWN(31,31),
2      DZ(31,31),UP(31,31),UZ(31,31),YY(31,31),XX(31,31),PL(31,31) ,
3      RR(31,31),SS(31,31)

```



```

DATA ((RR(K), K=1,99)= 1.0818,1.1326,1.1769,1.2177,1.2565,
11.2938,1.3300,1.3655,1.4004,1.4349, 1.4692,1.5032,1.5371,1.5709,
21.6047, 1.6385,1.6725,1.7065,1.7406,1.7750, 1.8095,1.8443,1.87
393,1.9146,1.9503, 1.9862,2.0226,2.0593,2.0964,2.1339,2.1718,
42.2103,2.2492,2.2887,2.3287, 2.3693,2.4105,2.4523,2.4947,2.5378,
5 2.5816,2.6261,2.6714,2.7176,2.7644, 2.8122,2.8609,2.9105,
62.9610,3.0126,3.0652,3.1189,3.1738,3.2298,3.2871,3.3457,3.4056,
73.4669,3.5297,3.5940,3.6600,3.7276,3.7969,3.8681,3.9412,4.0163,
84.0936,4.1730,4.2548,4.3390,4.4258,4.5152,4.6076,4.7029,4.8014,
94.9032,5.0085,5.1176,5.2306,5.3479,6.0064,6.8190,7.8509,9.2105)
DELT=1.0
M = 31
GAM=1.4
Y0=1.0
AM(1,1)=1.0
W(1,1)=0.0
AL(1,1)=90.0
TH(1,1)=0.0
PL(1,1)=90.
X(1)=500.
SUB(1,1)=-90.
Y(1)=(1000.-W(1,1)+TH(1,1))/2.
DO 30 I=2,M
A=I
TH(I,1)=(A-1.)*DELT
W(I,1)=1000.+TH(I,1)-Y(1)*2.
X(I)=(1000.+W(I,1)+TH(I,1))/2.
K=W(I,1) +.01
AM(I,1)=BB(K)
AM(2,1)=1.0818

```

```

AL(I,1)=ATANF(1./SQRTF(AM(I,1)*AM(I,1)-1.))*57.2963
PL(I,1)=TH(I,1)+AL(I,1)
SUB(I,1)=TH(I,1)-AL(I,1)
30 CONTINUE
C CALCULATION OF FIELD POINTS ALONG AXIS
DO 40 J=2,M
I=J
TH(I,J)=0.
W(I,J)=2.*X(I)-1000.
Y(J)=(1000.-W(I,J))/2.
K=W(I,J) +.01
AM(I,J)=BB(K)
IF ( K.EQ.0) AM(I,J)=1.0000001
AL(I,J)=ATANF(1./SQRTF(AM(I,J)*AM(I,J)-1.))*57.2963
PL(I,J)= TH(I,J)+AL(I,J)
SUB(I,J)=TH(I,J)-AL(I,J)
40 CONTINUE
C CALCULATION OF INTERNAL FIELD POINTS
MM=M-1
DO 50 J=2,MM
KK=J+1
DO 45 I=KK,M
TH(I,J)=X(I)+Y(J)-1000.
W(I,J)=X(I)-Y(J)
K=W(I,J) +.01
AM(I,J)=BB(K)
IF ( K.EQ.0) AM(I,J)=1.0000001
AL(I,J)=ATANF(1./SQRTF(AM(I,J)*AM(I,J)-1.))*57.2963
PL(I,J)=TH(I,J)+AL(I,J)
SUB(I,J)=TH(I,J)-AL(I,J)
45 CONTINUE

```

```

50 CONTINUE
DO 60 J=1,M
DO 55 I=1,M
PRATIO (I,J)=1./((1.+(GAM-1.)*AM(I,J)*AM(I,J)/2.)*(GAM/(GAM-1.)))
55 CONTINUE
60 CONTINUE

C CALCULATION OF CHARACTERISTIC AVERAGE ANGLES
KKK=M-1
DO 70 J= 1,KKK
DO 70 I= J,KKK
DOWN(I,J)=(SUB(I,J)+SUB(I+1,J))/2.0
DZ(I,J)=TANF(DOWN(I,J)/57.2963)
UP(I,J)=(PL(I,J)+PL(I,J+1))/2.
UZ(I,J)=TANF(UP(I,J)/57.2963)
70 CONTINUE

C CALCULATION OF X,Y COORDINATES
DO 80 J=1,KKK
DO 80 I= J,KKK
C INTERSECTION OF FIRST MACH WAVE (CHARACTERISTIC) WITH AXIS
IF (I-1) 90,90,100
90 YY(1,1)=0.0
XX(1,1)=-Y0/UZ(1,1)
GO TO 80

C DETERMINATION OF CHARACTERISTIC INTERSECTIONS JOINING CORNER
100 IF(J-1) 110,110,120
110 XX(I,J)=(YY(I-1,J)-Y0-XX(I-1,J)*UZ(I,J))/(DZ(I,J)-UZ(I,J))
YY(I,J)=XX(I,J)*DZ(I,J)+Y0
ANG=TANF(TH(I,J)/57.2963)
RR(I,J)=(YY(I-1,J)-Y0-XX(I-1,J)*UZ(I,J))/( ANG -UZ(I,J))
SS(I,J)=RR(I,J)*ANG +Y0
GO TO 80

```

```

C      DETERMINATION OF X INTERCEPTS ALONG AXIS
120 IF (I-J) 115,115,125
115 XX(I,J)=XX(I,J-1)-YY(I,J-1)/DZ(I,J)
   YY(I,J)=0.0
   RR(I,J)=0.0
   SS(I,J)=0.0
   GO TO 80

C      DETERMINATION OF CHARACTERISTIC INTERSECTIONS IN GENERAL
125 XX(I,J)=YY(I-1,J)-YY(I,J-1)+XX(I,J-1)*DZ(I,J)-XX(I-1,J)*UZ(I,J)
   XX(I,J)=XX(I,J)/(DZ(I,J)-UZ(I,J))
   YY(I,J)=(XX(I,J)-XX(I,J-1))*DZ(I,J)+YY(I,J-1)
   ANG=ATANF(TH(I,J)/57.2963)
   RR(I,J)=YY(I-1,J)-SS(I,J-1)+RR(I,J-1)*ANG   -XX(I-1,J)*UZ(I,J)
   RR(I,J)=RR(I,J)/(ANG-UZ(I,J))
   SS(I,J)=(RR(I,J)-RR(I,J-1))*ANG   +SS(I,J-1)
80 CONTINUE

   DO 210 J=1,M
   PRINT 180,J
180 FORMAT (1H1,* J= *,I3/)
   PRINT 200, (I,I=1,30)
200 FORMAT(*I*//(' 10I8' ))
   PRINT 201, (XX(I,J),I=1,30)
201 FORMAT(* XX*//('10F8.3'))
   PRINT 202, (YY(I,J),I=1,30)
202 FORMAT(* YY*//('10F8.3'))
   PRINT 203, (RR(I,J),I=1,30)
203 FORMAT(* RR*//('10F8.3'))
   PRINT 204, (SS(I,J),I=1,30)
204 FORMAT(* SS*//('10F8.3'))
   PRINT 205, (TH(I,J),I=1,30)
205 FORMAT(* TH*//('10F8.3'))

```

```

PRINT 206, (AM(I,J),I=1,30)
206 FORMAT(* AM*// (10F8.3))
PRINT 207, (PRATIO(I,J),I=1,30)
207 FORMAT(* PRATIO*// (10F8.3))
PRINT 208, (W(I,J),I=1,30)
208 FORMAT(* W *// (10F8.3))
PRINT 209, (X(I),I=1,30)
211 FORMAT (* X*// (10F8.3))
PRINT 211, (Y(I),I=1,30)
209 FORMAT (* Y*// (10F8.3))
210 CONTINUE
END
SCOPE
ALOAD
ARUN,5,5000,,1
[::::::::::::::::::::::::::::::::::::::::::::::::::[

```

BIBLIOGRAPHY

1. Stodola, A., (English Translation by Loewenstein, L.C.) "Steam and Gas Turbines, Volume I" McGraw-Hill Book Company, Inc., New York, N.Y., 1927, Sections 32, 33, 36, 42a.
2. Foster, C.R. and Cowles, F.B., "Experimental Study of Gas Flow Separation in Overexpanded Exhaust Nozzles for Rocket Motors," Jet Propulsion Laboratory, California Institute of Technology, Pasadena, California, Progress Report No. 4-103, May 1949.
3. Foster, C.R. and Cowles, F.B., "Experimental Study of the Divergence Angle Effect in Rocket Motor Exhaust Nozzles," Jet Propulsion Laboratory, California Institute of Technology, Pasadena, California, No. 20-134, Jan. 1951.
4. McKenney, J.D., "An Investigation of Flow Separation in a Two-Dimensional Transparent Nozzle," Jet Propulsion Laboratory, California Institute of Technology, Pasadena, California, Progress Report No. 20-129, April 1951.
5. Summerfield, M., Foster, C.R., and Swan, W.C., "Flow Separation in Overexpanded Supersonic Exhaust Nozzles," Journal of the American Rocket Society, September, October 1954.
6. Scheller, K., and Bierlein, J.A., "Some Experiments on Flow Separation in Rocket Nozzles," Wright Air Development Center, Dayton, Ohio, Journal of American Rocket Society, Vol. 23, p. 28, January, February 1953.
7. Green, L., "Flow Separation in Rocket Nozzles," Journal of American Rocket Society, Vol. 23, No. 1, p. 34-35, 1953.
8. Mager, A., "On the Model of the Free, Shock-Separated Boundary Layer," Journal of the Aeronautical Sciences, Vol. 23, p. 182-4, 1956.

9. Liepman, H.W., Roshko, A. and Dhawan, S., "On Reflection of Shock Waves From Boundary Layers," NACA TN 2334, April, 1951.
10. Lange, R.H., "Present Status of Information Relative to the Prediction of Shock-Induced Boundary Layer Separation," NACA TL 3065, February 1954.
11. Bogdonoff, S.M., and Kepler, E.C., "The Separation of a Supersonic Turbulent Boundary Layer," Journal of the Aeronautical Sciences, Vol. 22 No. 5, p. 414-424, June 1955.
12. Fraser, R.P., Eisenklam P., and Wilkie, D., "Investigation of Supersonic Flow Separation in Nozzles," Journal Mech. Engr. Sci., 1, p. 267-279, 1959.
13. Campbell, C.E., and Farley, J.M., "Performance of Several Conical Convergent-Divergent Rocket-Type Exhaust Nozzles," NASA TND-467, Sept. 1960.
14. Reshotko, E., and Tucker, M., "Effect of a Discontinuity on Turbulent Boundary Layer Thickness Parameters and Application to Shock-Induced Separation," NACA TN 3454, May 1955.
15. Bloomer, H.E., Antl, R.J., and Revas, P. ., "Experimental Study of Effects of Geometric Variables on Performance of Conical Rocket-Engine Exhaust Nozzles," NASA Technical Note D-846, June 1961. (Lewis Research Center, Cleveland, Ohio).
16. Page, R.H., "Flow Separation in Nozzles," Stevens Institute of Technology, Hoboken, New Jersey, Journal of Aerospace Science, p. 110, January 1962.
17. Arens, M. and Spiegler, E., "Shock Induced Boundary Layer Separation in Overexpanded Conical Exhaust Nozzles," AIAA Journal, Vol. 1, No. 3, p. 578-9, 1963.
18. Gadd, G.E., "Interactions Between Wholly Laminar or Wholly Turbulent Boundary Layers and Shock Waves Strong Enough to Cause Separation," Journal of the Aeronautical Sciences, Vol. 20, p. 729-739, 1953.
19. Moore, C.J., "An Experimental Study of Flow Separation and Instability in an Overexpanded Nozzles," M.S. Thesis, Southern Methodist University, 1964.

20. Simon, C.E., "Continued Study of Flow Separation and Instability in Overexpanded Nozzles," M.S. Thesis, Southern Methodist University, 1964.
21. Sunley, H.L.G. and Ferriman, D.L.C., "Jet Separation in Conical Nozzles," Royal Aeronautical Society Journal, Vol. 68, p. 808-17, 1964.
22. Kalt, S., and Badal, D.L., "Conical Rocket Nozzle Performance Under Flow-Separated Conditions," Journal of Spacecraft and Rockets, Vol. 2, No. 3, p. 447-449.
23. Chapman, D.R., Kuehn, D.M., and Larson, H.K., "Investigations of Separated Flows in Supersonic and Subsonic Streams with Emphasis on the Effect of Transition," NACA Report 1356, 1958.
24. Gadd, G.E., Holder, D.W., and Regan, J.D., "An Experimental Investigation of the Interaction Between Shock Waves and Boundary Layers," Proceedings of the Royal Society (London) A 226, p. 227-253, 1954.
25. Farley, J.M. and Campbell, C.E., "Performance of Several Methods-of-Characteristics Exhaust Nozzles," NASA TN D-293, October 1960.
26. Ahlberg, J.H., Hamilton, S., Migdal, D., and Nilson, E.N., "Truncated Perfect Nozzles in Optimum Nozzle Design," Journal of American Rocket Society, Vol. 31, p. 614-620, 1961.
27. Roshko, E.J., and Messier, P.F., "Flow Separation in a Contoured Nozzle," Journal of American Rocket Society, Vol. 32, p. 1612, October 1962.
28. Ionov, V.P., "Supersonic Flow at Different Reynolds Numbers in Contoured Nozzles Under Conditions of Overexpansion," Gas Dynamics and Physics of Combustion, NASA-TT-F-79 (Translated from Russian) p. 82-84, 1962.
29. Shapiro, A.H., "The Dynamics and Thermodynamics of Compressible Fluid Flow, Vol. 1," The Ronald Press Company, New York, p. 136, 1954.
30. Chow, W.L., "Axially Symmetric and Annular Supersonic Nozzle Profiles," Engineering Experiment Station, University of Illinois, ME-TN-394-1, 1963.

31. Lancaster, D.E., "Using New Low-Cost Integrated Circuits," Electronics World, Vol. 75, No. 3, March 1966.
32. Schlichting, H. (English Translation by Kestin, J.) "Boundary Layer Theory," McGraw-Hill Book Company, Inc., New York, N.Y., 1955.
33. Cohen, C.B., and Reshotko, E., "The Compressible Laminar Boundary Layer with Heat Transfer and Arbitrary Pressure Gradient," NASA-TN-3326.
34. Stewartson, K., "Correlated Incompressible and Compressible Boundary Layers," Proceedings of the Royal Society of London, Series A, Vol. 200, p. 84-100, 1949.
35. Howarth, L., "Concerning the Effect of Compressibility on Laminar Boundary Layers and Their separation," Proceedings of the Royal Society of London, Series A, Vol. 194, p. 16-42, 1948.
36. Shapiro, I, p. 535.
37. von Doenhoff, A.E., and Tetervin, N., "Determination of General Relations for the Behavior of Turbulent Boundary Layers," NACA Report 772, 1943.
38. Schubauer, G.B., and Klebanoff, P.S., "Investigations of Separation of the Turbulent Boundary Layer," NACA TN 2133, 1951.
39. Sandborn, V.A., "Preliminary Experimental Investigation of Low Speed Turbulent Boundary Layers in Adverse Pressure Gradients," NACA TN 3031, 1953.
40. Love, E.S., "Pressure Rise Associated With Shock-Induced Boundary Layers Separation," NACA TN 3601, 1955.
41. Bartz, D.R., "An Approximate Solution of Compressible Turbulent Boundary Layer Development and Convective Heat Transfer in Convergent-Divergent Nozzles," Transactions of the ASME, Vol. 77, p. 1235-1245, 1955.
42. Kays, W.M., "Convective Heat and Mass Transfer," McGraw-Hill Book Company, New York, N.Y., p. 93, 1966.

43. Shapiro, A.H., "The Dynamics and Thermodynamics of Compressible Fluid Flow," Vol. II, The Ronald Press Company, New York, N.Y., p. 1157, 1954.
44. Ibid., p. 1140-1153.